PHYSICAL REVIEW
LETTERS

VOLUME 7 SEPTEMBER 15, 1961 NUMBER 6

DENSITY OF LIQUID HELIUM-3 BETWEEN 0.045 AND 1.3°K*

John E. Rives and Horst Meyer†
Department of Physics, Duke University, Durham, North Carolina
(Received August 7, 1961)

We have measured the density of liquid helium-3 at various pressures up to 28.0 atm in the temperature range between 0.045 and 1.3°K. At pressures above about 15 atm, an unexpected minimum in density was found to occur, the temperature of this minimum increasing to 0.09°K when the pressure is increased to 28 atmospheres. For a pressure of 0.18 atm and below 0.08°K the coefficient of expansion was found to be proportional to T, as predicted by Brueckner.[1]

The method used for these measurements was the same as that used by Lee, Fairbank, and Walker,[2] who determined the density of liquid helium-3 down to about 0.15°K. It consisted in measuring the dielectric constant of the liquid from the resonant frequency of an LC circuit, in which the capacity was a coaxial cylindrical capacitor containing the liquid. The density of the liquid was then obtained using the Clausius-Mosotti relation. The assumption was, as in earlier work,[2] that the polarizability stayed constant with temperature and pressure.

The cylindrical capacitor was made of parts machined from electrolytic copper, the gap being 4×10^{-2} mm between the concentric cylinders. These were held together at their upper extremity by an araldite seal capable of withstanding pressures at least up to 29 atmospheres. Helium-3 could be introduced into the gap through a 2×10^{-1}-mm i.d. capillary. The inductance of the tank circuit consisted of a coil of copper wire soldered directly on top of the capacitor and shielded from external pickup by a thin copper cylinder connected to the ground side of the capacitor. The tank circuit was thermally connected via 500 No. 34 copper wires to the paramagnetic salt pill made up of about 30 g of freshly grown chromium methylammonium sulphate mixed with Apiezon oil J. The salt was adiabatically demagnetized from a field of about 12 kilogauss at about 0.45°K, and the lowest temperatures reached were about 0.035°K. The temperature was measured by two 470-ohm Speer carbon resistors, the first soldered to the tank circuit, the other embedded in the salt pill. These resistors were calibrated in each series of experiments against the susceptibility of the chrome alum, which in turn had been directly measured against that of cerium magnesium nitrate down to 0.06°K in a different apparatus. The temperatures below 0.06°K were determined by extrapolation of the calibration curve of the carbon resistors. While the temperature should be known to within 6% down to 0.07°K, the systematic error may increase to about 15% at the lowest temperatures.

The tank circuit was part of a Franklin oscillator[3] and the frequency was measured by a Hewlett Packard 524 B Electronic Counter. The resonance frequency of the tank circuit was about 31 Mc/sec and was stable within 5 cycles over periods of an hour. The power input into the tank circuit was so small that it did not affect the warming up of the sample even at the lowest temperatures. The change in frequency between 0.045°K and 1.2°K due to the change in density of liquid helium-3 at constant pressure was only of the order of 4 kc/sec, and hence during the experiments, the pressure had to be held very constant, as a change in pressure of 0.1% produced a frequency shift in the tank circuit of the order of 30 cps. During

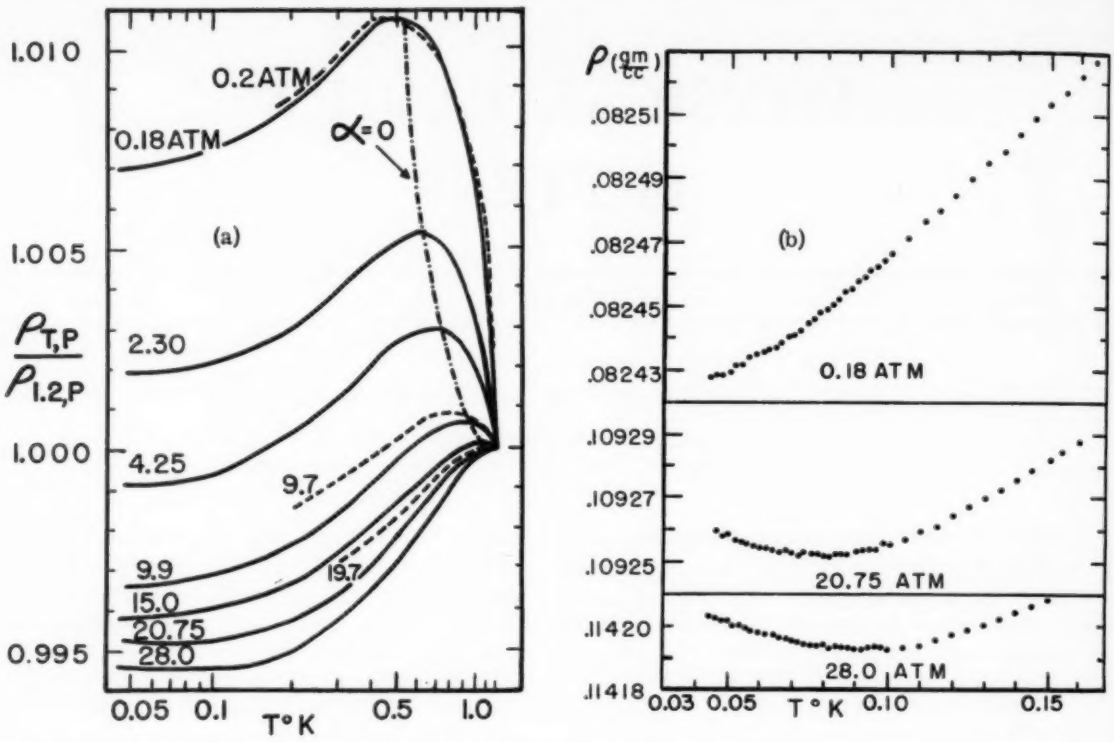

FIG. 1. (a) Density of helium-3 normalized to its value at 1.2°K for several pressures. --- Data of Lee, Fairbank, and Walker. (b) Some density curves of liquid helium-3 below 0.15°K.

each series of experiments, the frequency of the empty tank circuit was first measured over the whole temperature range. At several temperatures above 1°K the density of liquid helium-3, obtained in arbitrary units, was normalized to the accurate density values obtained by Sherman and Edeskuty[4] and the results were found to be very consistent.

Our results are shown in Fig. 1(a), where for convenience we have plotted the ratio $\rho(T,P)/\rho(1.2,P)$, where $\rho(1.2,P)$ is the density at 1.200°K and at the pressure P as found by Sherman and Edeskuty.[4] Our density results, extrapolated to zero pressure, agree satisfactorily with those of Kerr and Taylor[5] and are somewhat different from those of Lee, Fairbank, and Walker.[2] As can be seen from Fig. 1(a) and especially Fig. 1(b), the density at pressures above about 15 atm and at temperatures below 0.1°K passes through a minimum, the temperature of this minimum increasing with pressure. Several experiments were carried out to check this effect and gave reproducible results. The coefficient of expansion $\alpha_p = (1/V)(\partial V/\partial T)_p$ as derived from the ρ values is plotted in Fig. 2 for a few pressures. In the region below 0.08°K, we found $\alpha_{0.18\,\mathrm{atm}} = -(0.12 \pm 0.02)T$ in qualitative agreement with Brueckner's theory[1] which predicts $\alpha_p = -0.076T$. The figure also suggests that the density minimum

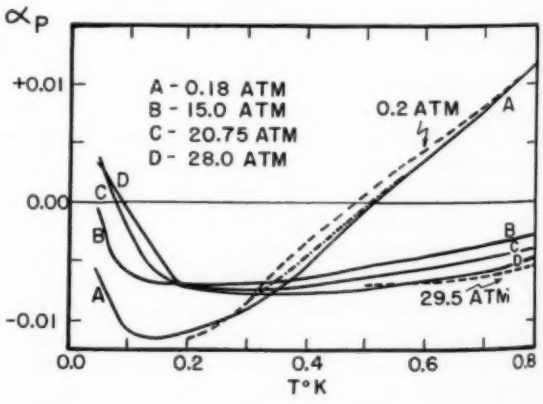

FIG. 2. The expansion coefficient of liquid helium-3 for some pressures. --- Data of Lee, Fairbank, and Walker; -·-·- data of Kerr and Taylor.

may be found for pressures below 15 atm at temperatures below 0.045°K. As a consequence, below 0.09°K, the entropy of isothermal compression ΔS, where

$$\Delta S = S_P - S_{svp} = -\int_{svp}^{P} V\alpha_p dp,$$

will pass through a maximum. Here S_{svp} is the entropy at saturated vapor pressure and V is the molar volume.

The quantitative value of ΔS as obtained from our density measurements can be checked by specific heat measurements at various pressures. At temperatures above 0.3°K, the agreement with ΔS as calculated by Brewer and Daunt[6] is very satisfactory. On the other hand, there are some systematic differences between our curves and those calculated from the earlier density measurements of Lee, Fairbank, and Walker.[2] It may be mentioned that no discontinuity of α_p, characteristic of a second order transition to another phase, such as predicted by Emery and Sessler[7] and by Brueckner et al.[8] for liquid helium-3, was found in these experiments over the whole temperature and pressure range. Previous specific heat measurements[9] on liquid helium-3 under a pressure of 0.18 atm down to 0.008°K had already failed to show this transition.

The temperature at which the maximum of density occurred for a given pressure agreed very well with the results of Brewer and Daunt[6] up to about 15 atmospheres and at higher pressures agreed better with those of Sherman and Edeskuty.[4]

A new and improved apparatus is being constructed in order to extend our measurements down to 0.01°K and obtain more accurate values for α_p below 0.07°K.

The initial stages of this experiment were supervised by Dr. W. M. Fairbank, whom we wish to thank for his valuable advice. We also acknowledge the help of Mr. C. Boghosian in some experiments. We also thank Dr. N. Kurti, Dr. H. London, and Dr. D. M. Lee for helpful discussions.

*This work has been supported by the National Science Foundation, the Alfred P. Sloan Foundation and the Office of Ordnance Research.

†Alfred P. Sloan Fellow.

[1]K. A. Brueckner, Helium-Three, edited by J. G. Daunt (Ohio State University Press, Columbus, Ohio, 1960).

[2]D. M. Lee, H. A. Fairbank, and E. J. Walker, Phys. Rev. 121, 1258 (1961).

[3]W. A. Edson, Vacuum Tube Oscillators (John Wiley & Sons, Inc., New York, 1953), p. 158.

[4]R. H. Sherman and F. J. Edeskuty, Ann. Phys. 9, 522 (1960).

[5]E. C. Kerr and R. D. Taylor, Proceedings of the International Conference on Low-Temperature Physics, Toronto, 1960 (University of Toronto Press, Toronto, 1960), p. 605.

[6]D. F. Brewer and J. G. Daunt, Phys. Rev. 115, 843 (1959).

[7]V. J. Emery and A. M. Sessler, Phys. Rev. 119, 43 (1960).

[8]K. A. Brueckner, T. Soda, P. W. Anderson, and P. Morel, Phys. Rev. 118, 1442 (1960).

[9]A. C. Anderson, G. L. Salinger, W. A. Steyert, and J. C. Wheatley, Phys. Rev. Letters 6, 331 (1961).

SELF-DIFFUSION COEFFICIENT AND NUCLEAR SUSCEPTIBILITY OF LIQUID HELIUM-THREE*

A. C. Anderson, W. Reese, R. J. Sarwinski, and J. C. Wheatley†
Department of Physics, University of Illinois, Urbana, Illinois
(Received August 14, 1961)

Recent measurements of the specific heat[1,2] and the thermal conductivity[3] of liquid He^3 at low pressures have demonstrated, for temperatures less than approximately 0.04°K, the temperature dependences predicted by the Fermi liquid theory of Landau[4] and Abrikosov and Khalatnikov.[5] However, the magnetization self-diffusion coefficient measured using the spin-echo method by Anderson, Hart, and Wheatley[6] (AHW) obeyed a $T^{-3/2}$ temperature dependence down to 0.03°K in contradiction with the T^{-2} dependence predicted by Hone[7] on the basis of the Fermi liquid theory. As pointed out by AHW, their experiment was susceptible to error, particularly at the lowest temperatures, because of long equilibrium times and difficulties with thermometry. Consequently, the experiment was repeated under much improved conditions and extended to lower temperatures. We now find the diffusion coefficient to be proportional to T^{-2} below 0.04°K - 0.05°K. The nuclear susceptibility is constant below 0.1°K and equal to the value previously measured (AHW) within experimental accuracy. The lowest temperature of these measurements was 0.02°K. The measurements were carried out at a pressure of 12 cm Hg.

The cell containing the He^3 was made from Epibond 100A,[8] and the plug which closed the cell was sealed with Epibond 121.[8] Both resins are nonmagnetic.[9] The space containing He^3 consisted of a cylinder 1.2 cm high and 1.2 cm in diameter with a coaxial cylindrical tail 5.1 cm long and 0.25 cm in diameter. The inside surface of the cell was lined with 400, 0.004-inch diameter, 99.999% pure annealed copper wires about half of which did not extend into the tail. The larger cylinder contained 1.29 g of powdered cerium magnesium nitrate (CMN) which served as a thermometer. The CMN was prevented from entering the tail by a cotton plug. The He^3 was introduced into the cell by a 1/64-in. o.d. by 0.003-in. wall 70-30 cupro-nickel tube which had a negligible magnetic effect.[9] A pi-wound, 3000-turn pickup coil of 0.002-in. diameter manganin wire was placed over 2.0 cm of the tail at the greatest possible distance from the CMN. The above construction gave internal equilibrium times of 15 minutes or less at the lowest temperatures while providing sufficient separation between the He^3 being measured and the CMN to give a negligible temperature-dependent magnetic gradient. The He^3 was cooled by 37.8 g of potassium chrome alum using techniques described elsewhere.[10]

The thermometer was calibrated in the temperature range of 1°K to 0.3°K using a 470-ohm Speer resistor which previously had been calibrated in this temperature range with a CMN magnetic thermometer. The accuracy of the temperature scale is estimated to be 2%.

The He^3 used had a He^4 content of less than 3 parts in 10^8 and a tritium decay rate of less than 900 disintegrations/sec. The apparatus outside the cryostat and the method used to obtain the echoes were similar to those described elsewhere.[11]

The self-diffusion coefficient, D, was measured by the method of spin echoes using an rf field of frequency 85 kc/sec and of amplitude $(2H_1)$ 0.6 gauss measured using a nutation technique. A 90°-180°-180° pulse sequence was used with a fixed time delay between the 90° pulse and the first 180° pulse and a variable time, τ, between the two echoes. The resulting echoes were displayed on an oscilloscope and photographed. The ratio, R, of the amplitudes of the two echoes is given by $R = \exp(-\gamma^2 G^2 D\tau^3/12 - \tau/T_2)$, where G is the magnetic field gradient, $\gamma = 2.038\times10^4$ (gauss-sec)$^{-1}$, and T_2 is the transverse relaxation time. The self-diffusion coefficient was calculated neglecting the effect of T_2, which had been found to be greater than 0.74 sec near $T = 0.03$°K.[6] Measurements of D were made with G alternately parallel and antiparallel to the steady field so as to eliminate to first order the effects of residual gradients.

The susceptibility was measured with the same apparatus but with no applied gradient and with only one 180° pulse applied between 2.5 and 5 msec after the 90° pulse. No systematic effect of the time of the echo on the echo height was observed, even at the lowest temperatures. In order to increase the echo height, the He^3 was magnetized in a field of about 100 gauss which was turned off just before the pulse train was initiated. This field remained the same throughout the experiment. The gain of the amplifiers was measured at each point and the echo heights were corrected to constant gain. With the above conditions, the echo height, corrected for gain,

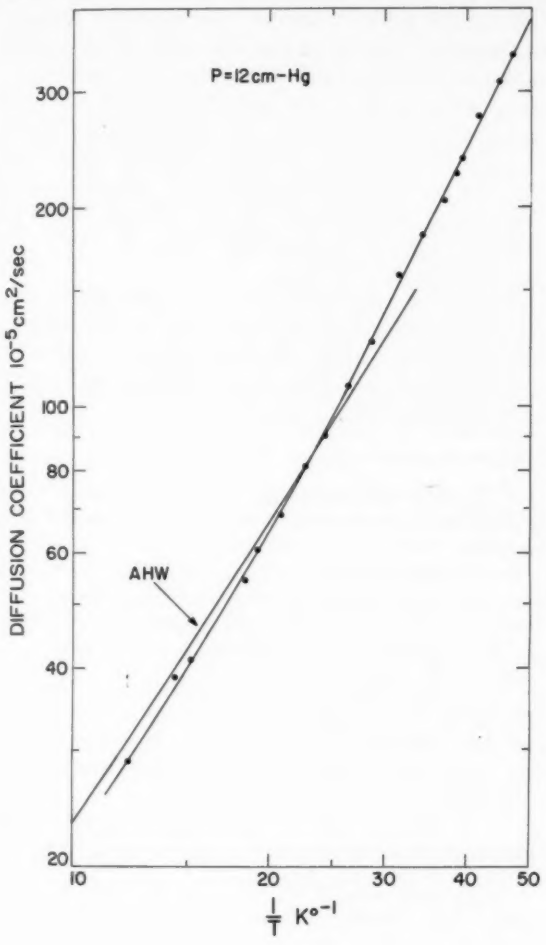

FIG. 1. Self-diffusion coefficient, D, vs $1/T$. The points represent averaged data. The curve has a slope of 2.00 ± 0.02 for T less than 0.04°K. The curve labeled AHW is the smoothed curve from reference 6.

should be proportional to the nuclear susceptibility.

The results of the diffusion measurements are shown in Fig. 1. For T less than 0.04°K to 0.05°K we find that $D = 1.54 \times 10^{-6} T^{-2}$ cm^2 °K^2/sec. The exponent of T in this temperature range is 2 with an estimated accuracy of 1%. The coefficient of D has an estimated accuracy of 7% on the basis of uncertainties in the temperature, time scale, and gradient. At higher temperatures the results are almost parallel to those of AHW but displaced about 5% toward lower T. Their low-temperature points lie below ours, giving a slower temperature dependence than that observed by us. The temperatures used by AHW were made uncertain, especially at the low-temperature end, by the presence of spurious magnetic materials. Moreover, their equilibrium times were several hours at the lowest temperatures, indicating that very small spurious heat inputs could adversely affect the results.

In Fig. 2 we have plotted $(\chi T)_{1.153°K}/\chi$ vs $1/T$, where the numerator is the product of the echo height at the bath temperature, the bath temperature (1.153°K), and the ratio of the density of the liquid at 0°K to that at 1.153°K as estimated from the data of Lee, Fairbank, and Walker[12]; and where the denominator is the echo height at the value of $1/T$ given on the abscissa. If it is assumed that He^3 obeys Curie's law at the bath temperature, then the ratio $(\chi T)_{1.153°K}/\chi$ is the effective magnetic temperature, T^*, of the He^3 at low temperatures. Below 0.1°K we find T^* to be constant within experimental accuracy. The average of the data for run 4, which is the best run for this purpose since the check at the bath temperature was made at its conclusion, gives $T^* = 0.347 \pm 0.010$°K for T less than 0.1°K, exactly

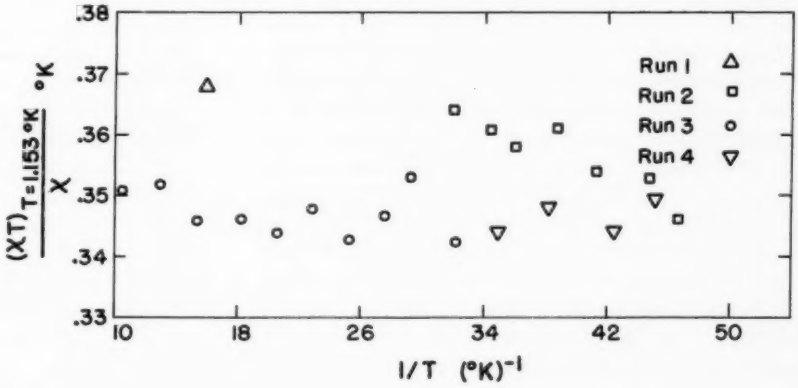

FIG. 2. Effective magnetic temperature $T^* = (\chi T)_{1.153°K}/\chi$ vs $1/T$. $(\chi T)_{1.153°K}$ is the product of the susceptibility and temperature at 1.153°K. χ is the susceptibility at temperature T. The points within each temperature interval represent averages for each run.

the result given by AHW. Within each run we found χ to be constant to within about 2%, so it is likely that χ is more nearly constant than is indicated by all the data collected in Fig. 2, for which there is about 5% scatter. The slight drop in χ below 0.05°K observed by AHW and attributed to experimental effects was not observed in these measurements.

The susceptibility can be written [Eq. (5.8), reference 5]

$$\chi = \frac{\beta^2 \quad (\partial\tau/\partial\epsilon)_\mu}{4\left[1+\frac{1}{4}\bar{\zeta}(\partial\tau/\partial\epsilon)_\mu\right]} = \frac{\beta^2 \quad N}{4\ VkT^*}, \tag{1}$$

an equation which defines T^*. In this equation N/V is the number of He^3 atoms per unit volume, $\beta=\gamma\hbar$ is the product of the gyromagnetic ratio and Planck's constant divided by 2π, k is Boltzmann's constant, $(\partial\tau/\partial\epsilon)_\mu$ is the density of states at the Fermi surface, and $\bar{\zeta}$ is the average of the effective spin interaction function over the Fermi surface. Using the most recent empirical values for the molar volume[12,13] and effective mass,[2] the value of T^* given above leads to $[1+\frac{1}{4}\bar{\zeta}(\partial\tau/\partial\epsilon)_\mu]=0.293$.

Hone[7] writes the diffusion coefficient in the form

$$D=\tfrac{1}{3}V_0^2\tau_D\left[1+\tfrac{1}{4}\bar{\zeta}(\partial\tau/\partial\epsilon)_\mu\right], \tag{2}$$

where $V_0=P_0/m^*$ is the quasi-particle velocity at the Fermi surface, τ_D is a relaxation time for diffusion, and the quantity in square brackets is given above. The resulting empirical value of τ_D is $4.6\times10^{-13}T^{-2}$ sec °K². If one uses in addition to the above information the most recent value for the speed of sound[14] to estimate[7] the value of τ_D from the Fermi liquid theory, one obtains $\tau_D = 1.0\times10^{-13}\,°T^{-2}$ sec °K². A relaxation time can also be computed from the measured values of thermal conductivity[3] in the Fermi liquid region giving $\tau_K = 6.4\times10^{-13}\ T^{-2}$ sec °K². If there were no dependence of the quasi-particle scattering probability on the azimuthal angle of scattering and in addition no spin effects, then by theory[5,7] one has $\tau_D/\tau_K=\frac{3}{5}$; experimentally we observe $\tau_D/\tau_K=0.70$.

Using the above values of the relaxation times, one finds in both cases that the ratio of the uncertainty in quasi-particle energy to kT is less than 1 at 0.04°K: $\hbar/kT\tau=0.5$ and 0.7 using τ_K and τ_D, respectively. Moreover, since the specific heat, thermal conductivity, and self-diffusion coefficient all have the predicted temperature dependences below 0.04°K, we conclude that the concept of He^3 as a Fermi liquid at temperatures less than this and at low pressures is valid.

We wish to acknowledge helpful discussions with Professor John Bardeen and D. Hone. We would like to thank William Abel for his expert assistance in constructing apparatus and for his help in making the measurements.

---

*This work has been supported by the Alfred P. Sloan Foundation and the U. S. Atomic Energy Commission.

†A. P. Sloan Fellow.

[1]A. C. Anderson, G. L. Salinger, W. A. Steyert, and J. C. Wheatley, Phys. Rev. Letters 6, 331 (1961).

[2]A. C. Anderson, G. L. Salinger, W. A. Steyert, and J. C. Wheatley (to be published).

[3]A. C. Anderson, G. L. Salinger, and J. C. Wheatley, Phys. Rev. Letters 6, 443 (1961).

[4]L. D. Landau, J. Exptl. Theoret. Phys. (U.S.S.R.) 30, 1058 (1956) [translation: Soviet Phys.—JETP 3, 920 (1959)].

[5]A. A. Abrikosov and I. M. Khalatnikov, Reports on Progress in Physics (The Physical Society, London, 1959), Vol. 32, p. 329.

[6]A. C. Anderson, H. R. Hart, and J. C. Wheatley, Phys. Rev. Letters 5, 133 (1960).

[7]D. Hone, Phys. Rev. 121, 669 (1961).

[8]Furane Plastics, Inc., 4516 Brazil Street, Los Angeles 39, California.

[9]G. L. Salinger and J. C. Wheatley (to be published).

[10]A. C. Anderson, G. L. Salinger, and J. C. Wheatley (to be published).

[11]H. R. Hart and J. C. Wheatley, Phys. Rev. Letters 4, 3 (1960).

[12]D. M. Lee, H. A. Fairbank, and E. J. Walker, Phys. Rev. 121, 1258 (1961).

[13]R. H. Sherman and F. J. Edeskuty, Ann. Phys. 9, 522 (1960).

[14]H. L. Laquer, S. G. Sydoriak, and T. R. Roberts, Phys. Rev. 113, 417 (1959).

OBSERVATIONS OF IONIC SOUND WAVES IN PLASMAS

I. Alexeff and R. V. Neidigh
Oak Ridge National Laboratory, Oak Ridge, Tennessee
(Received July 17, 1961; revised manuscript received August 31, 1961)

The object of this Letter is to report the observation of ionic sound waves in a typical discharge-tube kind of plasma, and also in a plasma restricted by the presence of a magnetic field. Earlier, partial reports of these experiments have been given local distribution.[1-3] The earliest work in this field is thought to be the prediction of ionic sound waves in plasmas by Tonks and Langmuir in 1929.[4] The fundamental frequency and first and second overtones were found in a mercury vapor discharge confined in a spherical tube by Revans in 1933.[5] He also showed evidence for radial standing waves in a cylindrical tube. Data from the recent discharge-tube experiments of Crawford[6] have been analyzed by this laboratory[1] and by Moore[7] and shown apparently to exhibit ionic sound waves. Additional work by Crawford[8] confirms this analysis.

The theory of propagation of ionic sound waves is much like that of ordinary sound waves. The velocity v of an ionic sound wave is related to the electron temperature T_e and the ion mass m_i by the expression

$$v = (\gamma k T_e / m_i)^{1/2}.$$

Here k is Boltzmann's constant and γ is the adiabatic compression coefficient which is $\frac{5}{3}$ for ordinary sound waves and may be as high as 3 in rare plasmas.[9]

If the plasma is restricted to a long cylindrical column by a magnetic field and the sound wave is reflected similarly at each end, standing ionic sound waves may result as ordinary sound waves do in an open organ pipe. Then the fundamental frequency should be $v/2L$, where L is the length of the column, and the harmonics should be integral multiples of the fundamental.

If the plasma is confined by a spherical discharge tube without a magnetic field, the frequency of the fundamental is v/CD, where D is the sphere diameter, and C is a constant that can be 1.51 or 1.0 depending on the plasma boundary conditions. Higher frequency modes of oscillation should occur, but their frequency also depends on the boundary conditions. For a pressure antinode at the wall ($C = 1.51$), the frequency ratios for the first six overtones to the fundamental are 1.61, 2.16, 2.17, 2.71, 2.85, 3.25.

A schematic diagram of the apparatus which produced the cylindrical plasma column is shown in Fig. 1 (inset). The plasma column was produced by a $\frac{1}{4}$-inch diameter electron stream (up to one ampere) from a negatively biased (up to -120 volts) hot filament. The magnetic field could be varied from 1000 to 7000 oersteds. The frequency as observed on a wire probing the column was found to be grossly independent of the magnetic field and the filament bias. It did not depend on background gas pressure which was uniform over the length of the column and in the range 10^{-4} to 10^{-3} mm Hg. The filament temperature had the most effect on the frequency which could be "pulled" slightly but which would change discontinuously to a higher mode if "pulled" too far. The amplitude of the probe signal varied considerably (more than 20 volts) with change in the above parameters. Sinusoidal frequencies were observed up to the fifth harmonic. At times the wave shape gave evidence of higher harmonics present with the fundamental.

The observed variation of frequency with ion mass for two lengths of plasma column is shown in Fig. 1. The solid lines are the theoretical curves for a γ of 3, and an electron temperature of 17 ev, the average of the first excitation potential of the inert gases. Electron temperature measurements made with a Langmuir probe were within a factor of two of this value. Obtaining reliable probe characteristic curves proved to be very difficult under the conditions of operation. In general, gases whose first excitation potential was greater than 17 ev supported standing waves with frequencies higher than predicted, and lower excitation potentials resulted in correspondingly lower frequencies.

For a convincing proof of the existence of these waves it was felt that they should be exhibited in a different system, one not using a magnetic field. After preliminary experiments, a spherical glass discharge tube was chosen instead of the usual cylindrical type. It was thought that the lowest mode of oscillation in a sphere might be less damped, as this mode involves no transport of matter parallel to the wall. The diagram of the sphere is shown schematically in Fig. 2 (inset). The sphere is glass with a hot cathode of tungsten wire and a metal disk as an anode. Both are flush

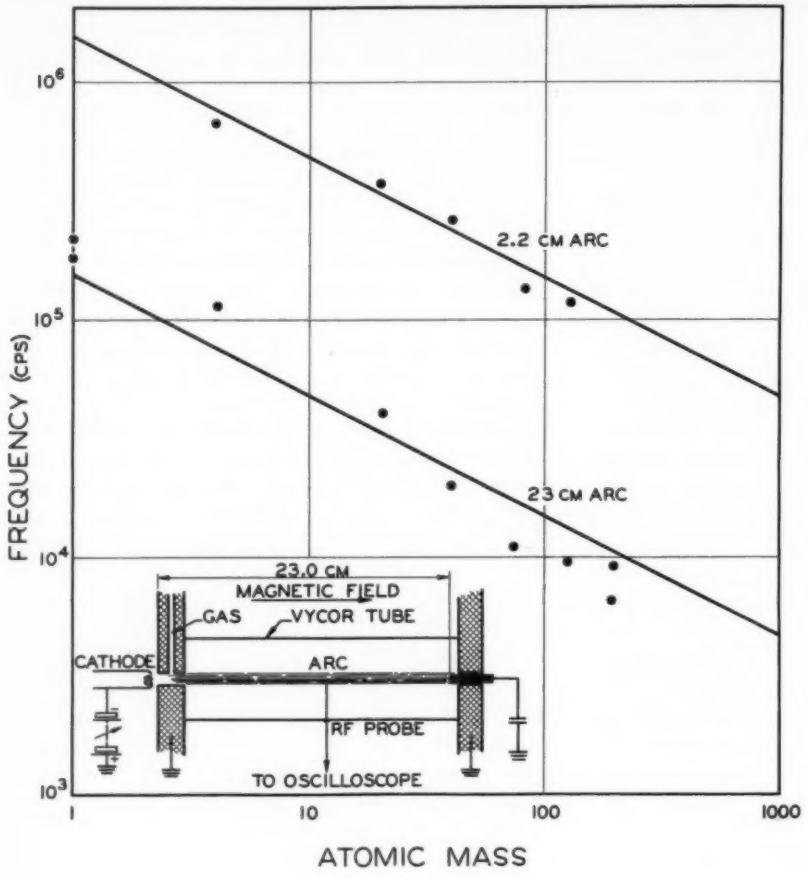

FIG. 1. Frequency vs atomic mass for two lengths of plasma column. The inset is a schematic diagram of the 23-cm arc. The 2.2-cm arc was excited in the same manner.

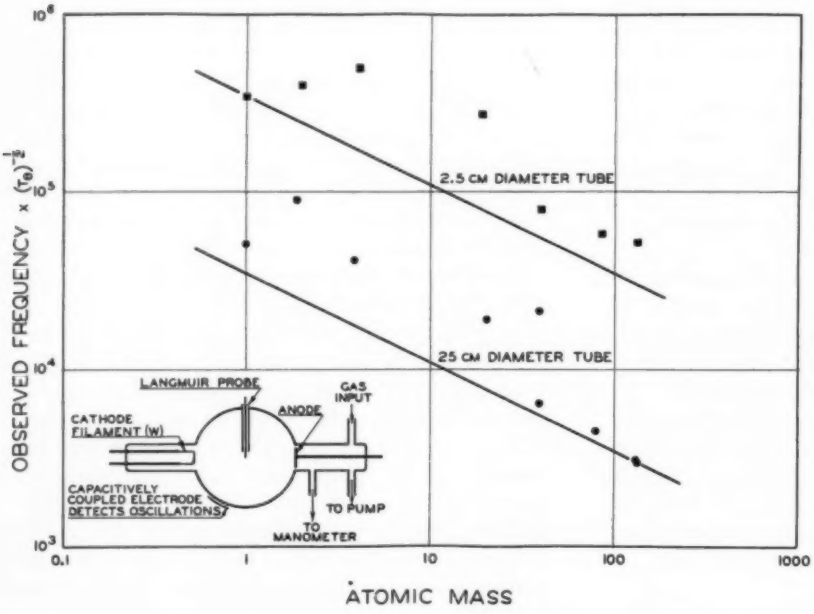

FIG. 2. Frequency vs atomic mass for two diameters of spheres. The inset is a schematic diagram of the sphere geometry. Electrode sizes were proportional to sphere diameter in each size sphere.

Table I. Ratios of frequencies observed to the fundamental for the different gases used. The calculated ratios are given in the left-hand column. The lowest frequency observed for helium, neon, and argon was thought to be the first overtone since this provided a better fit of the data.

$C=1.51$	Hydrogen	Helium	Neon	Argon	Krypton	Xenon
1	1				1	1
1.61	1.46	1.61	1.61	1.61	1.75	1.57
2.16			1.93		2.00	2.16
2.17		2.30	2.22	2.20		
2.71		2.72			2.59	2.63
2.85						
3.25			3.43			

with the wall and on opposite ends of a diameter. A Langmuir probe in the center was used to measure the electron temperature. Oscillations were detected by means of a capacitively coupled electrode outside of the sphere. Pressures of about 10^{-2} mm Hg and currents of 100 ma resulted in oscillation amplitudes of about one volt in the detection circuit. Varying the discharge parameters caused the oscillation frequency to change discontinuously to the higher frequency modes. The lowest frequency mode that was thought to correspond to the fundamental of the sphere was very difficult and sometimes impossible to excite. Probably some asymmetry in the sphere preferentially excited higher frequencies, and the high gas pressure needed to maintain the discharge in the sphere preferentially damped the lower frequencies.

In analogy with the plasma column work the lowest frequency observed in plasmas of different atomic mass and for spheres of 2.5 and 25 cm in diameter are plotted in Fig. 2. As the measured electron temperature now varied widely, all frequencies were normalized to an electron temperature of 1 ev. The solid lines represent the lines of slope $(-\frac{1}{2})$ which pass through the lowest observed frequency for both sphere diameters. Assuming that the lines pass through the fundamental frequencies, $\gamma=\frac{5}{3}$ and $C=1.51$. The value $\gamma=\frac{5}{3}$ is reasonable for the spheres in view of the high gas pressure in the discharge. In general the frequency is seen to be proportional to $(D)^{-1}$ and $(m_i)^{-1/2}$. Apparently the fundamental was not excited in some of the gases.

As many as four different frequencies have been observed for one gas. Classification is difficult because the fundamental might not have been excited and the frequency on an overtone may be altered by possible changes in the boundary conditions. An attempt at classification appears in Table I.

Another complication in working with ionic sound waves in discharge tubes appears if the pressure is too high. At about 1 mm Hg strong oscillations appear which are lower in frequency than the fundamental of the ionic sound waves. These frequencies apparently correspond to ordinary sound waves in the residual gas.

The authors gratefully acknowledge the suggestions, impetus, and continued support given the program by A. H. Snell and E. D. Shipley and the valuable discussions with many others of the Thermonuclear Division staff.

---

[1]I. Alexeff and R. V. Neidigh, Oak Ridge National Laboratory Report ORNL-CF-61-2-57, 1961 (unpublished); I. Alexeff and R. V. Neidigh, Thermonuclear Project Semiannual Report ORNL-3104, 1961 (unpublished), pp. 31-40.

[2]Igor Alexeff, Oak Ridge National Laboratory Report ORNL-CF-61-2-57, 1961 (unpublished); Igor Alexeff, Thermonuclear Project Semiannual Report ORNL-3104, 1961 (unpublished), pp. 40-45.

[3]I. Alexeff and R. V. Neidigh, Oak Ridge National Laboratory Report ORNL-CF-61-6-66, 1961 (unpublished).

[4]L. Tonks and I. Langmuir, Phys. Rev. 33, 195 (1929).

[5]R. W. Revans, Phys. Rev. 44, 798 (1933).

[6]F. W. Crawford, Stanford University Microwave Laboratory Report ML-762, 1960 (unpublished).

[7]Reference 4, F. W. Crawford, Stanford University Microwave Laboratory Report ML-813, 1961 (unpublished).

[8]F. W. Crawford, Phys. Rev. Letters 6, 663 (1961).

[9]Lyman Spitzer, Jr., Physics of Fully Ionized Gases (Interscience Publishers, New York, 1956), pp. 13, 59.

SUPERCONDUCTING-NORMAL TRANSITION TIME

A. H. Nethercot, Jr.

Thomas J. Watson Research Center, International Business Machines Corporation, Yorktown Heights, New York

(Received August 9, 1961)

The nonequilibrium properties of superconductors are of particular interest since these properties cannot be calculated directly from the standard Bardeen-Cooper-Schrieffer (BCS) theory. One such problem is the calculation of the speed at which transitions can occur between the normal and superconducting states when the magnetic field is varied. Since the theory does not clearly indicate what fundamental effects might limit this speed, a number of possible explanations have been suggested between which it is difficult to choose (see Appendix). It is the purpose of this Letter to propose a new explanation which proceeds in a relatively direct and straightforward fashion from the BCS theory and which, since it predicts a rather long time, overrides many of the previous suggestions.

In brief, the present explanation is that the switching speed is limited by a spatial rather than by a purely temporal effect: At fast switching speeds and therefore at high frequencies the skin depth becomes so small that this thin layer is prevented from changing its state by the presence of the large amounts of unswitched adjacent material. As will be described below, it appears from present theories[1,2] that skin depths corresponding to switching speeds of 10^{-10} sec are so thin that their properties are severely altered by the presence of the adjacent unswitched material. Hence these skin depths cannot be said to change their state sufficiently to define switching in times on the order of 10^{-10} sec.

The predictions of this theory are in accord with the presently known experimental facts. It is known from experiments with pulses that superconductors do switch in at least several millimicroseconds. However, experiments[3,4] on the nonlinear properties of superconducting tin at 10 000 Mc/sec indicate that switching is only very incomplete or partial in times on the order of 2×10^{-11} sec. Thus the switching time is bracketed between 10^{-9} and 10^{-11} sec. In these 10 000-Mc/sec experiments, the amount of second harmonic power generated when a high-amplitude rf magnetic field is incident against a bulk or thin film superconductor is compared with the harmonic power calculated under the assumption that there is an instantaneous change in the microwave surface impedance from its normal state value to its superconducting value when the field changes from above critical to below critical during a cycle. Distortion of the reflected wave is observed only when the rf field crosses the critical field curve during a cycle. The amount of this distortion is less than one percent of that calculated. This indicates that there is only a partial change in state. In addition, below 3.2°K harmonics are observed only if the bias field, H_0, is greater than H_C, indicating that at low temperatures switching from superconducting to normal is much more difficult than switching from normal to superconducting. Also, the amount of harmonics observed from thin films decreases very rapidly as the films become thinner than 2500 A. Thus, such films do not switch as readily as bulk materials, at least when the switching field is applied to only one side of the film.

The theoretical situation can be discussed from either the point of view of Parmenter[1] or that of Cooper.[2] The former shows that for superconducting-normal-superconducting (*S-N-S*) or *N-S-N* sandwiches there exists a critical distance, $2X_C$, for the central portion. For tin $2X_C \approx 1500$ A for both the *S-N-S* and *N-S-N* sandwiches. For thicknesses, d, smaller than $2X_C$ the central region shows the general properties only of the adjacent material, while for thicknesses, d, greater than $2X_C$ the central region displays its own properties (but if it is superconducting it has a reduced energy gap even if $d > 2X_C$). We will discuss first the case in which a bias field, H_0, is applied to a semi-infinite bulk superconductor, where $H_0 > H_C$. An additional microwave field, H_{rf}, of large amplitude is also applied to the surface. The effect of this field is to tend to restore the skin depth to the superconducting state during one-half of the cycle. Therefore we wish to consider a thin layer one skin depth thick of superconducting metal in contact with a bulk normal metal (if 0 denotes empty space, an *N-S-0* sandwich). Although the *N-S-0* sandwich is not treated by Parmenter, it would be expected that the central region could develop a gap only if the thickness is greater than a critical length, $2X_C'$. This distance, $2X_C'$, would be expected to be somewhat less than $2X_C$ since the presence of N material on only one side rather than on both would be less effective in preventing formation of the gap. A rough estimate

leads to a value for $2X_c'$ of $0.8(2X_c)$ or 1200 A for the N-S-0 sandwich. If the thickness is only slightly greater than $2X_c'$, the average gap in the central region is $\approx 1/30$ bulk gap.[1] Any gap, no matter how small, suffices to define the superconducting state for the dc currents. However, at high frequencies and $T > 0$, the gap, ΔE, must be greater than a certain amount for some property such as the microwave surface resistance to decrease by a factor of 2 from its normal state value. From inspection of data on the microwave surface resistance versus temperature, this decrease of a factor 2 is seen to occur when $kT \approx \Delta E$. If we consider the temperature range from 3.7 to 2.5°K, it follows that the gap must be less than the bulk gap only by a factor five (rather than by a factor thirty) for this given decrease in surface resistance to occur. This large a gap will occur only at distances rather greater than $2X_c'$, estimated to be 3 to $4X_c'$. Thus the normal skin depth (δ_N) must be greater than 2000 A if this depth is to be able to change its state from N to S. The skin depth becomes approximately 2000 A at $\nu \approx 3\times10^9$ cps, and hence it is predicted that switching cannot occur when the field is changed from greater than critical to less than critical in times shorter than $\tau = 1/2\pi\nu \approx 0.5\times10^{-10}$ sec.

It is predicted that switching from the S to N state is even slower than the above. When $H_0 < H_c$, the penetration of the field is governed by the superconducting skin depth, δ_S. Hence, at the lower temperatures where $\delta_S \approx \lambda$, switching will be extremely difficult since λ (the penetration depth) is only 500 A. This is in agreement with experiment[4] since no nonlinear effects are seen in tin at 10 000 Mc/sec if $H_0 < H_c$ and $T < 3.2°$. It might be objected that this approach leads at low temperatures to a frequency-independent limitation on switching. However, at sufficiently low frequencies new effects can occur such as motion of S-N boundaries and nucleation and growth of new sites. These effects will then allow switching to take place.

In the above, the S-N-0 case has been differentiated from the N-S-0 case with the important parameters being δ_S and δ_N, respectively. If switching is complete, the spatial variation in both N and S material should be included in some complex manner. However, as a first approximation, a high enough frequency can be chosen that switching is only partial and hence only one skin depth is important.

The above treatment can also be carried through on the basis of Cooper's theory.[2] This theory does not give a critical distance below which the gap completely disappears in a superconducting layer, but instead the gap decreases in size indefinitely as the layer becomes thinner. Adopting again the criterion that the gap cannot be less than one-fifth of its bulk value (to establish a change of a factor two in the microwave surface resistance) and discussing the case $H_0 > H_c$ (the N-S-0 sandwich), we find from Eqs. (1) and (3) of reference 2 that

$$\exp[-N(0)Vt_N/t_S] = \tfrac{1}{5},$$

where t_S is the skin depth and t_N is the effective thickness of the normal material. Since $N(0)V \approx 0.30$ for tin, $t_N/t_S = \frac{1}{3}$. If a limit to $(t_N + t_S)$ is set by the bulk correlation distance ($\xi_0 = 2500$ A), we find that $t_S \geq 1700$ A and that the switching time, τ, is longer than 0.3×10^{-10} sec. This value is in reasonable agreement with the 0.5×10^{-10} sec from Parmenter's theory. However, it appears that this value may be too short since, from the uncertainty principle, the correlation distance for reasonably pure bulk materials must be inversely proportional to the energy gap. If the modified gap is $\frac{1}{3}$ its bulk value, the correlation distance is 12 000 A and this leads to a switching speed of 3×10^{-9} sec, a very slow speed. Cooper's theory needs more development to clarify which correlation distance is involved.

The theory of Cooper is particularly suited for the case of thin films. If the switching field is applied to only one side of the film and if the film is thinner than the skin depth (either δ_S or δ_N), the microwave field varies approximately linearly across the film and falls to a very small value on the other side. Therefore, in general, the microwave field falls off more rapidly than it does in bulk material and at a given frequency the interaction potential $N(0)V$ is more diluted and the gap is less. Thus the degree of switching would be less in the thin film. These results for thin films are in accord with experiment[4] since nonlinear effects at $\nu = 10\,000$ Mc/sec rapidly decrease in amplitude for thicknesses less than ≈ 2500 A.

There is no experimental evidence on the case when the microwave field is applied to both sides of the thin film. If $H_0 < H_c'$, where H_c' is the thin-film critical field, the situation is very similar to the above except that the field varies even more rapidly in space. The switching should be very slow. The other case, $H_0 > H_c'$, is more difficult to treat since the fields do not vary greatly in space. However, the Gor'kov theory indicates that the transition becomes second order in the

magnetic field for the thinner films[5] and this causes a limitation on the switching. For first order transitions an infinitesimal change of H_0 from $(H_c' + \epsilon)$ to $(H_c' - \epsilon)$ causes a well-developed gap to appear and a large change in the microwave surface resistance to occur. In a second order transition a much larger change in field is necessary to produce the requisite gap. It is clearly much more difficult to produce a large change in field in a short time ($\approx 10^{-10}$ sec) than it is an infinitesimal change. The switching field should be at least several percent of the critical field to produce a gap $\frac{1}{3}$ of the bulk gap.[5] Since the critical field for thin films is very much greater than that for bulk materials, the requisite field may thus be quite appreciable. A clearer understanding of the relation between the Gor'kov and the spatial dependence theories would lead to a better understanding of these temporal effects as well as of the high-field superconductivity effects associated with filamentary behavior.

We have had informative and interesting conversations with a number of people. Discussions with R. J. von Gutfeld and R. H. Parmenter have been particularly helpful.

Appendix. Since no discussion of the various possible explanations for a limitation of the switching time has been given previously, a brief listing of some of these will be given here. The usual limitation, that of the growth of normal domains limited by eddy currents, has no relevance when skin depths small compared to the correlation distance are involved.

(I) The uncertainty relation $\Delta E \Delta t \approx \hbar$ leads to $\Delta t \approx 10^{-12}$ sec if ΔE is the energy gap. This time is too short.

(II) The correlation distance divided by the phonon velocity (ξ_0/v_s) leads to a time of about 10^{-10} sec and could be interpreted as a signaling time between correlated electrons by means of the interaction responsible for superconductivity. However, it is difficult to guess from the BCS theory whether such an effect should in principle be present and in addition the electrons are physically moving much faster than the phonons.

(III) A relaxation time such as l/v_f (where l is the electron mean free path and v_f the Fermi velocity) should come into the theory since an electron trajectory cannot be greatly altered until it is terminated. However, in the treatment of the anomalous skin effect by the ineffectiveness concept it is not always clear whether l/v_f or δ/v_f should be used.[6] The former would lead to switching times of from 10^{-9} sec to much shorter values and the latter to about 10^{-13} sec. The experimental fact that similar switching behavior is observed in situations where l should be drastically different indicates that l/v_f may not come in directly.

(IV) It has also been speculated[7] that the velocity of second sound (v_{II}) in the electron ensemble could possibly limit the rate of conversion of superconducting electrons to normal. This would lead to a time $\tau \approx \lambda/v_{II} \approx 10^{-9}$ sec if[8] $v_{II} \approx [H_c^2(1 - t^4)/2\pi\rho]^{1/2} \approx 10^4$ cm/sec. However, it is not clear that relaxation effects would allow this type of second sound to be propagated (especially in impure metals or in evaporated films) or even whether second sound of a different variety[9] and with a velocity of $\sim 10^6$ cm/sec would or would not be preferred.

---

[1]R. H. Parmenter, Phys. Rev. 118, 1173 (1960).
[2]L. N. Cooper, Phys. Rev. Letters 6, 689 (1961).
[3]A. H. Nethercot, Jr., Proceedings of the Seventh International Conference on Low-Temperature Physics (University of Toronto Press, Toronto, 1960), p. 231.
[4]A. H. Nethercot, Jr., and R. J. von Gutfeld (to be published).
[5]D. H. Douglass, Jr., Phys. Rev. Letters 7, 14 (1961), and references therein.
[6]A. B. Pippard, Advances in Electronics 6, 1 (1954), especially p. 33.
[7]J. Bardeen (private communication).
[8]See J. Bardeen and J. R. Schrieffer, in Progress in Low-Temperature Physics (North-Holland Publishing Company, Amsterdam, 1961), Vol. 3, p. 266.
[9]D. J. Thouless and D. R. Tilley, Proc. Phys. Soc. (London) 77, 1175 (1961).

TWO-PHOTON EXCITATION IN $CaF_2:Eu^{2+}$

W. Kaiser and C. G. B. Garrett
Bell Telephone Laboratories, Murray Hill, New Jersey
(Received August 28, 1961)

With the development of optical masers,[1-3] it is now possible to study two-photon processes which necessitate intense sources of monochromatic radiation. We have investigated the generation of blue fluorescent light around $\lambda_b = 4250$ A by illuminating $CaF_2:Eu^{2+}$ crystals with red light, $\lambda_r = 6943$ A, of a ruby optical maser.[2] Our experiments differ from the recent investigations by Franken et al.,[4] who observed the generation of optical harmonics in quartz. It is essential in their experiments that the crystal lacks a center of inversion and that it is transparent at ν_r and $2\nu_r$. In our investigations, the highly symmetric cubic CaF_2 structure is used and after an excitation to a real absorbing state of Eu^{2+} at $2\nu_r$, the fluorescent decay to a lower state is observed. CaF_2 crystals, with 0.1 % Eu^{2+} ions substituted for Ca^{2+}, exhibit strong absorption between 30 000 and 25 000 cm^{-1} resulting from electronic $4f \rightarrow 5d$ transitions of the Eu^{2+} ion.[5] Excitation of $CaF_2:Eu^{2+}$ with light absorbed in this wavelength range gives rise to a brilliant blue fluorescence (bandwidth ~300 A) which originates at levels around 4200 A and terminates at the ground state. There are no energy levels below 22 000 cm^{-1}, making $CaF_2:Eu^{2+}$ crystals transparent at $\nu = \nu_r$.

We have performed the following experiments. A $CaF_2:Eu^{2+}$ crystal of 1-mm thickness was mounted in front of the entrance slit of a quartz spectrometer, and the light beam of a ruby optical maser (~0.1-joule output) was focused onto the sample. Two red filters with transmission values $T < 10^{-4}$ for $\lambda < 6100$ A were mounted between the maser and the $CaF_2:Eu^{2+}$ crystal in order to eliminate the possibility that blue or ultraviolet stray radiation from the flash lamp reaches the sample. The fluorescence of the crystal was photographed at the exit slit of the spectrometer. Between the sample and the prism, a blue filter with $T \cong 10^{-3}$ at 7000 A was interposed to avoid excessive blackening of the photographic plate. In Fig. 1 a picture of the output spectrum is presented which was obtained by one flash (~500 μsec) of red light. The overexposed bright spot at 6943 A results from the incident maser light. Of particular interest is the observation of light around 4250 A, which is characteristic for the blue fluorescence of $CaF_2:Eu^{2+}$. The width of the blue streak is approximately 0.3 mm corresponding to the diameter of the incident light beam. When pure CaF_2 was illuminated by the optical maser in the same way, no light with $\lambda < \lambda_r$ was observed on the photographic plate. This observation is expected from the high symmetry of the CaF_2 lattice.

In a second experiment, the light beam leaving the quartz spectrometer was intersected by two mirrors in such a way that the red and blue parts of the spectrum were directed separately onto two photomultipliers. The signals of these photomultipliers were displayed simultaneously on a dual-beam oscilloscope. Load resistors of 10^5 ohms in the photomultiplier circuit were employed in order to smooth out the spikes (resulting from the relaxation oscillations) of the ruby optical maser and to allow a direct quantitative comparison between the two signals. In Fig. 2 the signal I_b obtained in the blue part of the spectrum is plotted against the signal in the red I_r, which is a direct measure of intensity incident on the crystal. The empirical line through our experimental points represents the quadratic relation $I_b \propto I_r^2$, which is a strong indication that we are dealing with a two-photon process. From the calibration of our photomultiplier, the number of blue photons at the exit slit of the spectrometer could be estimated to be 5×10^7 photons per flash. This number agrees well with the value of ~10^8 photons per flash estimated from the blackening of the photographic plate shown in Fig. 1.

We believe that in our experiments a real state of the Eu^{2+} ion at $\nu = 2\nu_r$ is excited by a two-photon process. The observed fluorescence is only an indication that the ion was indeed in the excited state. The probability of a process by which an atom is excited by two photons $h\nu_1$ and $h\nu_2$, the sum of which corresponds to an excited state of the atom, was first treated by Goeppert-Mayer in

FIG. 1. Positive of photographic plate, indicating the blue emission of a $CaF_2:Eu^{2+}$ crystal under strong illumination with $\lambda_r = 6943$ A.

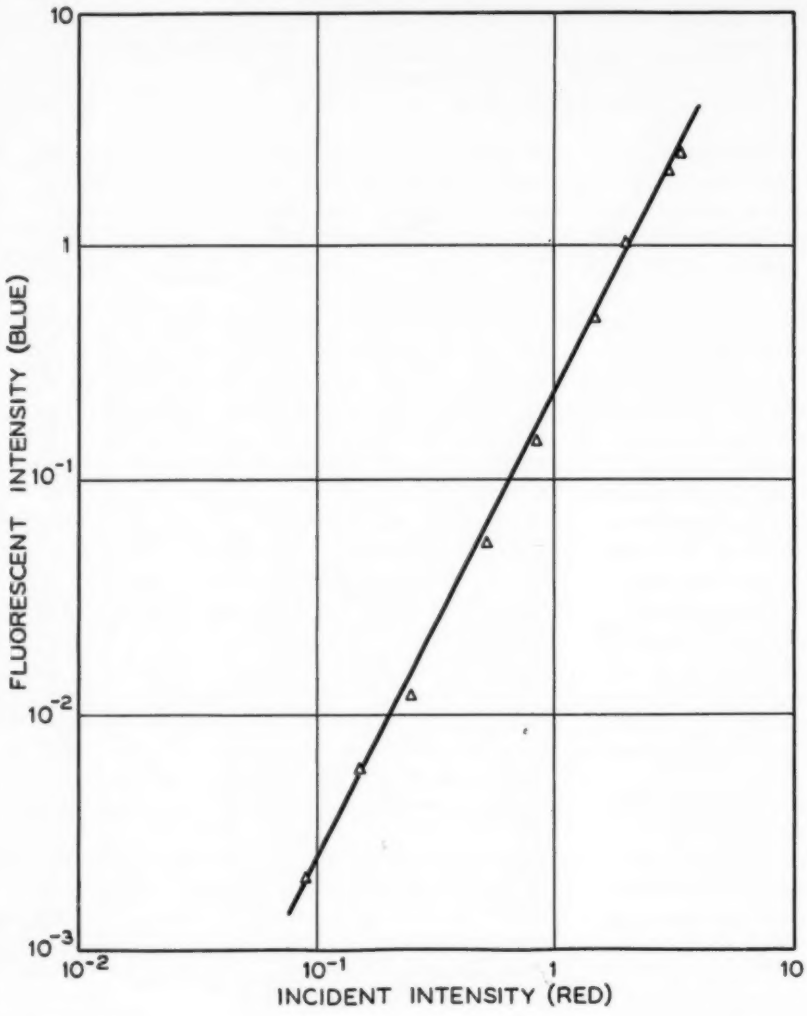

FIG. 2. Blue fluorescent intensity of sample versus incident red intensity.

1931.[6] More recently Kleinman[7] has reinvestigated the problem and has derived an equation for the cross section σ for such a two-photon excitation process which allows a direct quantitative estimate of the expected number of blue photons:

$$\sigma = (e^2/mc^2)^2(\lambda_\gamma{}^2/n^2\Delta\nu)F, \qquad (1)$$

where $e^2/mc^2 = 2.8\times10^{-13}$ cm, n is the dielectric constant of the material, $\Delta\nu$ is the width of the absorption band around $2\nu_\gamma$, and F is the incident photon flux. The number of excitations or, assuming a fluorescent quantum efficiency of one, the number of emitted fluorescent photons per unit volume of the specimen is

$$P_b = \sigma NF = (e^2/mc^2)^2(\lambda_\gamma{}^2/n^2\Delta\nu)NF^2. \qquad (2)$$

Here N denotes the number of fluorescent ions in the crystal. For an estimate of P_b, the following experimental data were used: $\lambda_\gamma = 7\times10^{-5}$ cm, $n(CaF_2) = 1.4$, $\Delta\nu = 1.5\times10^{14}$ sec^{-1} (5×10^3 cm^{-1}), and $N = 2.4\times10^{18}$ Eu ions per cm^3. The maser output of 4×10^{17} photons was concentrated into an area of approximately 10^{-3} cm^2; the incident photon flux F is, therefore, $F = 8\times10^{23}$ photon cm^{-2} sec^{-1}. From Eq. (2) we obtain $P_b = 10^{18}$ photons cm^{-3} sec^{-1}. Since the active volume was 10^{-4} cm^3, one calculates 5×10^{10} blue photons to be emitted per flash (500 μsec). The efficiency of this two-photon process is therefore ~10^{-7}. This value could be greatly increased if a system with a narrower excited state (smaller $\Delta\nu$) were employed. For a comparison with the observed number of blue photons, one has to consider the $f/4$ lens system and a number of reflection losses in the spectrometer. The number of photons leaving

the instrument is calculated to be 10^8. This value agrees quite well with the experimentally observed photon flux, giving strong support to the interpretation of our observations. The agreement is better than expected considering the simplifications made in the derivation of Eq. (2) and the estimates made during its application.

We would like to thank D. Kleinman for communication of his paper prior to publication, and H. Guggenheim for growing the CaF_2:Eu^{2+} crystal.

[1]T. H. Maiman, Brit. Commun. and Electronics 7, 674 (1960).
[2]R. J. Collins, D. F. Nelson, A. L. Schawlow, W. Bond, C. G. B. Garrett, and W. Kaiser, Phys. Rev. Letters 5, 303 (1960).
[3]A. Javen, W. R. Bennett, and D. R. Herriott, Phys. Rev. Letters 6, 106 (1961).
[4]P. A. Franken, A. E. Hill, C. W. Peters, and G. Weinreich, Phys. Rev. Letters 7, 118 (1961).
[5]P. P. Feofilov, Optica i Spektroskopiya 1, 992 (1956).
[6]M. Goeppert-Mayer, Ann. Physik 9, 273 (1931).
[7]D. Kleinman (to be published).

MAGNETIC BREAKDOWN IN CRYSTALS*

Morrel H. Cohen and L. M. Falicov
Institute for the Study of Metals, University of Chicago, Chicago, Illinois
(Received June 7, 1961)

To establish the various regimes of behavior of electrons in a magnetic field, the cyclotron frequency ω_c is usually compared with τ^{-1}, $\hbar^{-1}kT$, or $\hbar^{-1}E_F$, where τ is a typical relaxation time and E_F the Fermi energy. Comparison of ω_c with $\hbar^{-1}E_g$, where E_g is an energy gap of the pertinent band structure, has not been discussed except to note that the usual derivations of an effective Hamiltonian[1] for the motion of electrons in a magnetic field is no longer valid when $\hbar\omega_c \sim E_g$. No attention has been directed to the question of what actually happens when $\hbar\omega_c$ exceeds E_g; that is the subject of the present Letter.

The splitting of the energy levels due to magnetic fields is of the order of 10^{-8} ev per gauss, whereas gaps in ordinary band structures are rarely as small as 0.1 ev. Our question would be academic were it not for the existence of small gaps of the order 10^{-3} ev or less in some metals because of spin-orbit splitting[2] or of points of accidental degeneracy at or near the Fermi level.[3] These gaps are small compared with the Fermi energy and the remaining typical gaps in the band structure. In such a case the answer to our question is that as H increases, one passes from electron orbits determined semiclassically from the entire band structure to those determined semiclassically by ignoring the small gaps. We call this effect magnetic breakdown. Of course, some additional effects take place, i.e., a spreading of the magnetic levels into narrow bands and additional scattering processes, but these are not significant except in the transition range of magnetic field $\hbar\omega_c \sim E_g$.

Let us consider a simple example of a free-electron metal perturbed by a one-dimensional periodic potential. The one-electron Hamiltonian in the presence of a magnetic field in the z direction is

$$\mathcal{H} = \frac{1}{2m}\left(\vec{p} + \frac{|e|}{c}\vec{A}\right)^2 + V_0 \cos\kappa x,$$

where

$$\vec{A} = (0, Hx, 0), \quad k_F \gtrsim \kappa.$$

Since the electron distribution overlaps into the second zone, the Fermi surface consists of an undulating cylinder in the first zone with axis in the x direction and a small pocket of electrons in the second zone [Fig. 1(b)]. When H is small, i.e., $\hbar\omega_c \ll V_0$, the undulating cylinder gives rise to a set of open orbits; as consequences de Haas–van Alphen oscillations arise from the pocket but not from the cylinder and the R_{xx} component of the resistivity tensor increases quadratically with H. When $\hbar\omega_c \gg V_0$,[4] magnetic breakdown essentially restores the free-electron surface [Fig. 1(a)] and only the equatorial section of the "sphere" gives rise to a de Haas–van Alphen period. Moreover, because the open orbits have now disappeared, R_{xx} decreases as H^{-2} to a saturation value which is very approximately the free-electron value. The spreading of the magnetic levels into bands, which have a maximum width of about $2V_0$ for orbits which just intersect the zone faces, gives no appreciable effect, and the additional scattering processes give only second order corrections to the free-electron magnetoresistance[5]

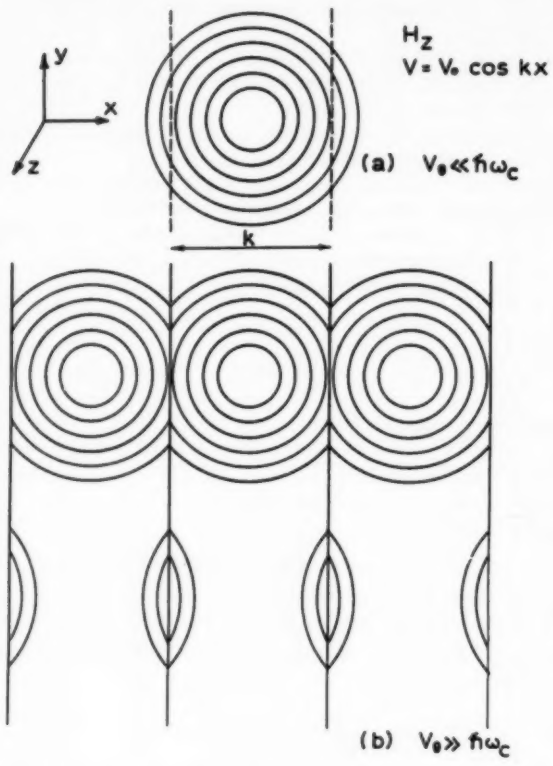

FIG. 1. A simple model to illustrate magnetic breakdown. (a) shows the orbits in k space for the free-electron case which are the same as the orbits when magnetic breakdown occurs; (b) shows the orbits for the low-field case.

that vanish as H^{-2}.

We have seen that in this simple illustration magnetic breakdown changes open orbits into closed orbits and so the H^2 term in the magnetoresistance disappears. More generally, the effect can cause a change of any orbit, i.e., closed, extended, or open, into any other of the same or different category. Consequently, as the field varies it must be possible to observe the disappearance of some periods and the appearance of new ones in experiments such as the de Haas–van Alphen effect, cyclotron resonance, and ultrasonic attenuation.

Possible experimental evidence for magnetic breakdown is the giant orbit observed by Priestley[6] in the de Haas–van Alphen effect in magnesium for fields very near the [000, 1] direction. Such an orbit, with an area larger than the section of the Brillouin zone, cannot occur in any ordinary band structure. However, the existence of an accidental degeneracy near the Fermi energy along the ΓK line (without spin-orbit coupling) and the detailed analysis of the structure of the levels[3] shows that the waist of the Fermi surface in the second zone contacts each "cigar" in the third zone just above and below the basal plane. Spin-orbit coupling should lift the degeneracy, but a sizeable region of k space must remain in which magnetic breakdown occurs for orbits which pass near one set of six points of contact. This would cause transitions between the Fermi surface in the second zone and the "cigars" in the third zone, giving rise to an orbit essentially the same as the equatorial section of the free-electron sphere (Fig. 2); its area gives a value of the period that exactly agrees with the experimental value 1.57×10^{-9} (gauss)$^{-1}$. The narrow angular region (about 4° in radius around the c axis) in which the orbit has been found further supports

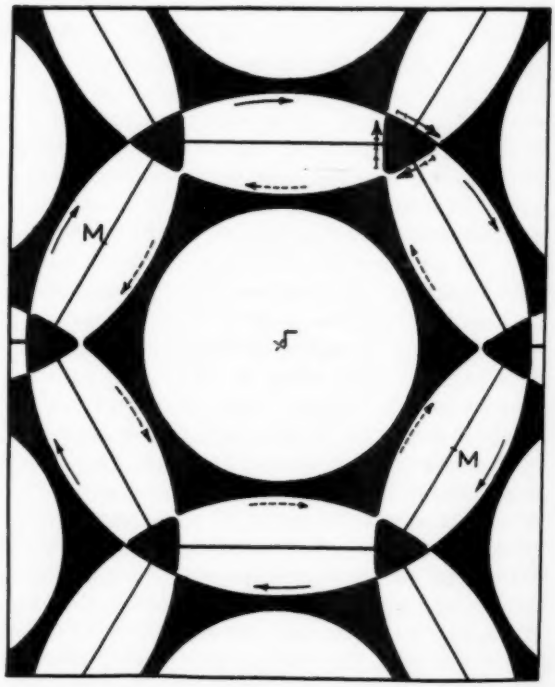

FIG. 2. The giant orbit in magnesium. The figure shows a section of the Fermi surface with a plane parallel to the basal plane and passing through the points of contact removed by spin-orbit splitting. ---→ orbit around the Fermi surface in the second zone at low fields; ⊢⊢→ orbit around "cigars" in the third zone at low fields; ⟶ giant orbit after magnetic breakdown occurs, showing transitions from second zone to third zone to second zone, etc.

this interpretation, because when the field is tipped only slightly off the c axis, the orbit can no longer pass near all six points of contact. The fields used in the experiments (57 to 191 kgauss) should have been enough to overcome the small gaps, but we have not estimated the splitting of the accidental degeneracy.

Another case of magnetic breakdown which may occur at relatively low fields is the magnetoresistance of beryllium for fields perpendicular to the c axis. If the H_1 level[7] of the band structure lies below the Fermi energy, spin-orbit coupling[2] causes the Fermi surface in the third zone to look like two similar cylinders with axes parallel to the c axis; the magnetoresistance must then increase quadratically with H. However, for fields of about 20 kgauss, magnetic breakdown connects these cylinders with the small pockets in the fourth zone, overcoming the small energy gap produced by spin-orbit splitting. The orbits close, and the magnetoresistance must saturate. A similar effect should occur in magnesium at fields very roughly about 200 kgauss from the change in topology of the Fermi surface in the second zone.[2]

In Mg,[3] Zn,[8] and Cd[8] there are two intersecting electron pieces of Fermi surface around L, which are separated by spin-orbit coupling, except at two points of contact on the AL line. For the magnetic field in a plane perpendicular to AL, magnetic breakdown is possible for orbits near the points of contact at any field strength. For arbitrary field orientation $\hbar\omega_c$ must exceed the spin-orbit splitting. In the hexagonal close-packed phases of Li and Na, the piece of Fermi surface around A which is split off from the main body of the Fermi sphere by spin-orbit coupling must show similar behavior because of the vanishing of the splitting along the three lines LAL.

The points of contact on the Fermi surface of graphite[9] are also removed by spin-orbit splitting.[10] Magnetic breakdown phenomena should in principle be observable when the field is nearly normal to the c axis.

Finally, it should be remarked that band gaps introduced by spin-orbit coupling can be magnetic field dependent via the interaction of the magnetic field with the unquenched orbital angular momentum and the electron spin. For the simple example of the degeneracy of p-like states in a reflection plane, the condition for magnetic breakdown is unchanged when the magnetic field is in the plane. On the other hand, magnetic breakdown can occur at somewhat different field strengths for the two different spin orientations when the magnetic field is perpendicular to the plane.

In conclusion we would like to acknowledge several stimulating discussions on this subject with W. A. Harrison.

---

*Work supported in part by the Office of Naval Research.

[1]See, for instance, R. Peierls, Z. Physik 80, 763 (1933); L. Onsager, Phil. Mag. 43, 1006 (1952); J. M. Luttinger and W. Kohn, Phys. Rev. 97, 869 (1955); W. Kohn, Proc. Phys. Soc. (London) 72, 1147 (1958).

[2]M. H. Cohen and L. M. Falicov, Phys. Rev. Letters 5, 544 (1960).

[3]This is the case in the Mg band structure as determined by L. M. Falicov (thesis submitted to the University of Cambridge, England, and to be published).

[4]The perturbation $V_0 \cos\kappa x$ mixes only unperturbed Landau levels which differ by at least $\hbar\omega_c$. A sufficient criterion for the convergence of the perturbation expansion is that $V_0 \ll \hbar\omega_c$ since the matrix elements of $\cos\kappa x$ must be less than unity in magnitude. A more detailed analysis by E. I. Blount (to be published) has shown that for typical orbits the necessary criterion is $V_0 \ll (\hbar\omega_c E_F \sin 2\varphi)^{1/2}$, $\varphi = \cos^{-1}(\kappa/k_F)$.

[5]See, for instance, E. N. Adams and T. D. Holstein, J. Phys. Chem. Solids 10, 254 (1959); P. N. Argyres, Phys. Rev. 117, 315 (1960).

[6]M. G. Priestley, private communication and reported by D. Shoenberg, in The Fermi Surface, edited by W. A. Harrison and M. B. Webb (John Wiley & Sons, New York, 1960), p. 80. We are grateful to Mr. Priestley for permission to quote his unpublished data on the range of orientation and field in which he observed the giant orbit.

[7]C. Herring and A. G. Hill, Phys. Rev. 58, 132 (1940). The related position of H_1 and the Fermi level cannot be determined within the accuracy of the calculation.

[8]W. A. Harrison, Phys. Rev. 118, 1190 (1960).

[9]See, for instance, J. W. McClure, Phys. Rev. 108, 612 (1957).

[10]J. C. Slonzewski and P. R. Weiss, Phys. Rev. 99, 636 (1955), have estimated the spin-orbit splitting to be about 10^{-4} ev as reported in reference 8.

MULTICOMPONENT MAGNETOPLASMA RESONANCE IN p-TYPE GERMANIUM

R. E. Michel and B. Rosenblum
RCA Laboratories, Princeton, New Jersey
(Received July 31, 1961)

In a field of sufficiently high frequency ω the electrical conductivity of a system of carriers exhibits a maximum (cyclotron resonance) when $\omega_C \equiv eH_0/m^*c = \omega$, where $\vec{H}_0$ is the applied magnetic field and m^* is the effective mass. At carrier concentrations high enough that the plasma frequency of the carriers is comparable to the experimental frequency, the usual cyclotron absorption maxima are shifted by plasma effects. We have observed such phenomena in p-type germanium where the plasmas of the light and heavy holes form a coupled system. The study of such a coupled system is particularly interesting in that it gives insight into certain aspects of carrier motion in metals and semimetals.

Magnetoplasma resonance was first observed in solids in the case of indium antimonide with an approximately fixed concentration of a single type of carrier.[1] It has also been studied in n-type germanium[2] as a function of carrier concentration.

In the present experiments a small, approximately ellipsoidal, sample of 7 ohm-cm indium-doped germanium was placed in a microwave cavity and its conductivity at 24 kMc/sec determined as a function of magnetic field in the [110] direction. The number of holes in the valence band was controlled by adjusting the temperature in the 10 to 40°K region. The carrier concentration was determined by Hall effect measurements. The ellipsoid for the plasma experiments was cut from between the potential arms of the Hall sample to minimize error due to doping inhomogeneities.

In an ellipsoidal sample which is small compared to the wavelength of the applied field and also small compared to the penetration depth, the microwave electric field will be uniform over the entire sample. For this case a simple equation of motion for the carriers has been derived.[1] Kittel[3] has extended this treatment to the case of a plasma consisting of two mobile particles and the fixed ions. The two coupled equations of motion can be written:

$$\ddot{\vec{r}}_1 + \frac{1}{\tau_1}\dot{\vec{r}}_1 + \omega_{p1}^2\vec{r}_1 + \frac{m_2}{m_1}\omega_{p2}^2\vec{r}_2 = \frac{e}{m_1}\vec{E} + \dot{\vec{r}}_1 \times \vec{\omega}_{c1},$$

$$\ddot{\vec{r}}_2 + \frac{1}{\tau_2}\dot{\vec{r}}_2 + \omega_{p2}^2\vec{r}_2 + \frac{m_1}{m_2}\omega_{p1}^2\vec{r}_1 = \frac{e}{m_2}\vec{E} + \dot{\vec{r}}_2 \times \vec{\omega}_{c2}, \quad (1)$$

where $\vec{r}_1$ and $\vec{r}_2$ are the position vectors for the average particle of the first and second kind (in the present case the light and heavy holes, respectively); $m_{1,2}$ are their masses; $\tau_{1,2}$ are the relaxation times; and $\vec{\omega}_{c1,2}$ are the cyclotron frequencies. The plasma frequencies are

$$\omega_{p1,2} = [Ln_{1,2}e^2/m_{1,2}^*(1+\chi L)]^{1/2},$$

where $n_{1,2}$ are the number of particles of the first and second kind, χ is the electric susceptibility of the crystal in the absence of the free carriers, and L is the depolarization or sample shape factor. The electric field is $\vec{E} = \vec{E}_0/(1+\chi L)$, where $\vec{E}_0$ is the applied field (which is taken to be along a principal axis of the sample). It is assumed that both types of particles have the same charge e.

For the interpretation of the present experiment we assume that the light- and heavy-hole masses are independent of energy and momentum. For the light holes this is an excellent approximation; the cyclotron mass of the heavy holes, however, has a momentum dependence which results in an anisotropy in the position of the cyclotron resonance of approximately 30%. We have used the appropriate cyclotron mass of the heavy holes for $\vec{H}_0$ in the [110] direction in the above equations but have determined the ratio $n_2/n_1 = 20$ from the density-of-states mass.

In Fig. 1 the positions of the resonance lines, as calculated from Eqs. (1), are plotted as a function of the total carrier concentration N. The arrows show the positions of the lines at low carrier concentration. The dashed lines indicate what would be the motion of each resonance if there were no coupling between the plasmas. In Fig. 1 it is assumed that the microwave field is circularly polarized. For linear polarization the two directions of $\vec{H}_0$ are equivalent, and Fig. 1 would have reflection symmetry in the horizontal axis. The thickness of the lines is a qualitative indication of the relative peak intensity at a given carrier concentration of the two resonances. It is thus seen that the absorption line which was initially the light-hole cyclotron resonance moves through zero field, increases in intensity, and eventually becomes the main magnetoplasma line; that which was initially the heavy-hole line decreases in intensity, never passes through zero

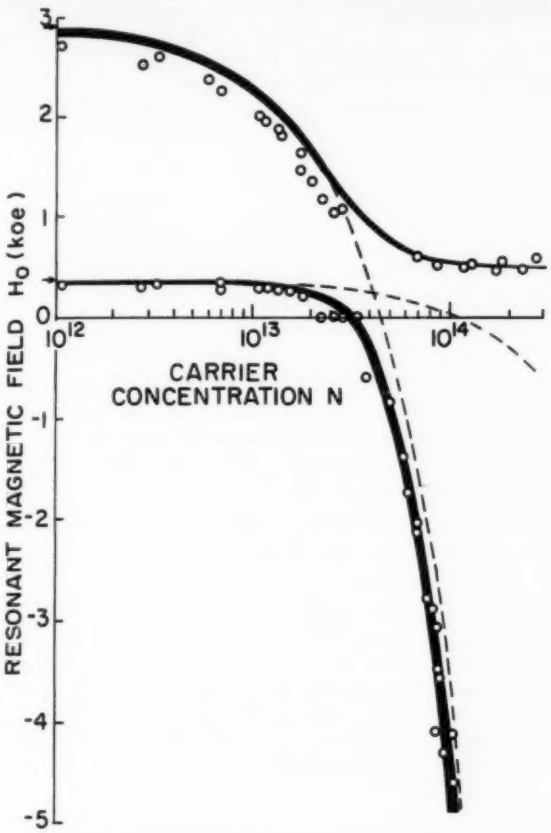

FIG. 1. The calculated resonant magnetic field for the magnetoplasma resonances vs carrier concentration. The thickness of the lines is approximately proportional to the relative intensity. The dashed lines indicate what would be the resonant fields if there were no coupling between the plasmas. The circles are experimental points.

field, and asymptotically approaches a field close to the cyclotron resonance field for the light holes. It is clear that the absorption at each resonance cannot be ascribed either to light or to heavy holes but is due to the cooperative effect of both carriers. The circles in Fig. 1 are experimental determinations of the resonance maxima positions. The discrepancy in the initial motion of the heavy-hole line is probably due to the assumption of isotropic mass.

The weak resonance which is observed at low magnetic field for large carrier concentrations is of particular interest. In the present case, where $\omega_{p2}=1.58\omega_{p1}$, this resonance approaches $\frac{1}{2}$ the light-hole cyclotron resonance field for $\omega_{p1,2}\gg\omega$. If $\omega_{p2}\gg\omega_{p1}\gg\omega$, the line would appear at the light-hole cyclotron resonance field. This resonance is an example of the phenomena discussed (for a somewhat different geometry) by Kittel[3] in which it is possible to observe the cyclotron resonance of a minority group of carriers in the presence of a majority group because the latter group acts to short-circuit the plasma effects of the first. This resonance is also similar to that discussed by Lax and Mavroides[4] for two-carrier systems in metals.

Since the signal was not always a very small perturbation of the cavity, it was simpler to take the data with linearly rather than with circularly polarized microwaves, and this was done in spite of the fact that the two lines were at times superimposed. In Figs. 2(a), (b), (c), and (d), the theoretical absorption curves for linear polarization are plotted for several representative total carrier densities N. The relaxation time for each group of carriers was chosen empirically to fit the experimental data.[5] The light solid line is the absorption due to the light holes, the dashed line that due to the heavy holes, and the bold solid line is the resultant. The arrows indicate the positions of the light- and heavy-hole cyclotron resonances at low carrier concentration. In Figs. 2(e), (f), (g), and (h) are experimental curves of the absorption at approximately corresponding N. In Figs. 2(a), (b), (e), and (f) the two lines are moving toward lower field with increasing carrier concentration. In Figs. 2(c) and (g) the strong line has passed through zero field and is moving to higher field as the carrier concentration increases. The weak line at about 0.8 koe is largely masked in the tail of the strong. At still higher concentrations [Figs. 2(d) and (h)] the main magnetoplasma line has moved off to the right and its tail is small enough that we can readily see the weak resonance line. The upper curve in Fig. 2(h) is the observed signal when the sample is placed in a region of uniform electric field in the microwave cavity. This is in approximate agreement with the theoretically calculated curve. When the sample is placed close to a node in the electric field, the line is greatly enhanced with respect to the main magnetoplasma resonance, as shown by the lower curve. A simple physical argument indicates that at least part of this enhancement results from less cancellation of the currents due to the light and heavy holes when there is a gradient in the electric field across the orbit of the carriers in the magnetic field.

In many resonance experiments the sharpness and resolution of the lines can be greatly improved

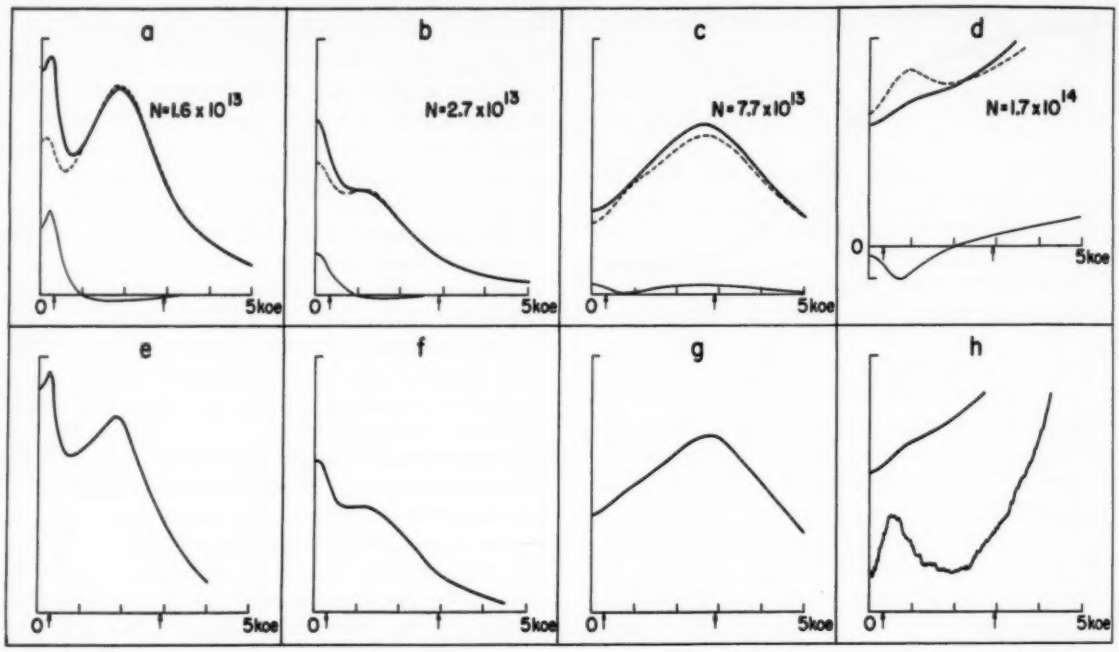

FIG. 2. The upper set of curves shows the theoretical power absorption as a function of magnetic field for the carrier concentrations indicated. The dashed line is the absorption by the heavy holes, the light solid line is that by the light holes, and the bold line is the resultant. The bottom set of curves is the experimental absorption for the approximately corresponding number of carriers. The arrows indicate the position of the cyclotron resonances at low carrier densities.

merely by making the observations at a higher experimental frequency. This is not true in the present case. If we approximate the scattering rate due to ionized impurities by $aNT^{-3/2}$ and the scattering rate due to thermal phonons by $bT^{3/2}$, where T is the temperature and a and b are constants, and assume that these scatterings are independent, and that neutral impurity scattering is negligible, then there is a maximum possible $\omega\tau$ which can be obtained for a given fractional shift of the resonance. This maximum is obtained by properly choosing the doping of the sample. The $\omega\tau$ in the present work is not far from that maximum.

We would like to thank Mr. Harold Hanson for his assistance throughout the experiment.

[1]G. Dresselhaus, A. F. Kip, and C. Kittel, Phys. Rev. 100, 618 (1955).

[2]R. E. Michel and B. Rosenblum, Bull. Am. Phys. Soc. 5, 375 (1960).

[3]C. Kittel, Proceedings of the Conference on Radio and Microwave Spectroscopy, Duke University, 1957 (unpublished).

[4]B. Lax and J. B. Mavroides, in Solid State Physics, edited by F. Seitz and D. Turnbull (Academic Press, Inc., New York, 1960), Vol. 11.

[5]It may be noted that the relaxation times for impurity scattering of the light and heavy holes are not equal while those for phonon scattering are.

ULTRASONIC AMPLIFICATION IN CdS

A. R. Hutson and J. H. McFee
Bell Telephone Laboratories, Murray Hill, New Jersey

and

D. L. White
Bell Telephone Laboratories, Whippany, New Jersey
(Received August 28, 1961)

We have observed substantial amplification of ultrasonic waves in photoconductive CdS, produced by applying a dc electric field in the direction of wave propagation. Results are reported showing gains of 18 db at 15 Mc/sec and 38 db at 45 Mc/sec in a 7-mm length of CdS.

Light-sensitive ultrasonic attenuation has been observed in CdS.[1-4] It was pointed out[5] that these effects result from the relaxation interaction of mobile charge carriers with the strong longitudinal electric fields of piezoelectric origin accompanying certain acoustic waves in CdS. In the course of developing a theory for the propagation of acoustic waves in piezoelectric semiconductors,[6] one of us (D. L. White) pointed out the possibility of achieving acoustic gain by applying a dc electric field which causes the interacting charge carriers to drift in the direction of wave propagation faster than the sound velocity.

Figure 1 shows the experimental arrangement. A 1-μsec pulse of rf is applied to the top Y-cut quartz transducer producing a shear wave which propagates down through the first buffer, CdS crystal, second buffer, and is converted by the bottom transducer to an rf output signal. The output is amplified, detected, and displayed on an oscilloscope whose time base is triggered at the initial rf input pulse. (The fused silica buffers provide time delay and electrical insulation.) The CdS crystal is oriented so that the shear wave propagates at right angles to the hexagonal axis with material displacement along the hexagonal axis. In the absence of electrical conductivity, a longitudinal piezoelectric field proportional to strain ($-e_{15}S/\epsilon$) accompanies the wave in the CdS. Mobile charge carriers are produced with relative uniformity throughout the sample by illuminating it with the weakly absorbed 5770/5790 A lines of mercury. The parallel polished faces of the CdS, which are bonded to the buffers, were prepared as electrical contacts by diffusing indium into a very thin surface region and then evaporating a metallic indium film onto the surface. A dc voltage pulse can be applied between these contacts to provide the carrier drift field. The voltage, duration, and time delay (with respect to the initial rf pulse) of the drift-field pulse are separately controllable. At the start of this experiment, the crystal appeared to be insulating in the dark with an acoustic attenuation of less than 7 db at 45 Mc/sec and less than 2 db at 15 Mc/sec.[4]

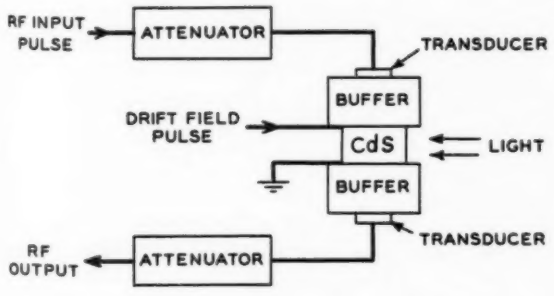

FIG. 1. Experimental arrangement.

We have measured the change in the output signal with respect to that obtained in the dark with no drift field, with the following results:

1. No illumination—drift-field pulse has no effect upon output signal.

2. No drift field—increasing illumination yields increasing attenuation and conductivity.

3. Sample illuminated—5-μsec drift-field pulse has no effect unless time delay is such that drift-field pulse overlaps 3.5-μsec transit time of 1-μsec ultrasonic pulse in the sample. When overlap occurs, the output signal is either increased or decreased, maximum effect corresponding to complete overlap.

4. Sample illuminated, drift-field pulse completely overlapping sound pulse in sample—variation of the drift-field strength produces changes in the output signal as shown in Fig. 2. (For those parts of the curves showing large gain, input attenuation was added in order to remain within the linear region of the effect.)

The striking features of these results are the appearance of negative attenuation (gain) and the

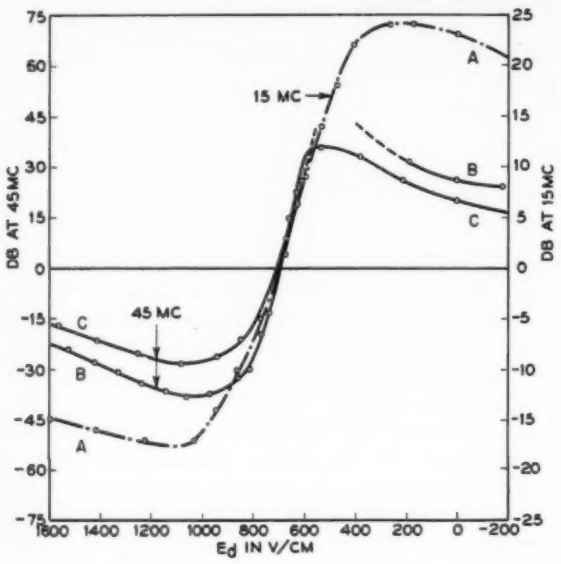

FIG. 2. Observed attenuation as a function of drift field. Zero db represents attenuation with sample unilluminated. Curve *A*: 15 Mc/sec, $\omega_c/\omega = 1.2$. Curve *B*: 45 Mc/sec, $\omega_c/\omega = 0.24$. Curve *C*: 45 Mc/sec, $\omega_c/\omega = 0.21$. (ω_c/ω values are average values for the whole sample computed from measured CdS conductivities.)

crossover at ~700 v/cm. The drift field at crossover corresponds to a drift velocity, v_d, equal to the appropriate CdS shear wave velocity ($v = 2\times10^5$ cm/sec) for negative carriers of $\mu \cong 285$ cm^2/volt sec. This drift mobility is in good agreement with the Hall mobility of about 300 cm^2/volt sec at 300°K reported by Piper and Halsted.[7] The change from acoustic loss to gain at a carrier drift velocity equal to the wave velocity corresponds to White's prediction.

A small signal theory of this attenuation behavior may be obtained by adding a constant drift field, E_d, to the equation for current density in reference 6. Basically, the theory amounts to obtaining an expression for the amplitude of the wave-periodic electric displacement, D, in terms of the wave-periodic E field from Poisson's equation and the current-density-space-charge continuity equation. This relation between D and E is then used to eliminate D from the piezoelectric equation, $D = eS + \epsilon E$, so that an expression for E in terms of the strain, S, and the appropriate piezoelectric e constant is obtained, which may be substituted in the elastic equation, $T = cS - eE$. The result is a complex elastic stiffness constant, c', which contains all of the electrical effects. The acoustic absorption constant, α, is obtained from the imaginary part of $(c')^{-1/2}$. If one is dealing only with a single carrier species, we find

$$\alpha = \frac{\omega}{v}\frac{e^2}{2c\epsilon}\left[\frac{(\omega_c/\gamma\omega)}{1+(\omega_c/\gamma\omega)^2(1+\omega^2/\omega_c\omega_D)^2}\right], \qquad (1)$$

where $(e^2/c\epsilon)$ is the square of the appropriate electromechanical coupling constant; $\omega_c = \sigma/\epsilon$, the conductivity relaxation frequency; $\gamma = 1 - v_d/v$; and $\omega_D = v^2/D$, where D is the carrier diffusion constant. When the Einstein relation between mobility and diffusion is valid, $(\omega^2/\omega_c\omega_D) = k^2\Lambda^2$, where $k = 2\pi/\lambda$ and Λ is the Debye length. Plots of the bracketed term in (1) are shown in Fig. 3. The effect of diffusion is to decrease the maximum value of this term as ω_c/ω is decreased. (If diffusion were neglected, the bracketed term would have maxima of ±0.5 and the maximum values of $\pm\alpha$ would remain constant even in the limit of small ω_c/ω.) The coefficient of the bracket term of (1) is $\simeq$150 db at 45 Mc/sec and $\simeq$50 db at 15 Mc/sec for our 7-mm sample.[5,6,8] Thus, Figs. 2 and 3 have the same vertical scales and can be compared directly.

Agreement between theory and experiment is semiquantitative for the data shown, which were taken at high light intensities. Closer agreement

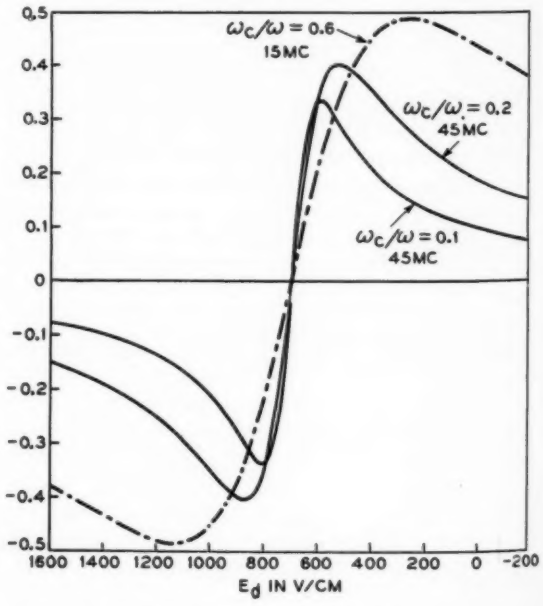

FIG. 3. Plots of bracketed term of Eq. (1).

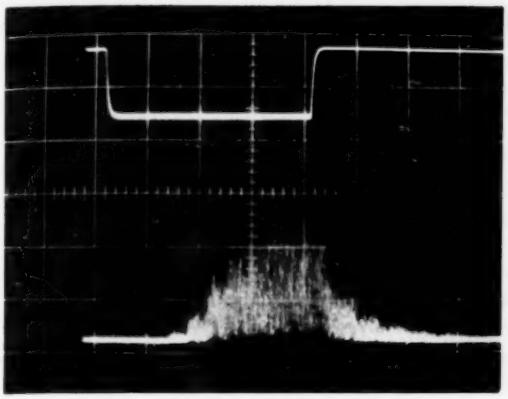

FIG. 4. Buildup of acoustic oscillations. Top trace: Drift-field pulse applied to CdS. Vertical scale, 715 volt/cm per large division. Lower trace: Signal from output transducer (transducer and receiver tuned to 15 Mc/sec). Horizontal scale for both traces, 20 μsec per large division.

probably is not to be expected for the following reasons: Inhomogeneities in the photoconductivity of the sample and a 7% ripple on the drift-field pulse probably caused blurring of the steep parts of the gain vs drift-field curves. Uncertainty may exist in the measured piezoelectric constant. There may be some photoconductivity due to holes. The Einstein relation (relating ω_D to μ) may fail because the electrons depart from thermal equilibrium under action of the drift field.

To demonstrate unequivocally the existence of net acoustic gain in our sample, we have lengthened the applied drift pulse, applying no input signal. There is sufficient gain in the downward direction to offset the attenuation in the upward direction as well as the losses incurred on reflection at the sample-buffer bonds, with the result that the sample breaks into oscillation. The lower trace in Fig. 4 shows the rapid buildup of acoustic energy from noise. A steady state is reached when the available carrier concentration can no longer support space-charge bunching sufficient to provide surplus gain at the high-strain amplitude.

We are grateful to T. B. Bateman and H. J. McSkimin for advice and assistance in ultrasonic techniques and to D. E. Collins, L. J. Heilos, and W. Pleibel for sample preparation.

---

[1]H. Gobrecht and A. Bartschat, Z. Physik 153, 529 (1959).

[2]H. D. Nine, Phys. Rev. Letters 4, 359 (1960).

[3]H. D. Nine and R. Truell, Phys. Rev. 123, 799 (1961).

[4]H. J. McSkimin, T. B. Bateman, and A. R. Hutson (to be published).

[5]A. R. Hutson, Phys. Rev. Letters 4, 505 (1960). This reference also includes piezoelectric constants for CdS.

[6]A. R. Hutson and D. L. White, J. Appl. Phys. (to be published).

[7]W. W. Piper and R. E. Halsted, Proceedings of the International Conference on Semiconductor Physics, Prague, 1960 (Publishing House of the Czechoslovak Academy of Sciences, Prague, 1961).

[8]H. Jaffe, D. Berlincourt, H. Krueger, and L. Shiozawa, Proceedings of the Fourteenth Annual Symposium on Frequency Control (U. S. Army Research and Development Laboratory, Fort Monmouth, New Jersey, 1960).

SPLITTING OF ELECTRON SPIN RESONANCE LINES BY AN APPLIED ELECTRIC FIELD

G. W. Ludwig and H. H. Woodbury
General Electric Research Laboratory, Schenectady, New York
(Received August 17, 1961)

Nuclei or paramagnetic ions in many solids occupy sites which lack inversion symmetry. Bloembergen has recently called attention to the possibility of observing shifts, proportional to the applied electric field $\mathcal{E}$, in the energy levels of such systems.[1] Consistent with Bloembergen's ideas, Kushida and Saiki[2] and Armstrong et al.[3] have detected a broadening of certain nuclear quadrupole resonance lines. In this Letter we report the first observation of changes, linear in $\mathcal{E}$, in the spin Hamiltonian of paramagnetic ions: The g tensor has been modified and its symmetry lowered, and a zero-field splitting of spin levels has been introduced. In the following Letter[4] a mechanism for such effects is proposed.

The measurements were made on transition metal ions occupying interstitial sites in the silicon lattice.[5] It was anticipated that effects of an electric field might be observable since the following criteria are met: Interstitial sites lack inversion symmetry; the t_2 functions of the transition metal ions are so hybridized that there are nonvanishing matrix elements of the electric field; and the separation between the ground and excited states of the ions are small. It is noted that some ions have orbital degeneracy which is partially lifted by spin-orbit interaction, and spectra of several ions are sensitive to uniaxial stress.

Samples were studied with $\vec{H} \perp \vec{\mathcal{E}}$ using a conventional TE_{011} mode cylindrical cavity. An $\mathcal{E} \sim 12$ kv/cm could be applied along the long dimension of the sample.

The ground state of interstitial neutral iron in silicon has an electron spin of one. So long as the tetrahedral symmetry is undisturbed, the three spin levels in a magnetic field are equally spaced, and the $M = 1$ to 0 and 0 to -1 transitions are equal in energy. For $\mathcal{E} \neq 0$ the single resonance line splits, proportional to $\mathcal{E}$, into two equally intense components, as shown in Fig. 1. It is believed that ions occupying one type of interstitial site display two fine structure components which differ in intensity by the Boltzmann factor (~1.17 under our experimental conditions). However, there are two types of interstitial sites, differing by the operation of inversion, which give complementary spectra. The position of the double-quantum transitions[6] is not sensitive to $\mathcal{E}$, indicating that one is observing a fine structure splitting rather than a g shift. For $\vec{\mathcal{E}}$ in a cubic direction, the splitting varies sinusoidally for $\vec{H} \perp \vec{\mathcal{E}}$, as shown in Fig. 2.

The ground state of interstitial Fe^+ in silicon can be described by an effective total angular momentum $J = \frac{1}{2}$; there are two energy levels and one resonance transition.[5] For $\mathcal{E}$ sufficiently large one observes two equally intense resonance lines, which show an angular variation similar to that described for Fe^0. Here, however, the appearance of two lines must represent an effect on the g tensor; the shift is of opposite sign for the two nonequivalent sites.

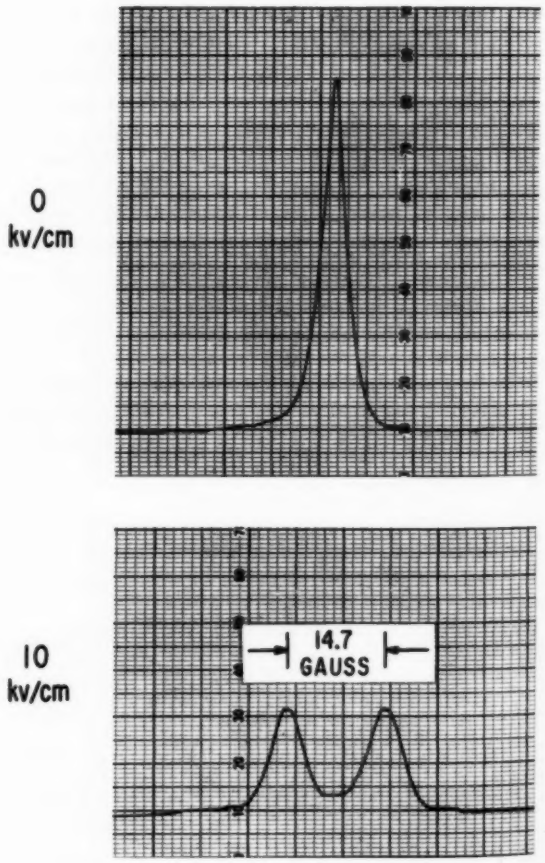

FIG. 1. Splitting of the spectrum of Fe^0 in silicon by an electric field applied in the [001] direction, for $\vec{H}$ in a [110] direction. The temperature is 4.2°K.

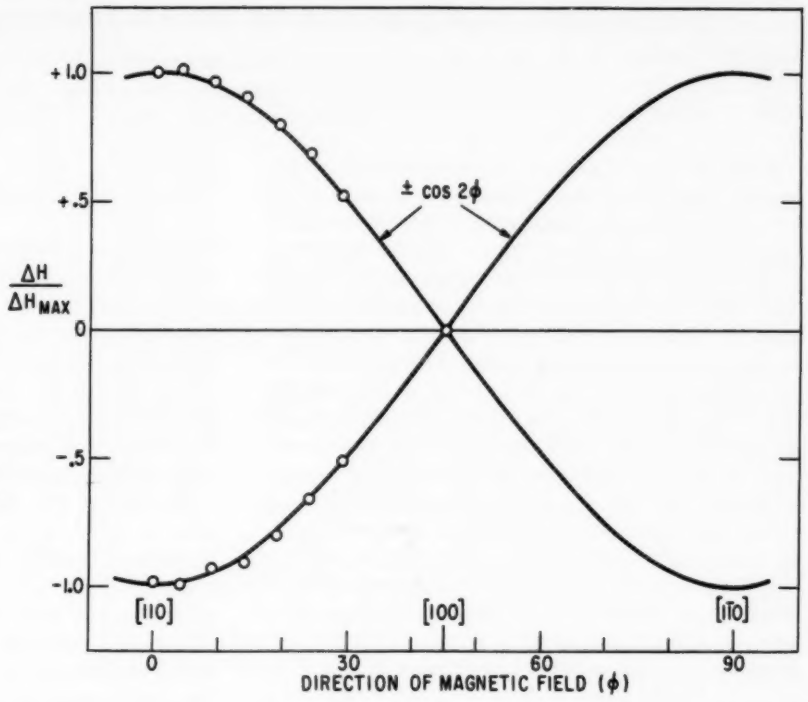

FIG. 2. Anisotropy of the splitting of the Fe^0 line for $\vec{\mathcal{E}}$ in the [001] direction and $\vec{\mathcal{K}}$ in the (001) plane.

The spin Hamiltonian describing the results for Fe^0 and Fe^+ with $\vec{\mathcal{E}}$ parallel to the [001] direction is

$$\mathcal{K} = g\beta\vec{J}\cdot\vec{H} \pm \mathcal{E}[b\beta(J_1H_1 - J_2H_2) + E(J_1^2 - J_2^2)]. \qquad (1)$$

Here the subscripts 1 and 2 denote the [110] and the [1$\bar{1}$0] directions, respectively, and the plus and minus signs correspond to the two different sites. To first order in $\mathcal{E}$ the M to M-1 transitions are

$$h\nu = g\beta H \pm \mathcal{E}[b\beta H + 3E(M - \tfrac{1}{2})]\sin^2\theta\cos 2\varphi, \qquad (2)$$

where θ and φ are polar angles describing the direction of $\vec{H}$, and $\theta = \pi/2$, $\varphi = 0$ is the [110] direction. We find $b \simeq 0$ and $|E| = (4.7 \pm 0.2) \times 10^{-8}$/kv for Fe^0; $|b| = (7 \pm 1) \times 10^{-4}$ cm/kv for Fe^+. Equations (1) and (2) are easily generalized to arbitrary direction of $\vec{\mathcal{E}}$.[4]

Effects of electric fields have also been observed for other ions in silicon.

One of us (G. W. L.) wishes to acknowledge his indebtedness to Professor Bloembergen, who suggested the possibility of observing electric field effects in silicon in an informal discussion. We are grateful to F. S. Ham for discussions which contributed to this work. C. R. Trzaskos assisted in the measurements.

---

[1]N. Bloembergen, Science 133, 1363 (1961); Phys. Rev. Letters 7, 90 (1961); J. Chem. Phys. (to be published).

[2]T. Kushida and K. Saiki, Phys. Rev. Letters 7, 9 (1961).

[3]J. Armstrong, N. Bloembergen, and D. Gill, Phys. Rev. Letters 7, 11 (1961); J. Chem. Phys. (to be published).

[4]F. S. Ham, following Letter [Phys. Rev. Letters 7, 242 (1961)].

[5]For a discussion of the electronic structure and resonance properties of these ions see H. H. Woodbury and G. W. Ludwig, Phys. Rev. 117, 102 (1960); G. W. Ludwig and H. H. Woodbury, Phys. Rev. Letters 5, 538 (1960). A further account is to be published.

[6]See J. W. Orton, P. Auzins, and J. E. Wertz, Phys. Rev. Letters 4, 128 (1960).

LINEAR EFFECT OF APPLIED ELECTRIC FIELD IN ELECTRON SPIN RESONANCE

Frank S. Ham
General Electric Research Laboratory, Schenectady, New York
(Received August 17, 1961)

In the preceding Letter,[1] Ludwig and Woodbury report observation of linear effects of an applied electric field on the electron spin resonance spectra of two charge states of interstitial iron in silicon, in accord with Bloembergen's prediction[2] that such effects should be in general observable for ions at crystal sites lacking inversion symmetry. The purpose of this Letter is to show explicitly how these effects arise for iron-series transition metal ions that form interstitial defects in silicon. Similar results pertain to other ions with d^n or f^n valence configurations in various crystals.

A phenomenological model that successfully describes interstitial iron series ions in silicon has been given by Ludwig and Woodbury[3]: The ions occupy sites of tetrahedral symmetry; all valence electrons are in the d shell; the threefold degenerate t_2 orbitals are lower in energy than the doubly degenerate e's; Hund's rule is obeyed. However, the t_2 and e wave functions of the interstitial are very different from the $3d$ functions of the free ion,[4] although they have the same behavior under symmetry operations of the tetrahedron. In particular, $3d\,t_2$ functions mix with functions of odd parity on the metal ion, such as $4p$, and form bonds with neighboring silicon atoms. Denoting by x, y, z coordinates with respect to the cube directions, we may represent the t_2 functions schematically by

$$\psi_x = \alpha(yz)_{3d} + \beta(x)_{4p} + \gamma(\varphi_1 - \varphi_2 + \varphi_3 - \varphi_4), \quad (1)$$

and ψ_y and ψ_z by cyclic permutation of x, y, z. Here φ_1, φ_2, φ_3, and φ_4 denote σ orbitals on nearest neighbors in the [111], [$\bar{1}\bar{1}$1], [1$\bar{1}\bar{1}$], and [$\bar{1}$1$\bar{1}$] directions, respectively, and for simplicity we ignore other possible bonds.

The interaction $\mathcal{H}_{\mathcal{E}} = e\,\mathcal{E}_z z$ of an electron with an electric field $\mathcal{E}_z$ in the z direction then has only one nonzero matrix element between the t_2 functions:

$$\langle \psi_x | e\,\mathcal{E}_z z | \psi_y \rangle = p\,\mathcal{E}_z. \quad (2)$$

This defines a parameter p. We may for convenience represent the matrix elements between t_2 functions in terms of an operator $\vec{\mathfrak{L}}$ which satisfies the commutation rules for angular momentum, with $\mathfrak{L} = 1$[5]:

$$\mathcal{H}_{\mathcal{E}} = -\mathcal{E}_z p(\mathfrak{L}_x \mathfrak{L}_y + \mathfrak{L}_y \mathfrak{L}_x). \quad (3)$$

$\mathcal{H}_{\mathcal{E}}$ lifts the orbital degeneracy of t_2, energy levels being at 0 and $\pm p\,\mathcal{E}_z$. Thus an electron in a t_2 state in tetrahedral symmetry responds to a field in a cube direction as if the state possessed an electric dipole moment of strength p. From (1) and (2), p is nonzero if the t_2 states are mixtures of functions of opposite parity on the central ion (α and $\beta \neq 0$) or if σ bonding occurs with the nearest neighbors ($\gamma \neq 0$).

For Fe^0 or Mn^- interstitial in Si, the ground state arises from the configuration $t_2^6 e^2$ and has $S = 1$ and no orbital degeneracy.[3] At an energy Δ higher, there is an orbital triplet of the form $t_2^5 e^3$ which is split by an electric field. Between these states and the ground state there are matrix elements of the spin-orbit interaction $\lambda(\vec{L}\cdot\vec{S})$, the orbital part of the Zeeman interaction $\beta(\vec{L}\cdot\vec{H})$, and the interaction $P(\vec{L}\cdot\vec{I})$ between the nuclear moment and the orbital moment of the electrons. Accordingly, from third-order perturbation theory we find for the spin Hamiltonian of the ground state[6]

$$\begin{aligned}\mathcal{H} = {} & g\beta\vec{H}\cdot\vec{S} + A\vec{I}\cdot\vec{S} - \gamma\beta_N\vec{H}\cdot\vec{I} \\ & + \mathcal{E}_z(2\lambda^2 p\alpha^2/\Delta^2)(S_x S_y + S_y S_x) \\ & + \mathcal{E}_z\beta(4\lambda p\alpha\alpha'/\Delta^2)(S_x H_y + S_y H_x) \\ & + \mathcal{E}_z(4\lambda pP\alpha\alpha''/\Delta^2)(S_x I_y + S_y I_x) \\ & + \mathcal{E}_z(2pP^2\alpha''^2/\Delta^2)(I_x I_y + I_y I_x) \\ & + \mathcal{E}_z\beta_N(4pP\alpha'\alpha''/\Delta^2)(\beta/\beta_N)(I_x H_y + I_y H_x). \quad (4)\end{aligned}$$

Terms in (4) arising from $\mathcal{E}_x$ and $\mathcal{E}_y$ may be obtained by permutation of indices. Here α, α', and α'' are factors arising because matrix elements of $\lambda(\vec{L}\cdot\vec{S})$, $\beta(\vec{L}\cdot\vec{H})$, and $P(\vec{L}\cdot\vec{I})$ are changed from their free-atom values. The isotropic shift in g provides the relation

$$(8\lambda\alpha\alpha'/\Delta) \cong -(g - 2.0023).$$

For $g\beta H \gg (\lambda^2\alpha^2/\Delta^2)p\mathcal{E}$ and arbitrary orientation of $\vec{\mathcal{E}}$ and $\vec{H}$, the energy levels to first order

in $\mathcal{E}$ are given by (with omission of nuclear terms)

$$E(M) = g\beta HM + (6\lambda^2 p\alpha^2/\Delta^2)\,\mathcal{E}M^2\phi + (8\lambda p\alpha\alpha'/\Delta^2)\,\mathcal{E}\beta HM\phi, \quad (5)$$

where

$$\phi = m_z n_x n_y + m_x n_y n_z + m_y n_z n_x, \quad (6)$$

n_x, n_y, n_z and m_x, m_y, m_z being the direction cosines of $\vec{H}$ and $\vec{\mathcal{E}}$, respectively.

For Fe^+ or Mn^0 the ground state is $t_2^5e^2$ with $S = \frac{3}{2}$ and a threefold orbital degeneracy describable by an effective orbital angular momentum operator $\vec{\mathcal{L}}$ with $\mathcal{L}=1$. With $\vec{J} = \vec{\mathcal{L}} + \vec{S}$, the spin-orbit interaction separates the levels with $J = \frac{1}{2}$, $\frac{3}{2}$, and $\frac{5}{2}$, placing $J = \frac{1}{2}$ lowest. The effect of $\mathcal{E}_z$ is represented by an operator of the same form as (3), and this, the Zeeman interaction

$$\mathcal{H}_H = g_{\mathcal{L}}\beta\vec{H}\cdot\vec{\mathcal{L}} + g_S\beta\vec{H}\cdot\vec{S},$$

and the hyperfine interaction

$$\mathcal{H}_I = A_{\mathcal{L}}\,\vec{\mathcal{L}}\cdot\vec{I} + A_S\vec{S}\cdot\vec{I}$$

have matrix elements between the $J = \frac{1}{2}$ and $\frac{3}{2}$ states. Accordingly, from second order perturbation theory the spin Hamiltonian for the $J = \frac{1}{2}$ states has the form

$$\mathcal{H}_{1/2} = (\tfrac{2}{3}g_S - \tfrac{2}{3}g_{\mathcal{L}})\beta\vec{H}\cdot\vec{J} + (\tfrac{2}{3}A_S - \tfrac{2}{3}A_{\mathcal{L}})\vec{J}\cdot\vec{I} - [2p(g_S - g_{\mathcal{L}})/3W]\,\mathcal{E}_z\beta\,(J_xH_y + J_yH_x) - [2p(A_S - A_{\mathcal{L}})/3W]\,\mathcal{E}_z(J_xI_y + J_yI_x),$$

where $W = [E(\frac{3}{2}) - E(\frac{1}{2})]$.

For interstitial Mn^+ and Cr^0 in silicon the ground state is $t_2^4e^2$ ($S=2$, $\mathcal{L}=1$). The effect of $\mathcal{E}_z$ is given by (3). This gives a direct Stark splitting of the ground level ($J=1$) as well as producing shifts in other resonance parameters.

The silicon lattice has two tetrahedral interstitial sites identical in their environments except that one is inverted with respect to the other. The dipole moment p has opposite sign for these sites, and resonance spectra should thus show a symmetrical splitting of lines to first order in $\mathcal{E}$, as is observed.

We have so far ignored the fact that the paramagnetic ion is displaced by the external field from its position of tetrahedral symmetry. This displacement gives rise to a perturbation in the potential seen by the electrons in addition to that produced directly by the applied field. However, we may show from symmetry that to first order in $\mathcal{E}$ this further perturbation can affect only those matrix elements already affected directly by the applied field. Thus the parameter p will be used to represent the net effect of both perturbations.

From the results of Ludwig and Woodbury and Eqs. (4) and (7) we can evaluate the effective one-electron dipole strength p for interstitial Fe^+ and Fe^0 in silicon, using estimates of the other parameters in these formulas obtained from other studies.[4] We obtain $p/e \cong 0.3\times10^{-8}$ cm for both Fe^0 and Fe^+. These values are, however, each uncertain to perhaps a factor of 3 because of uncertainties in making correction for local fields and in estimating the other parameters.

If p is of the same magnitude for Mn and Cr in silicon as for Fe, the ground states of Mn^+ and Cr^0 should suffer a linear Stark splitting of ~0.05 cm^{-1} with $\mathcal{E}=10^4$ v/cm, in zero magnetic field.

The author is indebted to G. W. Ludwig and H. H. Woodbury for helpful discussions.

---

[1]G. W. Ludwig and H. H. Woodbury, preceding Letter [Phys. Rev. Letters 7, 240 (1961)].

[2]N. Bloembergen, Science 133, 1363 (1961); Phys. Rev. Letters 7, 90 (1961).

[3]G. W. Ludwig and H. H. Woodbury, Phys. Rev. Letters 5, 538 (1960).

[4]G. W. Ludwig, H. H. Woodbury, and F. S. Ham (to be published).

[5]A. Abragam and M. H. L. Pryce, Proc. Roy. Soc. (London) A205, 135 (1951).

[6]In writing the coefficients of the terms in (4) we have omitted contributions arising from matrix elements between the ground state and two higher orbital triplets derived from the free atom ^3F and ^3P terms. These additional contributions have the same general form and relative size as those given and must be included in a quantitative treatment. They are proportional to a matrix element of $\mathcal{H}_{\mathcal{E}}$ between the t_2 and e functions instead of to p as defined by (2).

DE HAAS–VAN ALPHEN EFFECT IN RHENIUM, NIOBIUM, AND TANTALUM*

A. C. Thorsen and T. G. Berlincourt

Atomics International, Division of North American Aviation, Inc., Canoga Park, California

(Received July 24, 1961; revised manuscript received August 21, 1961)

The electronic structures of many low-melting-point metals have been extensively investigated and characterized by de Haas–van Alphen (dHvA), galvanomagnetic, cyclotron resonance, anomalous skin-effect, and magnetoacoustic absorption techniques.[1] In contrast, despite considerable interest in the electronic character of transition metals,[2] there have been very few applications of such techniques to these elements[3,4] due primarily to the difficulties of obtaining single crystals of the requisite high purity. In this paper we report on the first observations of dHvA oscillations in the transition metals Re, Nb, and Ta. As will be evident from the data, the ranges of the observed dHvA parameters are similar to those observed for polyvalent low-melting-point metals.

The single crystals of Re and Nb used in this investigation were grown, respectively, by Nadler and Buehler using electron bombardment techniques. The Ta sample was prepared by Budnick using a strain-anneal technique.[5] Chase Brass and Copper Company material was used for the Re crystal which had a room-temperature to liquid-helium-temperature resistivity ratio of 540. The corresponding ratios for the Nb and Ta crystals were 56 and ≈600, respectively. (The liquid helium temperature resistivities were measured at 4.2°K in magnetic fields just sufficient to quench all superconductivity.) The Re and Nb samples were approximately 1 mm in diameter by 9 mm in length and were obtained from single-crystal rods by a combination of etching and spark cutting techniques. The Ta sample was cut from a 0.51-mm diameter wire and was composed of several small single crystals whose orientations varied slightly along the length of the sample. The approximate crystallographic orientations for all three samples are indicated in Table I. The pulsed-field apparatus used in this study has been described briefly.[6,7]

A complex electronic structure might well be anticipated in Re. If one assumes seven valence electrons per atom, the free-electron Fermi sphere completely encloses the first two Brillouin zones for the hexagonal lattice. In such a situation, there may exist in higher zones a number of electron and hole surfaces capable of generating dHvA oscillations. The results are suggestive of such a complex structure, for no fewer than four oscillating susceptibility terms were observed in Re with the field approximately parallel to the $[10\bar{1}0]$ direction. Three of these terms can

Table I. Periods, corresponding Fermi surface extremal cross-sectional areas, and effective masses for de Haas–van Alphen oscillations in Re, Nb, and Ta. (Estimated accuracy of periods is ±5%.)

Crystal	Magnetic field orientation	P (10^{-8} gauss^{-1})	A (10^{15} cm^{-2})	m^*/m_0
Re	$[10\bar{1}0]$	1.65	5.79	1.9 ±0.7
		6.3	1.52	0.5 ±0.05
		7.1	1.34	0.53 ±0.05
		124	0.077	<0.1
Nb	[110]	1.16	8.23	1.0 ±0.1
		1.67	5.72	1.0 ±0.1
Ta[a]	12° from [110] in (001) plane	2.02	4.73	...
		2.16	4.42	0.8 ±0.1

[a]Only one effective-mass entry appears after Ta because the required data were taken during a second run when only one term was observable.

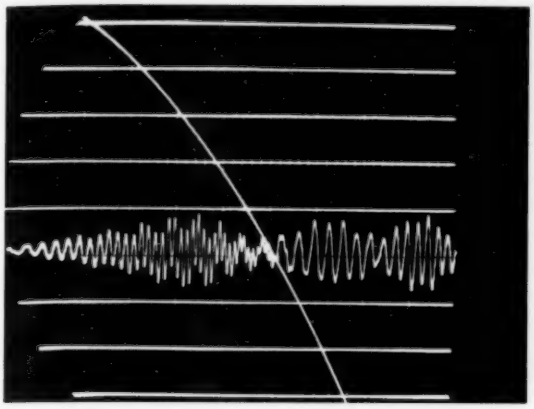

FIG. 1. de Haas–van Alphen effect in Re at 1.16°K. The oscillating trace shows the output from a pickup coil containing the sample. The curved trace shows the field increasing from 87.7 to 94.4 kilogauss during a portion of the oscillating trace. The total sweep time is two milliseconds (time increasing from right to left). Three oscillating terms are visible.

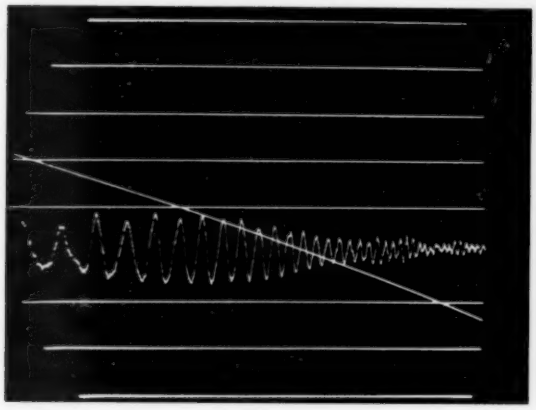

FIG. 2. Long-period de Haas–van Alphen oscillations in Re at 1.16°K. The diagonal trace shows the field increasing (from right to left) from 13.5 to 42.1 kilogauss during a sweep time of about 2.0 milliseconds.

be recognized in Fig. 1, while the fourth and much longer period term, observable at lower magnetic fields, is shown in Fig. 2. The periods P deduced from such data are given in Table I along with the corresponding Fermi surface extremal cross-sectional areas $A = 4\pi^2 e/chP$. The effective-mass values m^* listed in Table I were calculated from the temperature variations of the amplitudes of the oscillations in the usual manner.[4] It should be remarked, however, that for the longest period oscillations the corresponding m^* is so small that the exponential approximation in the temperature dependence of the amplitude was inapplicable and a comparison with the hyperbolic sine function was required. Even so, the temperature dependence of the amplitude was such that only an upper limit could be assigned to the effective mass.

The dHvA parameters in Re have values typical of those for nontransition metals. In fact, the longest period oscillations observed are comparable with those which occur in semimetals and should be easily observable with greater precision in modest magnetic fields by means of torsion balance techniques.

Two oscillating terms were observed in Nb with the magnetic field approximately parallel to a [110] direction. These are pictured in Fig. 3, and the corresponding parameters are listed in Table I. It is probable that additional oscillating terms exist but were masked by collision broadening of the Landau levels. The relatively low resistivity ratio suggests that such broadening might be quite pronounced. Little can be said as yet regarding the origin of the dHvA oscillations in Nb except that those we observe are probably not due to electrons or holes in the first two bands. The free-electron sphere completely encloses the first Brillouin zone for a pentavalent bcc metal, and on the basis of a nearly free elec-

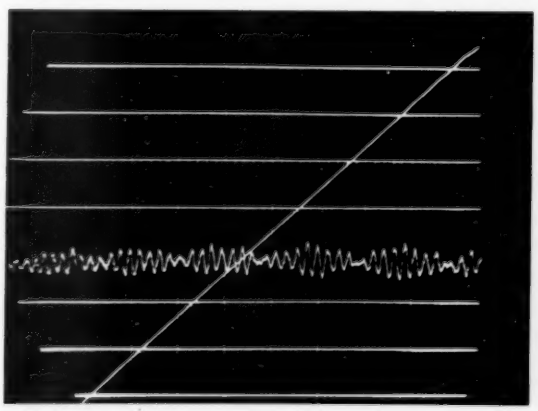

FIG. 3. de Haas–van Alphen effect in Nb at 1.14°K. The beating effect is due to two oscillating terms of different period and amplitude. The diagonal trace shows the field decreasing (from right to left) from 150.0 to 138.2 kilogauss during a sweep time of 1.6 milliseconds.

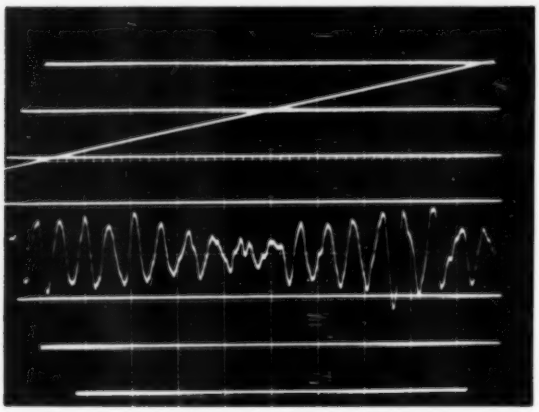

FIG. 4. de Haas–van Alphen effect in Ta at 1.13°K. The beating effect due to two oscillating terms can be seen as the field decreases (from right to left) from 141.6 to 134.9 kilogauss during a sweep time of 1.0 millisecond.

tron model[8,9] the holes in the second band would be expected to give rise to periods shorter than those observed.

Two oscillating terms were also observed in Ta (see Fig. 4), and the corresponding dHvA parameters are listed in Table I. Our measurements indicate that the shorter period term is quite sensitive to orientation, for it nearly disappeared when the sample was removed and remounted at a slightly different angle. It is interesting that Ta and Nb have the same valence and crystal structure, and have lattice parameters differing by less than one percent. For such a situation the nearly free electron model predicts almost identical periods. The observed differences (less than 50%) could be attributed to the difference in crystallographic orientation.

The authors wish to thank E. Buehler and J. E. Kunzler of Bell Telephone Laboratories for supplying the sample of Nb, J. I. Budnick of IBM Watson Research Laboratory for the Ta sample, and H. Nadler of this laboratory for the Re sample. We would also like to acknowledge many valuable discussions with R. E. Behringer.

*This research was supported by the U. S. Atomic Energy Commission.

[1]The Fermi Surface, edited by W. A. Harrison and M. B. Webb (John Wiley & Sons, Inc., New York, 1960).

[2]For a review see C. Herring, J. Appl. Phys. 31, 3S (1960).

[3]Shoenberg has reported periods for dHvA oscillations in W and Mo (reference 4). However, orientations and effective masses were not given.

[4]D. Shoenberg, Progress in Low-Temperature Physics, edited by C. J. Gorter (Interscience Publishers, Inc., New York, 1957), Vol. 2, pp. 226-65.

[5]D. P. Seraphim, J. I. Budnick, and W. B. Ittner, III, Trans. Am. Inst. Mining, Met., Petrol. Engrs. 218, 527 (1960).

[6]T. G. Berlincourt, Proceedings of the Seventh International Conference on Low-Temperature Physics, edited by G. M. Graham and A. C. Hollis Hallett (University of Toronto Press, Toronto, 1960), p. 231.

[7]A. C. Thorsen and T. G. Berlincourt, Phys. Rev. Letters 6, 617 (1961).

[8]A. V. Gold, Phil. Trans. Roy. Soc. (London) A251, 85 (1958).

[9]W. A. Harrison, Phys. Rev. 118, 1190 (1960).

FERROMAGNETIC EXCHANGE INTERACTION BETWEEN Mn^{2+} IONS IN Mn, ZnF_2

M. R. Brown, B. A. Coles, and J. Owen*
Clarendon Laboratory, Oxford, England

and

R. W. H. Stevenson
Marischal College, University of Aberdeen, Aberdeen, Scotland

(Received August 24, 1961)

Paramagnetic resonance techniques have been used to measure exchange interactions between nearest neighbor (nn) Mn^{2+} ions in mixed crystals of Mn, ZnF_2 with Mn:Zn ≈ 1:50. The two ions are separated by the short edge ($c \approx 3.2$ A) of the body-centered tetragonal unit cell. The general procedure has followed that used for previous investigations[1,2] of exchange-coupled pairs of spins, $S^i = S^j = \frac{5}{2}$.

The results can be described by the following spin Hamiltonians. For one ion of the pair, omitting interactions with the other ion,

$$\mathcal{H}^i = g\beta\vec{H}\cdot\vec{S}^i + D_c[(S_z^i)^2 - \tfrac{1}{3}S^i(S^i+1)] + E_c[(S_x^i)^2 - (S_y^i)^2], \qquad (1)$$

where $g = 2$, $S^i = \frac{5}{2}$, $D_c = -0.0135 \pm 0.004$ cm^{-1}, E_c

$= 0 \pm 0.006$ cm^{-1}. There is a similar Hamiltonian $\mathcal{H}^j$ for S^j. For the interacting pair the Hamiltonian is

$$\mathcal{H}^{ij} = \mathcal{H}^i + \mathcal{H}^j + J\vec{S}^i \cdot \vec{S}^j + D_e[3S_z{}^i S_z{}^j - \vec{S}^i \cdot \vec{S}^j], \quad (2)$$

where $J/k = -0.4 \pm 0.2$°K and $D_e = -0.051 \pm 0.009$ cm^{-1}. The z axis is parallel to c, that is, to the line joining the ions. The isotropic exchange term $J\vec{S}^i \cdot \vec{S}^j$ gives rise to states of total spin ($\vec{S} = \vec{S}^i + \vec{S}^j$) with $S = 0$, 1, 2, 3, 4, and 5, and with relative energies, 0, J, $3J$, $6J$, $10J$, and $15J$, respectively. Since J is negative for the present case, $S = 5$ is lowest and $S = 4$ is $5|J|$ higher in energy, and most of the measurements have been made on transitions within these two lowest total spin states.

The values of the parameters D_c and D_e, which determine the position and anisotropy of the lines in the spectrum, have been confirmed by fitting more than 20 transitions in the wavelength range 0.85 to 3.3 cm. The crystal-field contributions, $D_c = -0.0135$ cm^{-1}, $E_c = 0$, are of the same order as those found for isolated Mn^{2+} ions in very dilute crystals which are[3] $D_c = -0.0186$ cm^{-1}, $E_c = -0.0041$ cm^{-1}. The other contribution D_e appears to be consistent with the expected dipole-dipole interaction $-g^2\beta^2/r_{ij}{}^3$, since the value can be fitted by choosing $r_{ij} = 3.21$ A which lies between the expected[4] separations 3.13 A for ZnF_2 and 3.31 A for MnF_2.

The magnitude of the isotropic exchange J has been estimated by using intensity measurements to find the separation between different energy levels given by Eq. (2). This has involved the determination of the intensities of a number of lines in the spectrum both relative to each other and relative to a comparison specimen in the temperature range 1.5 to 20°K. All the measurements agree in giving the exchange ferromagnetic in sign and close to the value $J_{nn}/k = -0.4$°K. Preliminary measurements have also been made on next nearest neighbor (nnn) Mn-Mn pairs which give the approximate result $J_{nnn}/k = 4$°K (antiferromagnetic).

This preliminary result for next nearest neighbors is in reasonable agreement with a molecular field interpretation of the bulk properties of the antiferromagnetic MnF_2 as was expected. The ferromagnetic sign of the nearest neighbor exchange, on the other hand, was not expected. If, as seems reasonable, a similar ferromagnetic interaction is present in MnF_2, then in order to account for the susceptibility properties it may be necessary to assume appreciable antiferromagnetic exchange between further neighbors on the same magnetic sublattice, e.g., third, fourth, sixth, or seventh nearest neighbors.

Finally, it is of interest to note that the nearest and next nearest neighbor pair structure in MnF_2 is in some ways similar to that in MnO but the ratio J_{nnn}/J_{nn} is surprisingly different, being about -10 for MnF_2 and +1 for MnO.[1] This is not understood, but a possible explanation may be that there is direct ferromagnetic exchange of magnitude a few degrees Kelvin between nearest neighbors in both salts, and that this is the dominant interaction in MnF_2 where the antiferromagnetic superexchange interactions are smaller.

We would like to thank the General Electric Research Laboratory, Schenectady, and the British Board of Admiralty for supporting this work, and we are grateful to Dr. W. Marshall for helpful discussions.

---

*Royal Society Research Fellow.

[1]B. A. Coles, J. W. Orton, and J. Owen, Phys. Rev. Letters 4, 116 (1960).

[2]J. Owen, Suppl. J. Appl. Phys. 32, 213S (1961).

[3]M. Tinkham, Proc. Roy. Soc. (London) A236, 535 (1956).

[4]J. W. Stout and S. A. Reed, J. Am. Chem. Soc. 5, 5279 (1954).

POLARIZATION IN NEUTRON-PROTON SCATTERING BELOW 100 Mev

P. H. Bowen, G. C. Cox, G. B. Huxtable, A. Langsford, J. P. Scanlon, and J. J. Thresher*
Atomic Energy Research Establishment, Harwell, Berkshire, England
(Received August 17, 1961)

A systematic investigation of neutron-proton scattering in the energy range 20 to 120 Mev is being made by this group with the object of providing sufficient information for a phase-shift analysis of the $T=0$ state of the two-nucleon system. Since no polarization data on the n-p system have hitherto been available below 77 Mev, our first results appear to be of sufficient interest to publish at this stage.

A polarized neutron beam has been obtained from the neutron time-of-flight spectrometer of the Harwell cyclotron[1,2]; the beam polarization as a function of energy is given in Table I. Figure 1 is a schematic diagram of the apparatus. A liquid hydrogen target was placed at the end of the neutron flight path, and neutrons scattered by the target were detected by two large organic-liquid scintillation counters, placed symmetrically above and below the beam. In order to reject events in which a recoil proton from the hydrogen target was detected, anticoincidence counters were placed in front of the neutron counters. The polarizations were determined by measuring asymmetries in neutron scattering and, to reduce false asymmetries, a solenoid was used to rotate the polarization vector of the neutron beam alternately clockwise and anticlockwise through approximately 90°.[3] The use of a symmetrical two-counter system made it possible to analyze the data in such a way that the calculated scattering asymmetry was independent of the neutron beam intensity and the efficiencies of the counters. A beam monitor was necessary only to enable corrections for backgrounds to be made. These were determined in subsidiary measurements and were due to rescattering of neutrons from the walls of the experimental area after they had been scattered by the hydrogen target and to scattering of neutrons from the thin metal windows of the target.

Table I. Polarization of the neutron beam as a function of energy.

Neutron energy (Mev)	Neutron beam polarization
22.5	0.135 ±0.029
30	0.139 ±0.014
40	0.130 ±0.013
50	0.187 ±0.014
60	0.262 ±0.016
70	0.312 ±0.018
80	0.338 ±0.022
90	0.367 ±0.029

At neutron energies above 80 Mev, the number of detected neutrons varied rapidly with time of flight, and a small uncertainty in the alignment of the time spectra from the two neutron counters could have produced a large uncertainty in the measured asymmetry; for this reason it was necessary to reject most of the data at neutron energies above 85 Mev. Recent improvements in the electronic apparatus have virtually eliminated this source of error for future measurements.

The asymmetries were corrected for the effects of multiple scattering of neutrons in the hydrogen and its metal container. From preliminary estimates a correction factor which increases the asymmetry by about 13% of its value at 22.5 Mev, falling to 4.4% at 90 Mev, has been applied. The possible systematic error in making this correc-

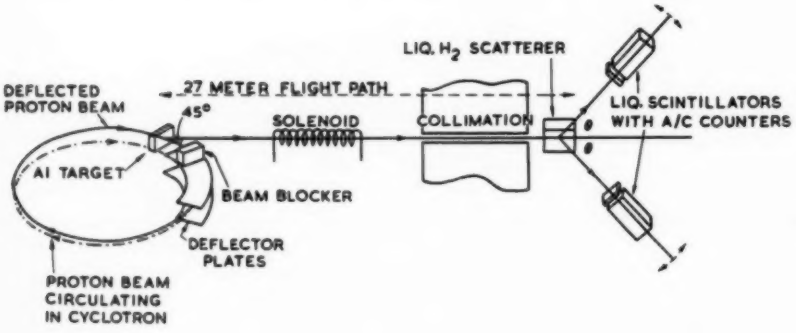

FIG. 1. Experimental arrangement—schematic diagram.

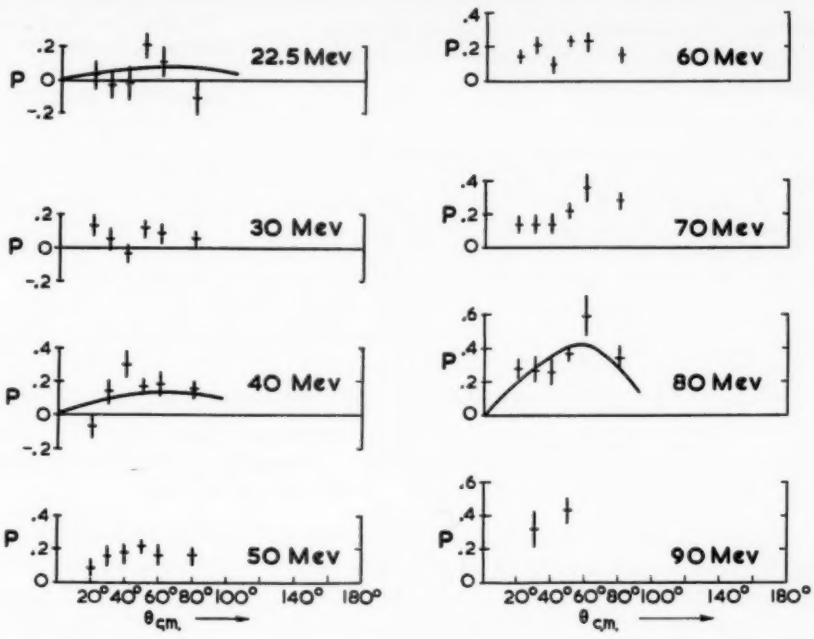

FIG. 2. Polarization in neutron-proton scattering. The curves are predictions of n-p polarization at 18, 40, and 77 Mev, made on the basis of the Signell-Marshak potential model.

tion, which should not be larger than the magnitude of the correction, has been combined with the somewhat larger statistical error in the measurement of beam polarization to give a "scale error" at each energy. The individual points on each curve have statistical errors which arise from the asymmetry measurements and are considerably larger than the scale errors.

The results have been grouped into 8 energy bands and are shown in Fig. 2 and Table II. At each energy, the over-all energy resolutions were obtained by combining the width of the energy band with the intrinsic energy resolution of the spectrometer. The results are in reasonable agreement with those obtained at 95 Mev[4] and 77 Mev[5] with considerably worse energy resolution.

Some predictions for n-p polarization, based on the Signell and Marshak potential model, are shown in Fig. 2 at 77 Mev[5] and at 18 and 40 Mev.[6]

The results presented here have enabled Phillips[7] to place some restrictions on proton-proton scattering phase shifts at low energies, assuming charge independence of nuclear forces.

A recent phase-shift analysis for the neutron-proton system,[8] which did not include the results presented here, has provided a number of possible sets of phase shifts, all of which give a good fit

Table II. Neutron-proton polarization as a function of energy and angle.

Nominal energy (Mev)	Total energy spread (Mev)	Scale error (%)	Neutron-proton polarization 20°	30°	40°	50°	60°	80°
22.5	5	25	0.03 ±0.09	-0.03 ±0.12	-0.02 ±0.10	0.20 ±0.08	0.10 ±0.09	-0.12 ±0.09
30	10	16	0.13 ±0.06	0.05 ±0.07	-0.04 ±0.06	0.11 ±0.04	0.08 ±0.06	0.05 ±0.04
40	10	12	-0.07 ±0.07	0.14 ±0.08	0.30 ±0.08	0.17 ±0.05	0.18 ±0.07	0.15 ±0.05
50	10	10	0.09 ±0.05	0.16 ±0.06	0.18 ±0.06	0.21 ±0.04	0.16 ±0.06	0.16 ±0.05
60	11	8	0.14 ±0.04	0.21 ±0.05	0.09 ±0.05	0.23 ±0.03	0.23 ±0.06	0.15 ±0.04
70	12	8	0.14 ±0.05	0.14 ±0.06	0.14 ±0.06	0.22 ±0.04	0.36 ±0.08	0.28 ±0.05
80	13	8	0.28 ±0.06	0.27 ±0.08	0.26 ±0.08	0.37 ±0.05	0.59 ±0.12	0.34 ±0.08
90	14	9		0.27 ±0.11		0.43 ±0.08		

to the present data.[8] Further measurements are, however, being made to reduce the statistical errors of the present data, and to extend the results to 160° c.m. and to 100 Mev.

---

*Now at the National Institute for Research in Nuclear Science, Harwell, Berkshire, England.

[1]J. P. Scanlon, G. H. Stafford, J. J. Thresher, and P. H. Bowen, Rev. Sci. Instr. 28, 749 (1957).

[2]P. H. Bowen, G. C. Cox, G. B. Huxtable, A. Langsford, J. P. Scanlon, and J. J. Thresher, Nuclear Instr. (to be published).

[3]P. Hillman, G. H. Stafford, and C. Whitehead, Nuovo cimento 4, 67 (1956).

[4]G. H. Stafford, C. Whitehead, and P. Hillman, Nuovo cimento 5, 1589 (1957).

[5]C. Whitehead, S. Tornabene, and G. H. Stafford, Proc. Phys. Soc. (London) 75, 345 (1960).

[6]J. Hamilton (private communication).

[7]R. J. N. Phillips, Nuclear Phys. 21, 686 (1961).

[8]M. H. Hull, Jr., K. E. Lassila, H. M. Ruppel, F. A. McDonald, and G. Breit, Phys. Rev. 122, 1606 (1961).

EVIDENCE FOR CHARGE INDEPENDENCE IN MEDIUM WEIGHT NUCLEI*

J. D. Anderson and C. Wong
Lawrence Radiation Laboratory, University of California, Livermore, California
(Received July 26, 1961)

The importance of isotopic spin considerations ($\Delta T = 0$) in "mirror nuclei" (p,n) reactions has been pointed out by Bloom et al.[1] If one goes to nonmirror nuclei such as V^{51}, Cr^{51}, the (p,n) reaction is assumed to go as follows: The incoming proton reacts with an $f_{7/2}$ neutron, exchanges its charge, and is emitted as a neutron. In the initial state there are eight $f_{7/2}$ neutrons available and three $f_{7/2}$ protons. Since, by definition of isotopic spin state (charge independence), all the nuclear interactions within the initial and final nucleus are the same, the Q for the (p,n) reaction between V^{51} ($T = \frac{5}{2}$) and its analog state in Cr^{51} is the Coulomb energy difference. It is the purpose of this Letter to point out that direct-reaction neutrons from the (p,n) reaction on medium weight nuclei do indeed leave the residual nucleus in a state which is the analog of the ground state of the bombarded nucleus.

It was pointed out previously[2] that the energy and angular distribution of the continuum neutrons from the $V^{51}(p,n)Cr^{51}$ reaction are in agreement with predictions of the statistical model of the compound nucleus for proton bombarding energies up to 8 Mev. Using time-of-flight techniques[2,3] to measure the neutron spectra, direct-reaction neutrons are observed for proton bombarding energies above 10 Mev. These neutrons do not come from groups leaving Cr^{51} in low-lying states as might be expected from a simple Born approximation calculation in which one considers only the radial overlap of the wave functions describing the initial and final states. These neutrons are observed to come from a level (or levels) in Cr^{51} at 6.5 Mev.

Neutron spectra at $\theta_L = 23°$ have been measured for proton energies between 9 and 13 Mev using a self-supporting 8-mg/cm² vanadium foil and a 10-meter flight path. The neutron spectra for three incident proton energies are shown plotted in Fig. 1. The compound statistical model predicts that if a sufficient number of nuclear levels are involved in both the compound nucleus and the residual nucleus, the energy distribution of neutrons emitted is given by

$$P(E)dE = KE\omega(E_{\text{excit}})\sigma_c(E)dE,$$

where $\omega(E_{\text{excit}})$ is the level density of the residual nucleus at its excitation energy, which is determined by the incident proton energy, the Q value of the reaction, and the emitted neutron energy; $\sigma_c(E)$ is the reaction cross section for the inverse reaction between the excited residual nucleus and a neutron of energy E; and the constant K is a function of the incident proton energy. Assuming that $\sigma_c(E)$ is a slowly varying function of neutron energy, the energy dependence of the level density of the residual nucleus is proportional to $P(E)/E$. The relative neutron spectra transformed to the center-of mass system and divided by the energy of the emitted neutron in the c.m. system are plotted as a function of the excitation of the residual nucleus in Fig. 2. From Fig. 2 it is clear that $P(E)/E$ (allowing for the change in energy resolution as a function of neutron energy) is only a function of the excitation of the residual nucleus up to $E_{\text{excit}} = 6.5$ Mev, indicating the assumption of compound nucleus formation in this region is valid. However, a fluctu-

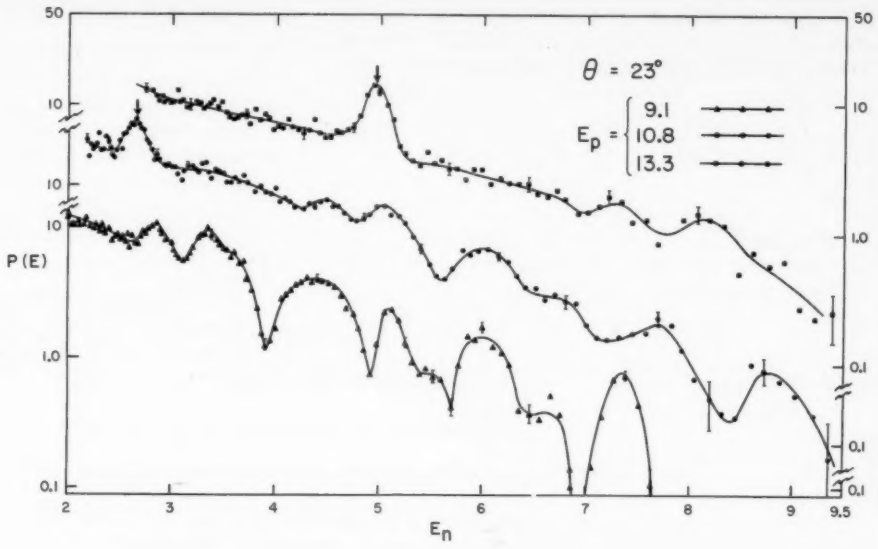

FIG. 1. Neutron spectra from proton bombardment of V^{51}.

ation in level density of a factor of 2 to 3 at E_{excit} = 6.5 Mev with a hundred levels being involved is incompatible with this level (or levels) being populated by a compound nucleus. As one increases the proton bombarding energy the continuum neutron cross section (E_{excit} = 6.5 Mev) decreases from 17 mb/sr Mev at E_p = 10.8 Mev to 4.5 mb/sr Mev at E_p = 13.3 Mev, while the cross section for the "level" remains at 2 mb/sr. The decrease in cross section for the continuum neutrons is in excellent agreement with our previous measurement of the Cr^{51} level density[2,4] and is to be expected on the basis of a compound nucleus while the direct-reaction cross section is expected to vary only slowly with energy which is borne out by the present experimental data. Thus it is concluded that the level at 6.5 Mev in Cr^{51} is excited via a direct reaction.

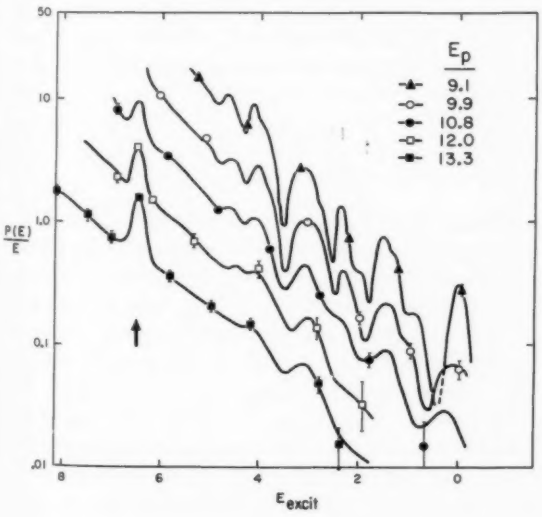

FIG. 2. The neutron spectra transformed to the center-of-mass system and divided by the energy of the emitted neutron are plotted as a function of the excitation of the residual nucleus Cr^{51}. The arrow denotes the position of the analog state.

If one calculates the V^{51}-Cr^{51} Coulomb energy difference using the results of Swamy and Green,[5] one obtains ΔE_C = 8.2 Mev for $R = 1.25A^{1/3}$ f. This is in excellent agreement with our measured value of 8.0 ± 0.2 Mev. [This is the (p,n) ground state Q(-1.54 Mev) plus the residual excitation in Cr^{51} (6.5 Mev).] Our conclusion is that the level in Cr^{51} at 6.5-Mev excitation is the analog of the ground state of V^{51} and is therefore a $T = \frac{5}{2}$ state.

Additional evidence for analog states is found in the $Fe^{56}(p,n)Co^{56}$ and $Co^{59}(p,n)Ni^{59}$ neutron spectra. Our Q values for the (p,n) reaction to the analog states are again in excellent agreement (see Table I) with the Coulomb energy differences calculated from reference 5.

Further experiments involving additional target nuclei and measurements of the angular distributions of the direct-reaction group are currently under way.

It is a pleasure to acknowledge the assistance of

Table I. Q values for the (p,n) reactions to the analog state.

	Q (measured) (Mev)	ΔE_C (calculated) (Mev)
$V^{51}(p,n)Cr^{51}$ [a]	8.0 ± 0.2	8.2
$Fe^{56}(p,n)Co^{56}$ [a]	8.9 ± 0.2	9.0
$Co^{59}(p,n)Ni^{59}$ [a]	9.1 ± 0.2	9.2

[a]Denotes isotopic spin analog state.

J. W. McClure and B. D. Walker in obtaining the data and of S. D. Bloom in its interpretation.

*This work was done under the auspices of the U. S. Atomic Energy Commission.

[1]S. D. Bloom, N. K. Glendenning, and S. A. Moszkowski, Phys. Rev. Letters 3, 98 (1959).
[2]R. D. Albert, J. D. Anderson, and C. Wong, Phys. Rev. 120, 2149 (1960).
[3]C. Wong, J. D. Anderson, C. C. Gardner, J. W. McClure, and M. P. Nakada, Phys. Rev. 116, 164 (1959).
[4]J. D. Anderson, C. Wong, J. W. McClure, and B. D. Walker (to be published).
[5]N. Swamy and A. Green, Phys. Rev. 119, 1719 (1958).

PHOTODISINTEGRATION OF POLARIZED AND ALIGNED DEUTERONS*

W. Zickendraht, D. J. Andrews, and M. L. Rustgi†
Yale University, New Haven, Connecticut
(Received August 7, 1961)

Information regarding dynamic and electromagnetic properties of the two-nucleon system obtainable from the photodisintegration of the deuteron can be extended by employing aligned and polarized deuterons. In the present note a partial and preliminary survey of the possibilities is attempted by confining oneself to unpolarized gamma rays and to differential cross sections without a consideration of the polarization of ejected nucleons. Since, as will be seen below, the effects of alignment are quite pronounced, one may hope that the assumptions underlying the usual theories of the photodisintegration process can receive a more thorough test by comparison of theory and experiment even to the limited extent gone into here. The calculations reported on have been made by employing a previously described arrangement[1] in terms of probability amplitudes S_{mi} corresponding to final states with combined proton-neutron spin projection m arising from initial states with spin orientation i. A modified Signell-Marshak potential, referred to as Potential I in reference 1, was used at six photon energies in approximation E in which all transitions of types $E1$, $M1$, and $E2$ are considered in the nonretarded approximation.

The line of orientation axis determined by the direction of fields external to the deuteron is a convenient choice for the quantization axis. In thermal equilibrium one deals essentially with a statistical mixture of magnetic substates with in general unequal population probabilities and without correlation. The calculations reported on are concerned with this somewhat idealized situation. Denoting the relative population numbers of the magnetic substates μ by w_μ with the normalization

$$w_1 + w_0 + w_{-1} = 1, \tag{1}$$

the polarization parameter P_1 and the alignment parameter P_2 in the notation of Blin-Stoyle and Grace[2] are, respectively,

$$P_1 = w_1 - w_{-1}, \tag{2}$$

$$P_2 = w_1 - 2w_0 + w_{-1} = 3(w_1 + w_{-1}) - 2. \tag{3}$$

Equations (1), (2), and (3) determine w_1, w_0, w_{-1} and therefore the w_μ are determined by the specification of P_1 and P_2. Consequently the cross section is expressible in terms of P_1 and P_2. From (2) and (3) and the inequalities $0 \leq w_\mu \leq 1$, $w_1 + w_{-1} \leq 1$ it is seen that $-1 \leq P_1 \leq +1$, the lower and upper limits corresponding to $(w_1, w_{-1}) = (0, 1)$ and $(1, 0)$, respectively. Similarly $-2 \leq P_2 \leq 1$, the lower limit corresponding to $w_0 = 1$ and the upper to $w_0 = 0$.

Parallel and perpendicular arrangements of the orientation axis relatively to the gamma-ray beam direction will be distinguished, respectively, by subscripts l for longitudinal, and t for transverse. In the longitudinal case the differential cross section for protons with unpolarized γ rays is

$$\sigma_l(\theta) = a + bS^2 + cC + dS^2C + eS^2C^2 + P_2[-2g - 2hC - (2i+j)S^2 - (2k+l)S^2C - (2m+n)S^2C^2 - pS^4C - qS^4C^2], \tag{4}$$

where

$$S=\sin\theta, \quad C=\cos\theta. \tag{4'}$$

The coefficients are given in Table I. The angle between the direction of the ejected proton and the gamma-ray beam is denoted by θ. The angular distribution is obviously axially symmetric in this case and θ suffices for the specification of σ_l. The polarization parameter P_1 does not enter Eq. (4), since the levels $\mu=\pm1$ contribute equally to σ_l, as may be seen by analyzing the incident beam in terms of circularly polarized photons. Reflection in a plane through the photon beam axis shows in fact that right-handed photons incident on $\mu=+1$ contribute equally with left-handed ones on $\mu=-1$ and vice versa.

If the orientation axis is perpendicular to the γ-ray beam, it is convenient to use polar coordinate angles (θ, Φ) for the proton direction with the photon beam as polar axis and the azimuthal angle Φ measured from the orientation axis in the right-handed sense. The differential cross section for protons in this "transverse" case is

$$\sigma_t(\theta,\Phi)=a+bS^2+cC+dS^2C+eS^2C^2+P_2\{g+hC+iS^2+kS^2C+mS^2C^2+[jS^2+lS^2C+nS^2C^2+pS^4C+qS^4C^2]\cos^2\Phi\}$$
$$+P_1\{S[r+sC+tS^2+uS^2C]\sin\Phi\}. \tag{5}$$

For checking calculations and possibly also experiments, it is useful to have available the relation

$$\tfrac{1}{3}[\sigma_t(\theta,\Phi)+\sigma_t(\theta,\Phi+\pi/2)+\sigma_l(\theta)]_{0,-2}=[\sigma(\theta)]_{0,0}. \tag{6}$$

The values of P_1, P_2 are here indicated as subscripts. The left-hand side refers to complete alignment and zero polarization, the right-hand side to unoriented deuterons. The relation follows from the fact that $P_1=0$, $P_2=-2$ corresponds to $w_1=w_{-1}=0$, $w_0=1$ which implies that, keeping the proton direction fixed, the three cross sections correspond to a complete set of three mutually orthogonal spin functions.

The coefficients a, b, etc., which occur in Eqs. (4), (5) are listed in Table I for the same values of the incident gamma-ray energy E_γ as in reference 1. The dependence of $\sigma_l(\theta)$, $\sigma_t(\theta,0)$, $\sigma_t(\theta,\pi/2)$ on θ is shown in Figs. 1, 2, 3, respectively, for $E_\gamma=22.2$ Mev and 102.2 Mev. The differential cross section $\sigma(\theta)$ for the unoriented case is shown for comparison by the dashed curves when this is feasible. The plots refer to three cases I, II, III corresponding to cross sections $\sigma_{\rm I}$, $\sigma_{\rm II}$, $\sigma_{\rm III}$, respectively. Case I corresponds to complete alignment along the orientation axis and zero polarization, i.e., $P_1=0$, $P_2=1$, $w_1=w_{-1}=\frac{1}{2}$, $w_0=0$. Case II similarly represents the condition for the opposite extreme of the alignment parameter and zero polarization, i.e., $P_1=0$, $P_2=-2$, $w_1=w_{-1}=0$, $w_0=1$. The case of maximum polarization and alignment along the orientation axis is obtained if $w_1=1$, $w_0=w_{-1}=0$,

Table I. Values of coefficients for Eqs. (4) and (5).

E_γ (Mev)	a	b	c	d	e	g	h	i	j	k
22.2	5.26	51.6	0.844	15.5	1.16	0.83	0.104	0.111	-4.57	0.115
32.2	5.57	29.1	1.04	10.9	1.00	1.01	0.105	0.329	-5.76	0.393
62.2	5.42	7.54	1.05	4.41	0.67	1.45	0.094	0.529	-7.14	0.932
102.2	4.11	2.50	0.796	2.01	0.401	1.14	0.053	0.426	-5.56	0.82
152.2	2.87	1.18	0.616	1.02	0.219	0.766	0.044	0.35	-3.97	0.525
177.2	2.45	1.13	0.582	0.876	0.175	0.58	0.035	0.411	-3.57	0.455

	l	m	n	p	q	r	s	t	u
22.2	7.10	-0.029	29.9	-8.78	-0.768	-0.906	-3.40	0.812	0.046
32.2	6.79	0.021	25.9	-9.30	-0.795	-0.688	-3.29	0.874	0.065
62.2	4.63	0.15	16.2	-8.03	-1.07	-0.177	-0.569	0.874	0.178
102.2	2.98	0.16	9.74	-5.61	-0.885	-0.008	0.405	0.746	0.222
152.2	1.92	0.10	6.18	-3.64	-0.623	0.061	0.561	0.502	0.194
177.2	1.74	0.085	5.80	-3.28	-0.552	0.076	0.508	0.424	0.169

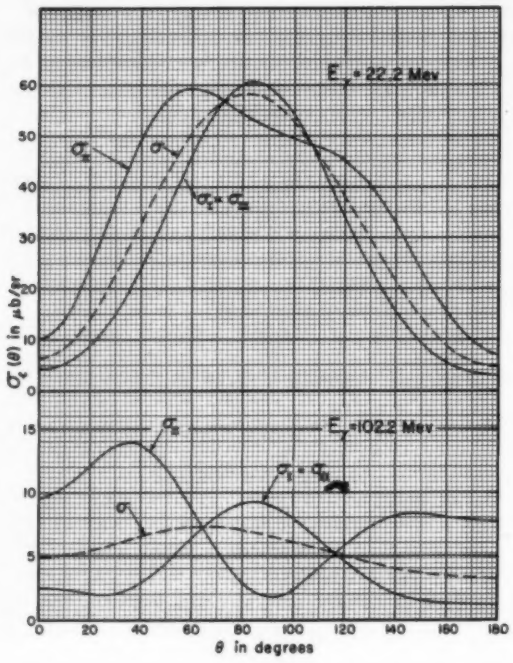

FIG. 1. Differential cross section for the $d(\gamma,n)p$ reaction with unpolarized gamma rays of energy 22.2 and 102.2 Mev and orientation axis being along the gamma-ray beam. Subscripts I, II, III correspond to (P_1, P_2) having the values (0,1), (0,-2), (1,1), respectively.

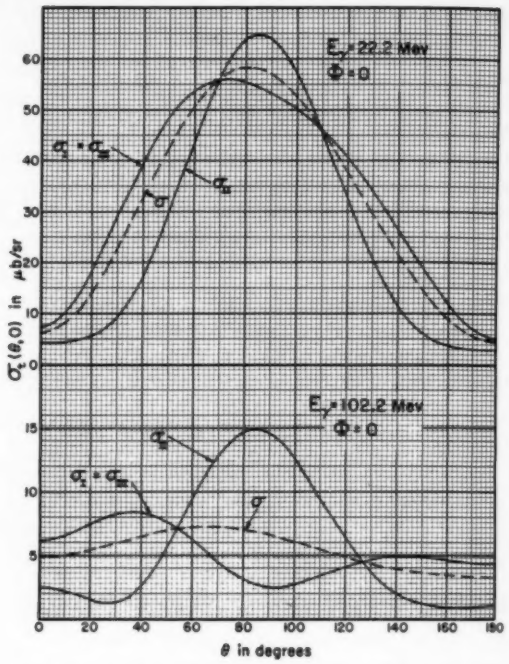

FIG. 2. Differential cross section for the $d(\gamma,n)p$ reaction with unpolarized gamma rays for orientation axis perpendicular to gamma-ray beam and proton direction in the plane of these two directions. Other conventions as in Fig. 1.

for which $P_1 = P_2 = 1$. This condition is referred to as Case III. The cross section for any values of P_1 and P_2 is obtainable from the graphs by means of

$$\sigma(\theta,\Phi;P_1,P_2) = (\tfrac{2}{3}+\tfrac{1}{3}P_2 - P_1)\sigma_{\mathrm{I}} + (\tfrac{1}{3}-\tfrac{1}{3}P_2)\sigma_{\mathrm{II}} + P_1\sigma_{\mathrm{III}}. \quad (7)$$

The differential cross section for unoriented deuterons is obtainable according to this formula as $\sigma = (2\sigma_{\mathrm{I}} + \sigma_{\mathrm{II}})/3$. The difference between σ_{II} and σ is therefore expected to be larger in absolute value than that between σ_{I} and σ.

According to (4) and (5), the polarization parameter P_1 does not affect either $\sigma_l(\theta)$ or $\sigma_t(\theta,0)$. Its effect on $\sigma_t(0,\pi/2)$ is also small as is seen from Fig. 3 and the fact that according to Eq. (7) P_1 enters through $(\sigma_{\mathrm{III}} - \sigma_{\mathrm{I}})P_1$.

The authors are indebted to Professor G. Breit for many valuable consultations and particularly for having planned the arrangement of the calculation[1] in terms of amplitudes with a view towards

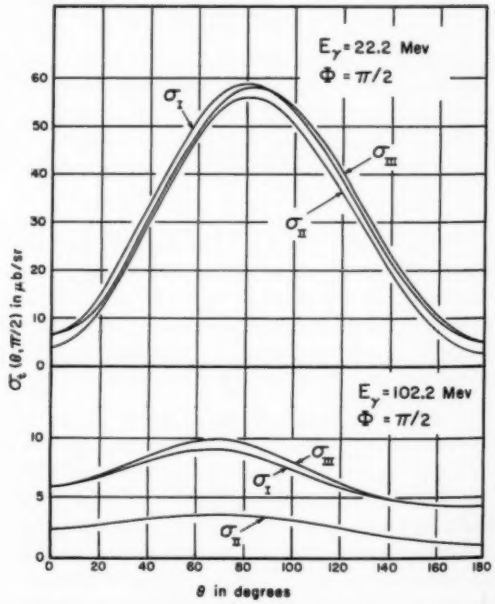

FIG. 3. Differential cross section for the $d(\gamma,n)p$ reaction with unpolarized gamma rays for the case of gamma-ray beam and proton directions both perpendicular to the orientation axis. Other conventions as in Fig. 1.

extensions such as that reported on here.

---

*This research was supported by the U. S. Air Force under a grant monitored by the Air Force Office of Scientific Research of the Office of Aerospace Research and by the U. S. Atomic Energy Commission.

†Now at Harvard University, Cambridge, Massachusetts.

[1]M. L. Rustgi, W. Zernik, G. Breit, and D. J. Andrews, Phys. Rev. 120, 1881 (1960). The convention regarding the definition of E_γ used in that reference is followed here.

[2]R. J. Blin-Stoyle and M. A. Grace, Handbuch der Physik, edited by S. Flügge (Springer-Verlag, Berlin, 1957), Vol. 42, p. 555, especially pp. 557-559.

K_2^0 DECAYS AND INTERACTIONS*

D. Luers,† I. S. Mittra, W. J. Willis, and S. S. Yamamoto
Brookhaven National Laboratory, Upton, New York
(Received August 29, 1961)

We have performed an experiment with low-energy K_2^0 mesons in the BNL 20-in. hydrogen bubble chamber. In this Letter, we wish to report results of two types: those bearing on the structure of the strangeness-changing weak interaction; and those which give information concerning K^0p and $\bar{K}^0p$ interactions.

The beam was made by 1250 ± 40 Mev/c π^- on a CH_2 target. K_2^0's at 47° in the lab were selected, and charged particles were removed by a sweeping magnet before the beam passed into the chamber, some 110 in. from the target. The direction of the K_2^0 beam in the chamber is known to ±2° but the momentum has a spread from ~200 to ~650 Mev/c, due to associated production of both Λ^0K^0 and Σ^0K^0, Fermi momentum in the target, etc.

We have made the usual assumptions (consistent with our observations) that the only common modes of K_2^0 decay into charged particles are[1]:

$$K_2^0 \to \pi^\pm + e^\mp + \nu,$$

$$K_2^0 \to \pi^\pm + \mu^\mp + \nu,$$

$$K_2^0 \to \pi^\pm + \pi^- + \pi^0,$$

which we shall call $\pi e\nu$, $\pi\mu\nu$, and $\pi\pi\pi$.

Under the present conditions, the K_2^0 momentum is calculable from measurements of the decay particles but is not overdetermined. (There is in general an ambiguity in the momentum which is not serious for the present analysis.) The most serious backgrounds, $\pi\mu$ and μe decays in flight, which might be interpreted as neutral decays, were eliminated by restrictions on the events which also threw out a small and calculable fraction of the K_2^0 decays (4 to 6% for the different decay modes).

A sample of 124 identified $\pi e\nu$ decays was obtained by identifying all electrons with momentum < 200 Mev/c by bubble density. Any track which was not clearly identified on inspection was measured by gap counting.[2] (A muon at the limiting momentum has $1/\beta^2 = 1.29$.) The remainder of the events was classified into two groups, one containing 52 events which gave a physical value of the K_2^0 momentum when interpreted as a $\pi\pi\pi$ decay, and a group of 222 events which are $\pi e\nu$ or $\pi\mu\nu$.

If polarizations are not measured, the configuration of a three-body decay is specified by two variables. We choose to use the energy of the charged particles in the center-of-mass system of the K_2^0. For each configuration, we have determined the probability of identifying a $\pi e\nu$ and of not rejecting each of the modes. This involves integrating over the uninteresting angles and over the experimentally observed K_2^0 spectrum. Given this information, we are prepared to make several comparisons with the theory.

1. The ratio $\pi^-e^+\nu/\pi^+e^-\nu = 1.16 \pm 0.17$. This ratio is one if CP is conserved, but no larger than 1.08 in any case.[3]

2. Pais and Treiman[4] have shown that the electron energy spectrum in the $\pi e\nu$ decay for a given pion energy has a form which is dependent only on the type of interaction involved. The pion spectrum is given, to be multiplied by a form factor which is expected to be roughly constant.[4-6] We have divided the Dalitz plot into three strips in T_π, each of which is subdivided as shown in Fig. 1.

We multiply the probability for observation and detection at each point times the expected distribution function for pure scalar, vector, and tensor interactions and integrate over each region. Theory and experiment are normalized to one in regions 1 and 2; 3, 4, and 5; and 6, 7, 8, and 9; thereby giving a comparison essentially

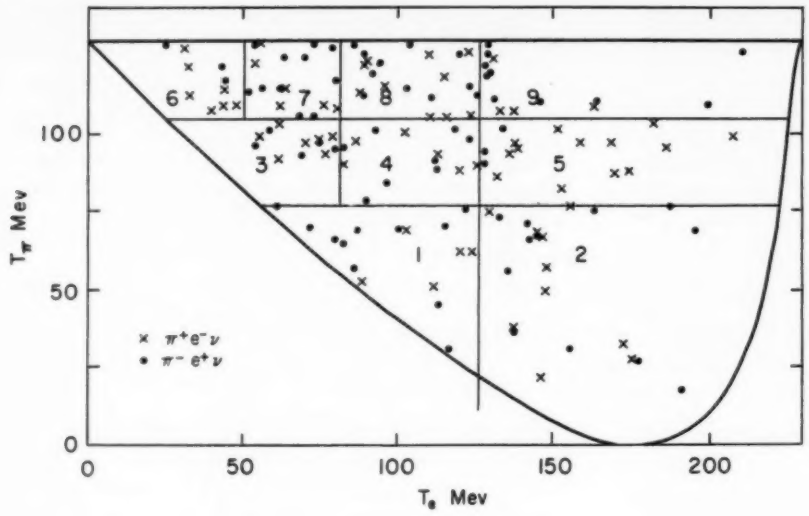

FIG. 1. Regions on Dalitz plot for $\pi e\nu$ to be used for comparison with experiment are shown, together with the distribution of events.

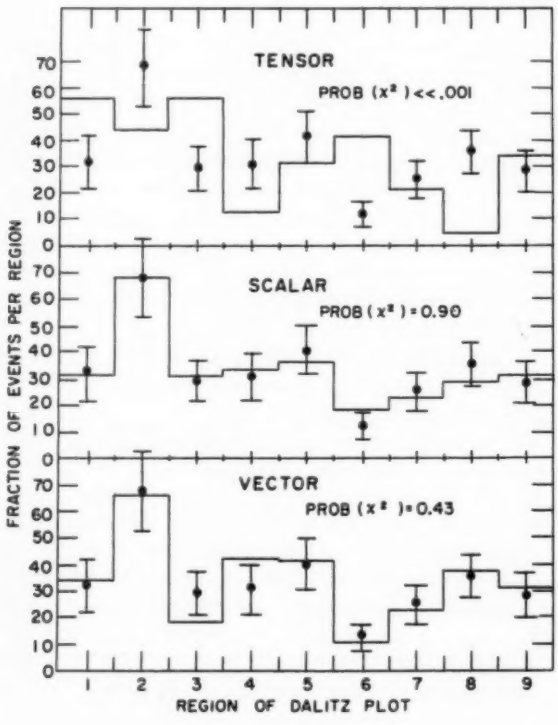

FIG. 2. Comparison of $\pi e\nu$ events with theory. Histograms represent the theoretical distribution of events, corrected for detection efficiency and normalized in each set of regions with the same range of T_π.

independent of the form factor. The results are shown in Fig. 2. Tensor is excluded; scalar and vector are allowed.

3. If the interaction is assumed to be scalar, the form factor is found to increase by a factor of ~14 from the region with $T_\pi < 76$ Mev to the region with $T_\pi > 104$ Mev. Such a large increase with pion energy is not expected, and probably allows this interaction to be excluded.

4. The vector form factor (Fig. 3) is roughly constant. The conclusion, then, is that the data are consistent with a pure vector interaction—in agreement with the universal V-A theory.[7]

5. If that part of the form factor due to strong interactions is constant, and an intermediate boson exists, the energy dependence of the form factor may be given in terms of the boson mass,[8] as shown by the curves on Fig. 3. From the present data a boson with mass >500 Mev/c^2 cannot be excluded.

6. The detection and identification probabilities may be integrated over all the decay configurations with weights appropriate to the vector interaction. This allows the $\pi e\nu$ branching ratio to be determined. The number of $\pi e\nu$ (0.1%) and $\pi\mu\nu$ (4.4%) in the sample fitting $\pi\pi\pi$ may be calculated. This allows a complete set of K_2^0 branching ratios into charged modes to be given in Table I.

7. Given the $\Delta I = \frac{1}{2}$ rule,[9] the $\Delta I = \frac{1}{2}$ current rule,[10] and the K^+ branching ratios[11] and lifetime, the K_2^0 branching ratios may be predicted, Table I. There is reasonable agreement with the exper-

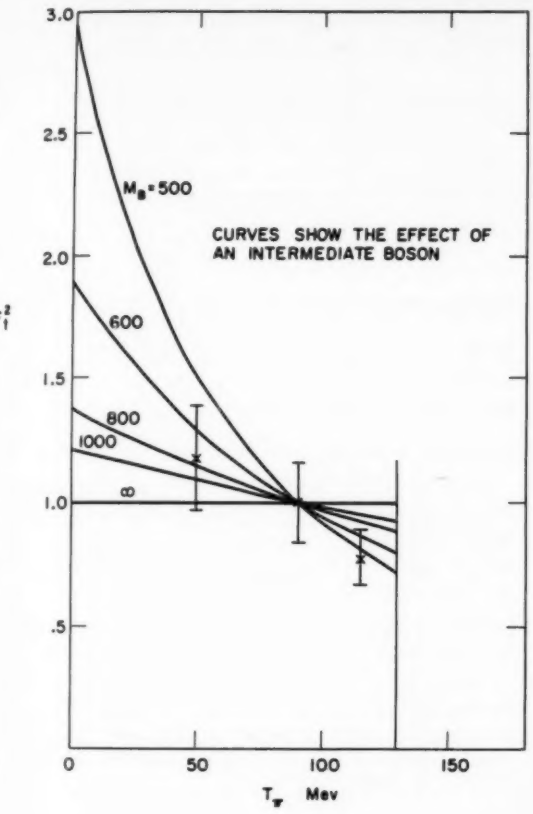

FIG. 3. The square of the form factor for $\pi e\nu$ decay with vector interaction. The curves show the form-factor dependence due to a possible intermediate boson.

imental numbers. If a $\Delta I = \frac{3}{2}$ current is assumed, together with $\Delta S = \Delta Q$,[10] the numbers obtained, also in Table II, are in disagreement with the experiment. Since there is evidence for $\Delta I = \frac{1}{2}$, but little information concerning the currents, we see this as a test of the current rule.

8. The π^0 energy spectrum in $\pi\pi\pi$ decay has been given by Weinberg[12] and Sawyer and Wali[13] as $W(T_{\pi 0}) = (1 + aT_{\pi 0})$(phase space). Using the $\Delta I = \frac{1}{2}$ rule, he predicts $a = -0.0109 \pm 0.022$. We find $a = 0.0171 \pm 0.0065$.

We turn now to the interactions. We have observed 111 events representing comparable numbers of

$$K_2^0 + p \to K_1^0 + p,$$
$$K_2^0 + p \to \Lambda^0 + \pi^+,$$
$$K_2^0 + p \to \Sigma^0 + \pi^+.$$

Biswas[14] has pointed out that a measurement of $K_1^0 p/(\Lambda^0\pi^+ + 2\Sigma^0\pi^+)$ provides a method for distinguishing among the various scattering length solutions for $\bar{K}p$ interactions, if the K^+-N scattering is known.

Unfortunately, most of our K_2^0's have a momentum greater than the limit of applicability of the zero-range theory (estimated to lie between 200 and 300 Mev/c).[15] The results are given in Fig. 4. Also shown are shaded regions indicating the result which might be expected, within the errors on the scattering lengths, using the $\bar{K}$ scattering lengths given by a recent χ^2 analysis of K^--p interactions.[16] Also shown are the range of expected values for the ratio at 175 Mev/c, using the four Dalitz solutions[17] to the same data: The momentum dependence is similar to that of solutions (1) and (2). Our data would seem to agree better

Table II. Values of the quantity $\epsilon = \Lambda^0/(\Lambda^0 + \Sigma)$, $T = 1$.

K momentum (Mev/c)	ϵ
0	$0.5^{+0.35}_{-0.15}$ [a]
~175	0.40 ± 0.03 [b]
~230	0.33 ± 0.14
~360	0.19 ± 0.07
~500	0.32 ± 0.08

[a] From K^--p data, quoted in reference 17.
[b] From K^--p data, reference 16.

Table I. Experimental branching ratios for charged modes of K_2^0 decays, together with predictions based on the $\Delta I = \frac{1}{2}$ rule and the $\Delta I = \frac{1}{2}$ and $\Delta I = \frac{3}{2}$ current rules. The ratio $\pi\mu\nu/\pi e\nu$ is given because the individual errors are correlated.

Quantity	Experiment	$\Delta I = \frac{1}{2}$ current	$\Delta I = \frac{3}{2}$ current
$\pi e\nu$	48.4 ±5 %	40.5 ±4.5%	27.4 ±3%
$\pi\mu\nu$	38.2 ±8 %	43.4 ±4.5%	29.1 ±3%
$\pi\pi\pi$	13.4 ±1.8%	16.1 ±1.0%	43.5 ±4%
$\pi\mu\nu/\pi e\nu$	0.79 ±0.19	1.06 ±0.15	1.06 ±0.15

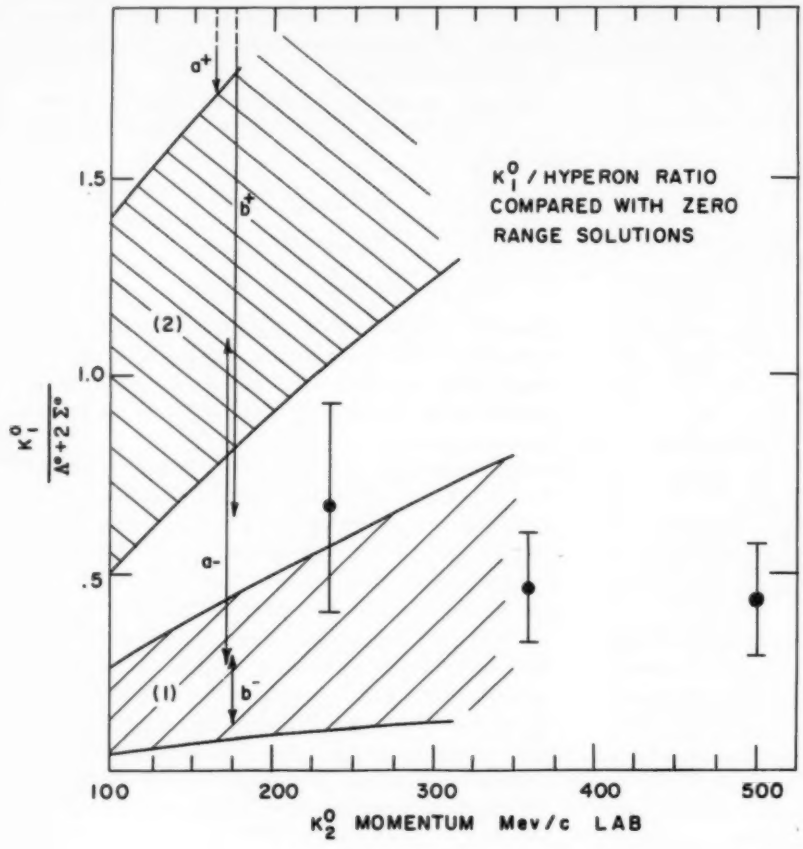

FIG. 4. The experimental values of $K_1^0/(\Lambda^0+2\Sigma^0)$ compared with the approximate values expected from K^+- and K^--nucleon scattering.

with solution (1) than with solution (2), or better with a^- or b^- than with a^+ or b^+, or, in general, with a $T=1$ scattering length which is not large and positive. A more quantitative conclusion must await consideration of effective-range effects.

We have also measured the ratio $\epsilon=\Lambda^0/(\Lambda^0+\Sigma)$, $T=1$, using the charge-independent relation $\Sigma^0\pi^+=\Sigma^+\pi^0$ for $\bar{K}^0$-p, which is a pure $T=1$ state. The results, with some K^--p values,[16,17] are given in Table II.

We would like to acknowledge the aid of Dr. E. L. Hart and Dr. P. C. Connelly.

---

*Research carried out under the auspices of the U. S. Atomic Energy Commission.

†On leave from Max-Planck Institut für Physik, Munich, Germany.

[1]M. Bardon, K. Lande, and L. M. Lederman, Ann. Phys. 5, 156 (1958).

[2]W. J. Willis, Phys. Rev. 116, 753 (1959). (For a more detailed description of our method and results, see R. Lea and C. Vittitoe, submitted to the Review of Scientific Instruments.)

[3]S. Weinberg, Phys. Rev. 110, 782 (1958).

[4]A. Pais and S. B. Treiman, Phys. Rev. 105, 1616 (1957). In this paper it is actually the angular correlation function which is calculated; we have transformed this into an energy correlation function.

[5]S. W. McDowell, Phys. Rev. 116, 1047 (1959).

[6]J. Bernstein and S. Weinberg, Phys. Rev. Letters 5, 481 (1960).

[7]R. Feynman and M. Gell-Mann, Phys. Rev. 109, 193 (1958).

[8]N. Brene, L. Egardt, and B. Quist, Nuclear Phys. 22, 553 (1961).

[9]R. H. Dalitz, Proc. Phys. Soc. (London) A69, 527 (1956).

[10]R. E. Behrends and A. Sirlin, Phys. Rev. 121, 324 (1961).

[11]D. Sinclair and J. Vandervelde (private communication).

[12]S. Weinberg, Phys. Rev. Letters 4, 87 (1960), Phys. Rev. Letters 4, 585 (1960).

[13]R. F. Sawyer and K. C. Wali, Nuovo cimento 17, 938 (1960). These authors point out that this may not be a good test of the $\Delta I=\frac{1}{2}$ rule.

[14]N. N. Biswas, Phys. Rev. 118, 866 (1960).
[15]R. H. Dalitz and S. F. Tuan, Ann. Phys. 3, 307 (1960).
[16]W. Humphrey and R. R. Ross (private communication). The real and imaginary parts of the scattering length used were: solution (1), $a_1 = 0.02 \pm 0.33$, $b_1 = 0.384 \pm 0.08$; solution (2), $a_1 = 1.2 \pm 0.06$, $b_1 = 0.56 \pm 0.15$. For the positive-strangeness scattering lengths, we have used $a_1 = -0.36 \pm 0.02$, and $a_0 = -0.20$ to -0.05, the latter in some doubt: see W. Chinowsky, G. Goldhaber, S. Goldhaber, W. Lee, T. O'Halloran, T. Stubbs, W. E. Slater, D. H. Stork, and H. K. Ticho, Proceedings of the 1960 Annual International Conference on High-Energy Physics (Interscience Publishers, Inc., New York, 1960), p. 451.
[17]R. H. Dalitz, Revs. Modern Phys. 33, 471 (1961).

METHOD FOR DETERMINING THE SPIN OF THE K-π RESONANCE

David O. Caldwell*
CERN, Geneva, Switzerland
(Received June 12, 1961; revised manuscript received August 31, 1961)

In order to understand the recently observed[1] resonance in the K-π system, which is here labeled K^*, it is essential to determine its spin. Recently there have appeared arguments[2] favoring a spin of 1 and a proposal[3] for determining the spin. The appearance of the latter has prompted the writing of this note describing a method of spin determination which may be simpler experimentally and can perhaps provide more information than that of reference 3. It has been tacitly assumed in that paper that the measurements[1] limit the K^* spin to 0 or 1 and the isotopic spin to 1/2, and that because the decay $K^* \to K + \pi$ is seen to be rapid, parity is conserved and hence the K^* has either spin 0 and parity opposite to that of the K, or spin 1 and the same parity as the K. Under these same restrictions, if one observes the process

$$K + \mathrm{He}^4 \to K^* + \mathrm{He}^4, \qquad (1)$$

then the K^* must have spin 1, since for the spin 0 case angular momentum and parity cannot be conserved in this reaction. If (1) is not seen, the K^* spin assignment can be checked by observing

$$K + \mathrm{He}^4 \to K^* + \mathrm{He}^4 + \pi, \qquad (2)$$

and looking at the K^*-decay distribution.

There are two circumstances under which (1) will be forbidden and a third reason why it would be inhibited, however. Thus if (1) is observed, surely (a) the spin of the K^* is greater than zero (and presumably one) and (b) the isotopic spin of the K^* is the same as that of the K, which is 1/2. If the K^* had an isotopic spin of 3/2, which is allowed by its decay into $K + \pi$, then (1) would not occur, and hence this point can be checked for a nonzero spin K^*.

The inhibition of (1) will be discussed shortly, but first let us investigate what could in principle be learned from observing the decay angular distributions from the K^* produced by (1). These results will then be applied to (2), which is not inhibited, but which is more difficult to discuss.

It is well known[4] that one can obtain information on the spin of an unstable particle if one observes such particles produced near the beam direction. A reaction like (1) is, however, particularly useful for this purpose because the decay angular distribution for the K^* is uniquely determined by its spin, and because most of the observed reactions could be utilized for this analysis. In justifying the first of these statements, let us begin by considering the initial state of (1): There can be no orbital angular momentum (l) about the direction (z) of the incident K, and since there is no spin, the total angular momentum in that direction (j_z) is zero also. Therefore in the final state $j_z = 0$ too, and since for forward production $l_z = 0$, then the spin (S) can have no component in z direction. Thus for a K^* of any possible spin, if the K^* is produced forward there will be a unique angular distribution[5] for its decay, given by the spherical harmonic $|Y_{S,0}(\theta)|^2$, where θ is the angle between the direction of the incoming K and the decay momentum in the center-of-mass system of the K^*. According to the uncertainty principle, the decay distribution should not change appreciably over K^* emission angles of the order of the reciprocal of the largest orbital angular momentum contributing to the production process, which is $\sim\hbar/pR$, where p is the incident K momentum and R is the "radius" of He^4. This, however, is just the typical emission angle for events in which the He^4 stays bound. To keep the He^4 together, the momentum transferred to the He^4, q, must be kept small. From the uncertainty principle, $q \sim \hbar/R \sim 0.2$ Bev/c. To satisfy this condition,

p must be rather large ($\gtrsim 1.5$ Bev/c), and hence the emission angle, $\sim q/p \sim \hbar/pR$ is quite forward and is just that obtained above as a limiting one for the spin determination. Thus most events would be useful ones for this spin analysis, which not only permits distinguishing between the likely values of 0 or 1, but also affords a means to measure possibly higher values in a less ambiguous way than is presently available.[1]

There is a second method of using (1) [and (2), as will be discussed later] to determine the K^* spin, and this method can be utilized also to check parity conservation in the production and decay of the K^*. One uses not-too-forward events so as to define better the direction, x, of the normal to the plane formed by the relative momentum of the incident particles and that of the outgoing particles (before K^* decay). Performing an inversion about that plane followed by a 180° rotation about x would change the initial wave function by $(-1)^{P_K}$, where P_K is the parity of the K, and the final wave function by $(-1)^{P_{K^*}}(-1)^{S_x}$.[6] Therefore, if $P_{K^*} = P_K$, the projection of the K^* spin in the x direction, S_x, is even, whereas if $P_{K^*} = -P_K$, S_x is odd. Thus for example if the K^* spin is 1, the decay distribution should be given by $|Y_{1,0}(\theta')|^2 \propto \cos^2\theta'$ (where θ' is the angle between x and the decay momentum in the rest system of the K^*), because $P_{K^*} = P_K$ for $S = 1$ if parity is conserved in $K^* \to K + \pi$. However, if parity is not conserved, then P_{K^*} can be $-P_K$ and one would see a $\sin^2\theta'$ distribution.

Thus one can in principle determine from observations of (1) the spin of the K^*, no matter how large it is, and also get information on its isotopic spin and on whether parity is conserved in its decay or production. However, the previously mentioned inhibition of this reaction limits its usefulness in practice. That (1) will not occur with large probability even if it is allowed by spin and isotopic spin considerations can be seen by considering the case in which the K^* is produced forward, followed by K^* decay also along the beam direction. In this case one has $K + \mathrm{He}^4 \to K + \pi + \mathrm{He}^4$, with all the momenta essentially along a line, the z axis. If parity is conserved in the production and decay process, a reflection of the system about any plane containing the z axis should not alter the parity. However, this is not true for the postulated system because the π is pseudoscalar, and there can be no compensating parity change provided by angular momentum, since there is no orbital angular momentum about the z axis. Since we have seen above that forward K^* decays would otherwise be highly probable, this conflict can be resolved only if the amplitude for K^* production goes to zero in the forward direction. Thus reaction (1) is inhibited, and it would be difficult to obtain the information for the analysis of the decay distributions.

This analysis can, however, be applied to reaction (2), which is not forbidden by spin or isotopic spin considerations, and is not inhibited as (1) is, because for (2) there are two pions in the final state, and hence there is no difficulty in conserving the parity. For (2), one must look at those cases in which both the K^* and the π travel near the z direction; then, as with (1), the K^* decay distribution about z is the same unique function of the K^* spin. Even the analysis of the decay distributions with respect to x to determine spin and to check parity conservation can be applied to (2) provided x is as defined above; i.e., the K^*, π, and He^4 lie essentially in a plane, although the noncoplanarity angle can again be of the order of $\hbar/pR$. Then because of the additional π, $P_{K^*} = P_K$ makes S_x odd, whereas $P_{K^*} = -P_K$ makes S_x even.

An important experimental problem in any of the above observations is being sure that one has He^4 in the final state. Fortunately He^4 has no excited states, and its disintegration into hydrogen isotopes is clearly distinguishable, but the emission of $\mathrm{He}^3 + n$ instead of He^4 provides some difficulty. Of presently available techniques, the helium bubble chamber appears the most suitable for this investigation, and in such a device with a magnetic field the $\mathrm{He}^3 + n$ events should usually be rejected on the basis of a kinematic fit. In some cases, the fraction of the total depending strongly upon the incident K energy and the chamber size, the He^4's and He^3's can be separated on the basis of momentum and range. In fact, observation of the He^4 range and angle alone clearly separates reaction (1) from other processes, such as elastic scattering. Reaction (2) is harder to measure than (1), but all of the final particles can be charged, and hence clear cases can be obtained. Thus although the mere observance of (1) can determine whether the K^* spin is 0 or 1 under the highly probable assumptions of reference 3, it seems possible to settle this important question with fewer restrictions by observing the decay distributions from (2) and perhaps from the much rarer (1).

I wish to express my gratitude to B. T. Feld and D. B. Lichtenberg for discussions, and particularly to T. D. Lee, who considerably altered the contents of this note.

*National Science Foundation Senior Postdoctoral Fellow on leave from the Physics Department, Massachusetts Institute of Technology, Cambridge, Massachusetts.

[1]M. Alston, L. W. Alvarez, P. Eberhard, M. L. Good, W. Graziano, H. K. Ticho, and S. G. Wojcicki, Phys. Rev. Letters 6, 300 (1961).

[2]Chia-Hwa Chan, Phys. Rev. Letters 6, 383 (1961); M. A. B. Bég and P. C. DeCelles, Phys. Rev. Letters 6, 145, 428(E) (1961).

[3]M. Schwartz, Phys. Rev. Letters 6, 556 (1961).

[4]R. K. Adair, Phys. Rev. 100, 1540 (1955).

[5]Interactions resulting from the decay of the K^* within the He nucleus could distort these distributions, but this effect is probably not very important because He^4 is tightly bound and the K^* would be moving much faster than K^*'s and Y^*'s observed so far.

[6]This argument has been used by T. D. Lee and C. N. Yang, Phys. Rev. 104, 254 (1956), and has been explicitly applied to the type of problem considered here by A. Bohr, Nuclear Phys. 10, 486 (1959).

QUASI-ELASTIC INTERACTION OF 155-Mev PROTONS WITH PROTONS IN Li^6 AND Li^7

J. P. Garron, J. C. Jacmart, M. Riou, C. Ruhla, J. Teillac, and C. Caverzasio
Laboratoire Joliot-Curie de Physique Nucléaire, Orsay, France

and

K. Strauch
Harvard University, Cambridge, Massachusetts

(Received August 1, 1961)

We have studied the reactions $Li^6(p, 2p)He^5$ and $Li^7(p, 2p)He^6$ by detecting the product protons in coincidence. The 155-Mev proton beam of the Orsay synchrocyclotron had a 10-20% duty cycle.[1] The experimental apparatus has been used for a similar study in carbon.[2] It consists of two telescopes, each with (1) two plastic scintillation counters to define the scattered beams and (2) one NaI counter to measure the energy of each product proton. The two telescopes are used to study the angular distribution of two protons emitted in coincidence in a plane which includes the incident beam and at angles θ_1 and θ_2 with the incident beam and arranged symmetrically around it. The angular resolution in the scattering plane is ±2.5°. At each angle, the summed energy of the two coincident protons is displayed on a pulse-height analyzer when the energy of one of the two protons lies between 62 and 82 Mev for Li^6 and 60 and 80 Mev for Li^7. This limits the events studied to an energy ratio, $x^2 = E_1/E_2$, of $0.7 < x^2 < 1.0$ for low-binding-energy protons and $0.6 < x^2 < 1.0$ for high-binding-energy protons. The energy calibration is carried out with free p-p scattering events from a CH_2 target. The targets were prepared from material supplied by Oak Ridge National Laboratory and had a purity of 95.6% (Li^6) and 99.9% (Li^7).

The summed energy spectra at $\theta_1 = \theta_2 = 40°$ displayed in Fig. 1 are typical. Two peaks are observed for each target, corresponding to binding energies of the target proton of 23.5 ± 0.7 Mev and 10.0 ± 1.4 Mev for Li^7 and 20.0 ± 0.7 Mev and 4 ± 1.4 Mev for Li^6.[3] The position and width of the low-binding-energy peaks correspond to the residual nuclei He^6 and He^5 being left in their ground state, although excitation of the 1.71-Mev level[4] in He^6 cannot be excluded. The binding energies involved

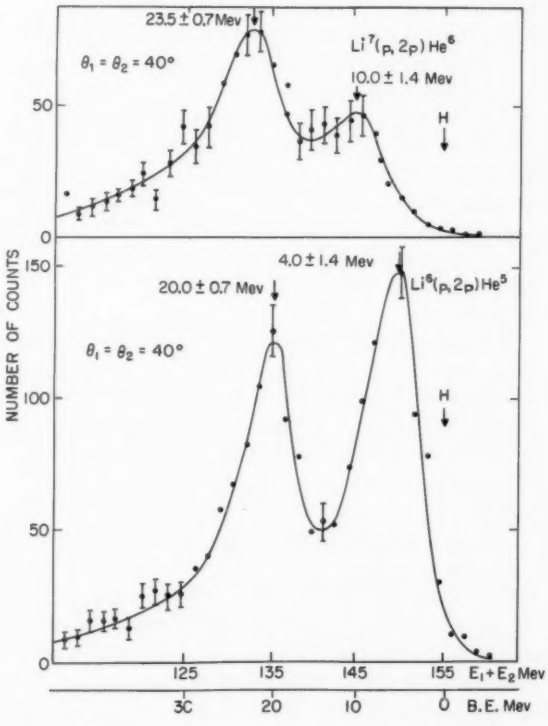

FIG. 1. Summed energy spectra of Li^6 and Li^7 at $\theta_1 = \theta_2 = 40°$. The abscissa also indicates the binding energy of the target protons.

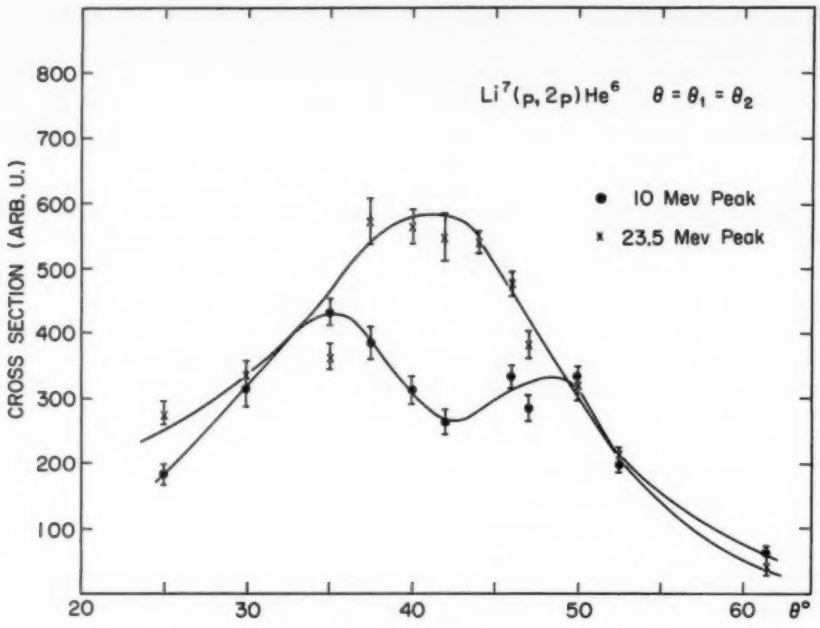

FIG. 2. Angular correlation distributions for Li^7.

suggest that the higher binding energy peaks are produced by the interaction of the incident protons with "inner core" protons in the target nuclei while the lower binding energy peaks are produced by the interaction with "outer shell" protons. This conclusion is based on the fact that the interaction time in the $(p, 2p)$ reaction is much smaller than the rearrangement time of the residual nucleus. Even for the ground state of He^5, these two times differ by a factor of 30 as calculated from the level width of 0.5 Mev reported in reference 4. The binding energies for the inner core protons are similar to those for He^4.

We have obtained angular correlation distributions from energy spectra measured at several angles $\theta = \theta_1 = \theta_2$ by integrating the number of events observed in a fixed summed energy interval of 15 Mev centered around each peak. For the higher binding energy protons this method yields only an upper limit to the cross section at small and large angles ($\theta < 30°$, $\theta > 50°$) since the corresponding peaks ride on a continuum which becomes appreciable. The results are presented in Figs. 2 and 3. The cross-section scale is in arbitrary units, but the same units are used for all curves. The errors shown are of statistical origin. The results for Li^7 are in agreement with previous studies[5] with ordinary targets in the regions where comparison is possible.

The angular correlation distributions for Li^7 (Fig. 2) have characteristic features previously observed with C^{12}.[2,5,6] The high-binding-energy peak has a maximum at about 41° as expected for s-shell protons, and the low-binding-energy peak has a minimum at about 42°, characteristic of p-shell protons. At small and large angles the cross sections fall off much more rapidly than for C^{12}. On the usual Born approximation interpretation, this observation means that the wave functions of the target protons in Li^7 have fewer high-momentum components than in C^{12}. The same conclusion has been reached from a study of the energy-sharing[7] in the same reaction.

The angular correlation distribution for the high-binding-energy protons in Li^6 (Fig. 3) is very similar to that of the corresponding protons in Li^7; the 23% difference in peak cross section can be explained by the difference in absorption. However, the angular correlation distributions of the low-binding-energy protons in Li^6 and Li^7 are very different, that for Li^6 being instead very similar to that of the high-binding-energy protons. The observation of the narrow peaks in the summed energy spectrum suggests that this difference is not the result of the difference in lifetime of the residual nuclei but rather due to differences in the properties of the low-binding-energy proton in Li^6 and Li^7. Using the impulse approximation interpretation, the wave function of the low-binding-energy proton in Li^7

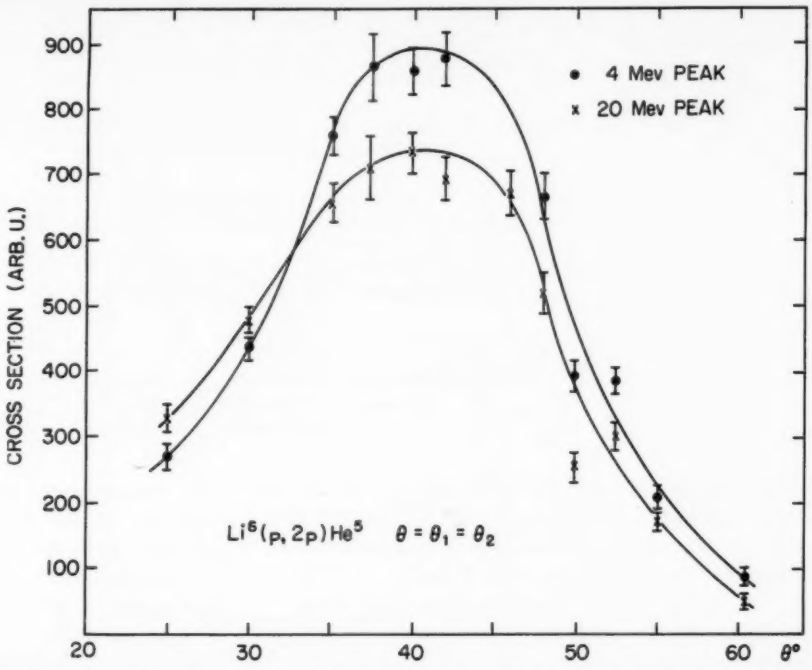

FIG. 3. Angular correlation distributions for Li^6.

contains many more low-momentum components than the corresponding proton in Li^7. In fact our Li^6 distribution is consistent with an s-proton interpretation, but we do not know whether a p proton with important low-momentum components might not yield a similar distribution.

The observed dip at about 41° in the angular correlation distribution for the low-binding-energy protons in Li^7 indicates that these protons have a pronounced minimum in their linear momentum distribution at zero momentum. Therefore the shell-model description of the low-binding-energy protons in Li^7 as p-shell protons is consistent with our observations. The results with the low-binding-energy protons in Li^6 are difficult to understand on the basis of the usual shell model, especially the large difference between the Li^6 and Li^7 distributions. Target protons with a maximum in their linear momentum distribution at zero momentum yield an angular correlation distribution with a maximum at about 41°. A model for Li^6 which yields such low-binding-energy s protons (a description consistent with our results) is the (alpha + deuteron) complex, in which the Li^6 spin is entirely due to the intrinsic spins of the neutron and proton in the deuteron.

The differences reported in this note seem to us to illustrate well the usefulness of studies of $(p, 2p)$ reactions at high energies in order to obtain information on nuclear structure. A complete report of similar studies with light elements will be published elsewhere.

We wish to thank the synchrocyclotron crew and the electronics group for their assistance. One of us (K. S.) wishes to thank the Laboratoire Joliot-Curie de Physique Nucléaire for their hospitality, and the Alfred P. Sloan Foundation for support.

---

[1]A. Cabrespine, J. phys. radium 21, 334 (1960).

[2]J. P. Garron, J. C. Jacmart, M. Riou, and C. Ruhla, J. phys. radium (to be published).

[3]We have verified in the case of Li^6 that the peaks correspond primarily to protons and not deuterons by observing the energy shift due to an absorber in one telescope.

[4]F. Ajzenberg-Selove and T. Lauritsen, Nuclear Phys. 11, 1 (1959).

[5]H. Tyrén, P. Hillman, and T. A. J. Maris, Nuclear Phys. 7, 10 (1958), and H. Tyrén, quoted in Proceedings of the International Conference on Nuclear Structure, Kingston, edited by D. A. Bromley and E. W. Vogt (University of Toronto Press, Toronto, 1960), p. 429.

[6]B. Gottschalk and K. Strauch, Phys. Rev. 120, 1005 (1960).

[7]B. Gottschalk and K. Strauch (to be published).

HELICITY OF THE PROTON FROM Λ DECAY*

J. Leitner, L. Gray, E. Harth, S. Lichtman, and J. Westgard
Syracuse University, Syracuse, New York

M. Block, B. Brucker, A. Engler, R. Gessaroli, A. Kovacs, T. Kikuchi, and C. Meltzer
Duke University, Durham, North Carolina

H. O. Cohn and W. Bugg
Oak Ridge National Laboratory, Oak Ridge, Tennessee

A. Pevsner, P. Schlein, and M. Meer
Johns Hopkins University, Baltimore, Maryland

and

N. T. Grinellini, L. Lendinara, L. Monari, and G. Puppi
University of Bologna, Bologna, Italy
(Received August 16, 1961)

The purpose of this note is to report a result for the helicity of the proton from Λ decay. We find that our data strongly favor positive helicity.

This result is obtained from a study of about 2000 Λ's produced by K^- absorption in He using the Duke helium chamber,[1] and a low-energy K^- beam at Berkeley.[2] The study, based on 105 proton scattering events from Λ decays, was made as part of a continuing experiment, a portion of which is described in detail elsewhere.[3]

The helicity of the proton in Λ decay is defined as the sign of the proton polarization measured in the decay rest frame. As shown by several authors,[4] this polarization is given by

$$\vec{\sigma}^* = -\alpha \vec{k}^*/|\vec{k}^*|, \tag{1}$$

where α is the asymmetry parameter of the decay $\Lambda \to \pi^- + p$, or in terms of the s and p amplitudes, $\alpha = 2\mathrm{Re}(s^*p)/(s^2+p^2)$ and $\vec{k}^*$ is the c.m. momentum of the proton. The proton polarization, longitudinal in the Λ rest frame, becomes partially transverse when transformed into the laboratory frame since (nonrelativistically) the spin remains rigid while the momentum $\vec{k}^*$ transforms into $\vec{k}_i$(lab), making an angle Γ with respect to $\vec{k}^*$. The transverse component, $\vec{\sigma}^* \sin\Gamma$, can then be measured by means of subsequent elastic scattering.

In principle both the magnitude and the sign of α can be obtained by measuring the (azimuthal) angular distribution of the scattered protons. In practice, however, since only a small portion of the available data has as yet been analyzed, only the sign of α is determined with good accuracy in this report.

Severe limits on the magnitude of α have already been set from the results of the up-down asymmetry experiments at Brookhaven and Berkeley.[5] The latest unpublished Berkeley results[6] indicate that $|\alpha| \geq 0.85$. We employ this result as a constraint on the determination of the sign of α in the present experiment. Details of the analysis are given below.

If an incoming proton beam of (lab) momentum $\vec{k}_i$ and arbitrary polarization $\vec{\sigma}$ is scattered from a spin 0 nucleus, the angular distribution[7] of the elastically scattered protons which emerge with polarization $\vec{P}_{an}(\theta,\epsilon)$ is

$$f(\theta,\epsilon) \sim 1 + \vec{\sigma} \cdot \vec{P}_{an}(\theta,\epsilon), \tag{2}$$

where θ = (proton) center-of-mass scattering angle, ϵ = lab proton energy at the point of scattering, $\vec{k}_f$ = outgoing proton lab momentum, and $\vec{P}_{an}(\theta,\epsilon) = P_{an}(\theta,\epsilon)\vec{k}_i \times \vec{k}_f / |\vec{k}_i \times \vec{k}_f|$ = analyzing polarization.[8] This expression can be written in a form more useful for analysis by expressing $\vec{\sigma} \cdot \vec{P}_{an}(\theta,\epsilon)$ in terms of the angle Γ defined above, and Ψ, an azimuthal scattering angle which is conveniently chosen as the angle between the Λ decay plane and the p-He scattering plane. The distribution then becomes

$$f(\Psi)d\Omega = [1 + \alpha \sin\Gamma P_{an}(\theta,\epsilon) \sin\Psi]\, d\Omega. \tag{3}$$

The quantities Γ and Ψ are directly obtainable[9] from a kinematic analysis of each event, and since the analyzing polarization is known[10] (see Fig. 1), α may be determined by an appropriate best-fit procedure using (3) as the theoretical distribution.

The important characteristics of the various subsamples chosen for analysis are given in Table I. Of the total of ≈150 Λ-decay proton scattering events found by the scanners, only 105 survived the selection criteria for sample A which were imposed in order to remove the Coulomb scatter-

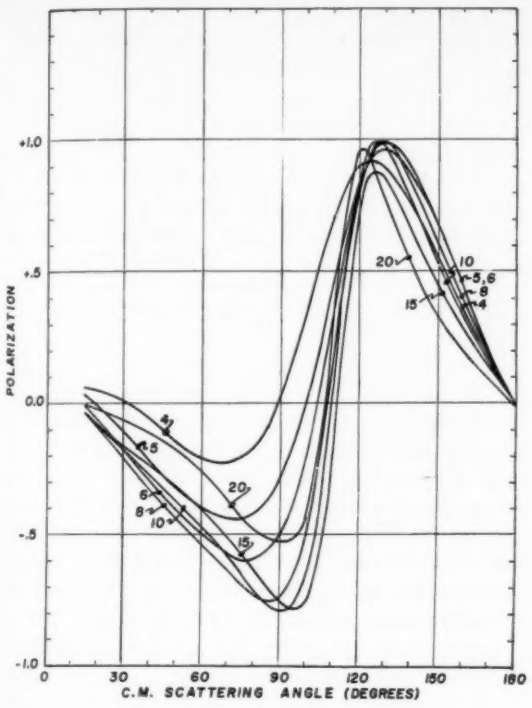

FIG. 1. Analyzing polarization for proton helium scattering as a function of c.m. angle for various proton (lab) kinetic energies. Data at and above 10 Mev are taken from J. L. Gammel and R. M. Thaler, Phys. Rev. 109, 2041 (1951). Data below 10 Mev are calculated from phase shifts given by A. Juveland and W. Jentschke, Z. Physik 144, 521 (1956).

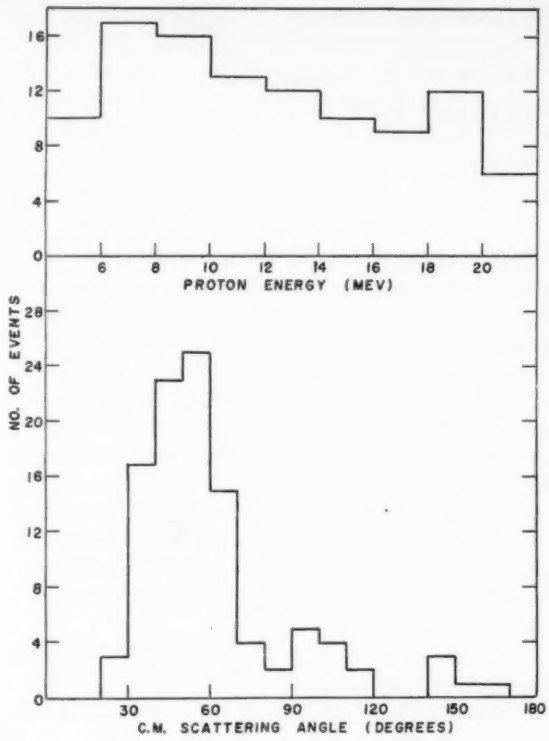

FIG. 2. (a) Proton energy spectrum of Sample A ($\theta \geq 26°$, 4 Mev $\leq \epsilon \leq$ 22.5 Mev). (b) Center-of-mass angular distribution of Sample A.

ings and possible inelastic contamination. These selection criteria are: (1) $\theta \geq 26°$, (2) 4 Mev $\leq \epsilon \leq$ 22.5 Mev. Of the total of 105 events in A, 100 stop in the chamber. The energy spectrum and angular distribution of all events is shown in Fig. 2.

Each event in the sample was subjected to a full kinematic analysis which yielded best-fit values of the dip and azimuth of each track. This information, when coupled with the accurate energy determination provided by the range of the scattered proton, permitted the calculation of $\sin\Psi$ and P_{an} to an average accuracy of 15% and 10%, respectively.[11]

The determination of the sign of α was carried out using three techniques, (a) the method of maximum likelihood, (b) comparison of the measured

Table I. Characteristics of the proton scattering sample. N = No. of events in sample; ϵ = average proton energy at scattering point; θ = average c.m. scattering angle; $\bar{P}_{an}$ = average analyzing polarization; $\langle P_{an}\sin\Gamma\rangle_{av}$ = average effective polarization of sample; η_{exp} = experimental value of right-left asymmetry; $\langle\eta\rangle$ = predicted value of right-left asymmetry using the measured $\langle P_{an}\sin\Gamma\rangle_{av}$.

Sample definition	N	$\bar{\epsilon}$	$\bar{P}_{an}$	$\langle\sin\Gamma\rangle_{av}$	$\langle P_{an}\sin\Gamma\rangle_{av}$	η_{exp}	$\langle\eta\rangle$	$\bar{\theta}$
A. $\theta \geq 26°$, 4 Mev $\leq \epsilon \leq$ 22.5 Mev	105	12.0	0.36	0.77	0.28	0.20	-0.18α	60.5°
B. $\theta \geq 26°$, 4 Mev $\leq \epsilon \leq$ 22.5 Mev, $P_{an}\sin\Gamma > 0.25$	57	10.6	0.47	0.86	0.40	0.15	-0.26α	69.0°
C. $\theta \geq 40°$, 4 Mev $\leq \epsilon \leq$ 22.5 Mev	85	11.8	0.41	0.76	0.31	0.20	-0.20α	66.5°

right-left asymmetry with its expected value, and (c) a χ^2 fit of (7) to the Ψ distribution.

The likelihood function, $L(\alpha)$, representing the total probability for observing our 105 events in sample A, is a product of the distributions (3) evaluated for each event:

$$L(\alpha) = \prod_{i=1}^{20} [1 + \alpha P_{an}(\theta_i, \epsilon_i) \sin\Gamma_i \sin\Psi_i]. \quad (4)$$

A plot of $L(\alpha)$ vs α for sample A is shown in Fig. 3. Although the best-fit magnitude of α, as determined from the position of the maximum of $L(\alpha)$, is quite consistent with the limits set by the up-down asymmetry experiments ($0.85 \leq |\alpha| \leq 1$), it is clear from the width of $L(\alpha)$ that the present data cannot determine $|\alpha|$ with comparable precision. We therefore accept the previous determination of $|\alpha| \approx 1$, and ask the question: "Given the magnitude of α, what is the likelihood of the hypothesis $\alpha = -1$, relative to the hypothesis $\alpha = +1$"? One such relative likelihood measure is given by the ratio $L(\alpha=-1)/L(\alpha=+1) \approx 2\times10^3$ which strongly favors[12] $\alpha = -1$.

Another such relative measure can be obtained by comparison of the measured azimuthal angle asymmetry η, defined[13] by

$$\eta_{exp} = [N_R(\sin\Psi \geq 0) - N_L(\sin\Psi < 0)]/(N_R + N_L), \quad (5)$$

with its expected value $\langle\eta\rangle$ given by

$$\langle\eta\rangle = (2/\pi)\alpha\langle\sin\Gamma P_{an}(\theta,\epsilon)\rangle_{av}. \quad (6)$$

For our sample A, $\langle\eta\rangle = -0.18\alpha$, and the measured asymmetry is $\eta_{exp} = 0.20 \pm 0.1$. Thus the data are consistent with the requirement $|\alpha| \approx 1$, and are in good agreement with the hypothesis $\alpha = -1$, but are in disagreement with the hypothesis $\alpha = +1$ by about 3.8 standard deviations.[12]

An alternate approach is based on a χ^2 analysis of the observed distribution in Ψ (see Fig. 4). The expected distributions $g(\Psi)d\Psi$ for $\alpha = \mp 1$, respectively, follow from (3), integrated over solid angle:

$$g(\Psi)d\Psi = [1 + \alpha\langle\sin\Gamma P_{an}(\theta,\epsilon)\rangle_{av} \sin\Psi]d\Psi, \quad (7a)$$

$$g(\Psi)d\Psi = [1 - \alpha\langle\sin\Gamma P_{an}(\theta,\epsilon)\rangle_{av} \sin\Psi]d\Psi, \quad (7b)$$

where $\langle\sin\Gamma P_{an}(\theta,\epsilon)\rangle_{av}$ is the experimental average given in Table I.[14] The most probable value of χ^2 for this fit is 5.0. The distribution (7a) is in excellent agreement with the data of Fig. 4, yielding a χ^2 of 3.9, corresponding to a probability of 56% for the observation of the data, if $\alpha = -1$. On the other hand, the distribution (7b) has a χ^2 of 25.7, corresponding to a probability of less

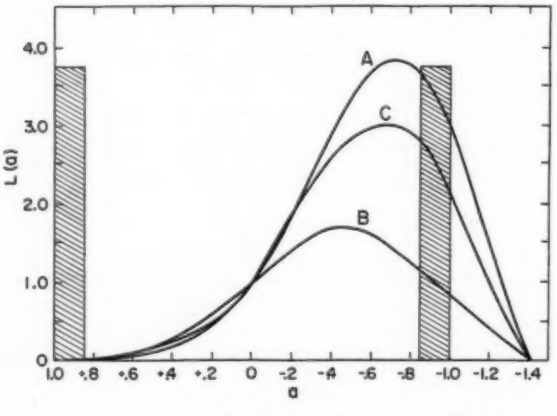

FIG. 3. Likelihood function $L(\alpha)$ vs α for Samples A, B, and C. The shaded areas represent regions allowed by up-down asymmetry experiment. Sample B is defined by $P_{an}\sin\Gamma \geq 0.25$, 4 Mev $\leq \epsilon \leq$ 22.5 Mev; sample C is defined by $\theta \geq 40°$, 4 Mev $\leq \epsilon \leq$ 22.5 Mev.

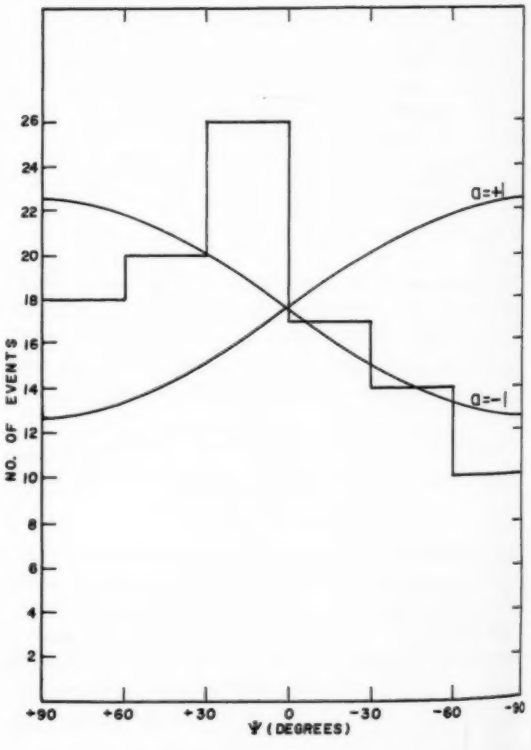

FIG. 4. Distribution of angle Ψ between Λ decay and proton scattering planes. The expected distributions for $\alpha = \pm 1$ are represented by smooth curves.

than 1% for the observation of the data, if $\alpha = +1$.

Aside from the purely statistical errors given above, we have considered several possible sources of systematic error—inelastic contamination, Coulomb contamination, scanning bias against events in certain regions of energy and scattering angle (see Fig. 2), and finally polarization of the Λ sample. We believe all of these effects to be either small or nonexistent for reasons discussed below.

Firstly, each of the scattered protons had an energy below threshold for $p + He^4 \rightarrow d + He^3$, which constitutes 90% of the inelastic cross section at low energy. Secondly, the $\theta \geq 26°$ criterion was designed to eliminate ~90% of the Coulomb events. In any event a small contamination of Coulomb scatters will not affect the maximum-likelihood estimate of α because these events, at small θ, would be assigned a small P_{an} (see Fig. 1).

In principle, since the angle Ψ between the production and decay planes is uncorrelated with scattering energy and the angle, the bias against low ϵ and small θ events should not affect the Ψ distribution. To test this point experimentally, we selected two subsamples B and C according to the criteria given in Table I. B is a high effective polarization sample rich in low-energy events; C is a sample composed of large scattering angle events. Both the likelihood functions (see Fig. 3) and the asymmetries (see Table I) for B and C are in good agreement with their expected values, thus confirming the internal consistency of the data.

Lastly, we consider the possibility of the existence of a polarization of the Λ sample, which would complicate the analysis to some extent.[4] The majority of the Λ's in the sample were produced via a two-step Σ-conversion process,[15] i.e.,

$$K^- + N \rightarrow \Sigma + \pi, \tag{8a}$$

$$\Sigma + N' \rightarrow \Lambda + N'. \tag{8b}$$

The outgoing Λ's, if polarized at all, must be polarized perpendicular to the production plane of (8b). However, since all such production planes are accepted, the outgoing Λ's must be polarized.

Owing to all the above considerations, we include no systematic effects in our estimation of the errors in this experiment.

In order to make a direct comparison of our results with those of other experiments of this type, we must disregard the constraint placed on the magnitude of α by the up-down asymmetry experiments. Then, from the likelihood function of Fig. 3, the most likely value of α is

$$\alpha = -0.75^{-0.15}_{+0.50}, \tag{9}$$

where the error on the positive side corresponds to the half-width of $L(\alpha)$. The result (9) can be compared with those of Boldt et al.[16] and Birge et al.,[17] who find $\alpha = +0.85 \pm 0.20$ and -0.45 ± 0.5, respectively. Our result is clearly in disagreement with the former; it is in agreement with that of Birge et al., but is even more indicative of a negative α.

Furthermore, we should like to emphasize that by taking the known limits on $|\alpha|$ properly into account, as described above, one obtains considerably stronger results. We prefer to summarize these results as follows: For values of $|\alpha|$ consistent with the known limits, our data favor the hypothesis that α is negative over the hypothesis that α is positive by at least 3 standard deviations.

One of us (JL) would like to acknowledge some stimulating correspondence with Dr. R. Birge.

---

*This research is supported in part by the Office of Naval Research, U. S. Atomic Energy Commission, Office of Scientific Research, and the National Science Foundation.

[1]M. M. Block, H. A. Fairbank, E. M. Harth, T. Kikuchi, C. M. Meltzer, and J. Leitner, Proceedings of the International Conference on High-Energy Accelerators and Instruments, CERN (European Organization for Nuclear Research, Geneva, 1959), p. 461.

[2]N. Horwitz, J. Murray, M. Ross, and R. Tripp, University of California Radiation Laboratory Report UCRL 8269, 1958 (unpublished). J. Murray and P. Schlein (private communication).

[3]M. M. Block et al., Proceedings of the 1960 Annual International Conference on High-Energy Physics at Rochester (Interscience Publishers, Inc., New York, 1960), p. 419 ff.

[4]T. Lee and C. Yang, Phys. Rev. 108, 1353 (1957), R. Gatto, University of California Radiation Laboratory Report UCRL 3795, 1957 (unpublished); J. Leitner, Nuovo cimento 8, 68 (1958).

[5]F. Eisler et al., Phys. Rev. 108, 1353 (1957). F. S. Crawford, M. Cresti, M. L. Good, K. Gottstein, E. M. Lyman, F. T. Solmitz, M. L. Stevenson, and H. K. Ticho, Phys. Rev. 108, 1102 (1957).

[6]Private communication from F. Crawford. A similar estimate (~0.8) is given by M. Schwartz (private communication).

[7]L. Wolfenstein, Ann. Rev. Nuc. Sci. 6, 43 (1956).

[8]This is the definition of polarization adopted by L. Wolfenstein, Phys. Rev. 75, 1664 (1949).

[9]The angle Γ is directly obtainable from Λ-decay kinematics at the decay vertex. It must then be corrected because of the difference in rotation frequencies of the

proton spin and momentum vectors during the flight path from the decay vertex to the scattering point. This frequency difference is proportional to the anomalous moment of the proton. See D. F. Nelson, A. A. Schupp, R. W. Pidd, and H. R. Crane, Phys. Rev. Letters 2, 492 (1959). The average correction in our experiment is quite small (~2°).

[10]J. L. Gammel and R. M. Thaler, Phys. Rev. 109, 2041 (1958). A. Juveland and W. Jentschke, Z. Physik 144, 521 (1956). The phase shifts of the latter paper and the formula given in reference 8 were used to calculate the values of P_{an} for energies below 10 Mev.

[11]This is true only for events in which the proton stops. Events in which the proton leaves the chamber have more severe errors in general.

[12]The value $|\alpha| > 0.85$ given in reference 6 may be somewhat uncertain since it is based on the assumption that only s and p waves are present in $\Lambda + K^0$ production by 1-Bev/c π^- on protons. However, even if we take $|\alpha| = 0.7$, our measured asymmetry η_{exp} would still differ by about 3 standard deviations from its expected value for $\alpha = +0.7$, and the ratio $L(-0.7)/L(+0.7)$ is $\approx 10^{+2}$.

[13]This definition holds only for events in which P_{an} is of one sign—viz, $P_{an} < 0$. For events in which $P_{an} > 0$, "right" and "left" must be interchanged.

[14]This is not an algebraic average, but rather is the average magnitude of $(\sin\Gamma P_{an})$. We associate a negative sign with it since most of the scattering events have $P_{an} < 0$. For events with $P_{an} > 0$, we reverse the sign of $\sin\Psi$ in Fig. 4.

[15]See reference 3, page 423.

[16]E. Boldt, H. S. Bridge, D. O. Caldwell, and Y. Pal, Phys. Rev. Letters 1, 256 (1958).

[17]R. W. Birge and W. B. Fowler, Phys. Rev. Letters 5, 254 (1960).

ERRATUM

SELF-CONSISTENT CALCULATION OF THE MASS AND WIDTH OF THE $J=1$, $T=1$, $\pi\pi$ RESONANCE. Fredrik Zachariasen [Phys. Rev. Letters 7, 112 (1961)].

Due to an error in the numerical computations the mass value $m_\rho \sim 950$ Mev is wrong and should be changed to $m_\rho \sim 350$ Mev. While the agreement with the experimental value is slightly less good, it is perhaps encouraging to have too large a coupling constant going with too small a mass. An improved calculation might then give a smaller coupling constant, corresponding to a weaker attraction which could be consistent with a larger mass, while it is hard to see how a smaller coupling constant could go with a smaller mass.

I am indebted to J. Mathews for pointing out that the mass was incorrect, and to C. Zemach for aid in computing the correct value.